

# Complete analysis of the background and anisotropies of scalar-induced gravitational waves: primordial non-Gaussianity $f_{\text{NL}}$ and $g_{\text{NL}}$ considered

Jun-Peng Li,<sup>a,b</sup> Sai Wang<sup>1, a</sup>, Zhi-Chao Zhao,<sup>c</sup> Kazunori Kohri<sup>d,e,f</sup>

<sup>a</sup>Theoretical Physics Division, Institute of High Energy Physics, Chinese Academy of Sciences, 19B Yuquan Road, Shijingshan District, Beijing 100049, China

<sup>b</sup>School of Physics, University of Chinese Academy of Sciences, 19A Yuquan Road, Shijingshan District, Beijing 100049, China

<sup>c</sup>Department of Applied Physics, College of Science, China Agricultural University, 17 Qinghua East Road, Haidian District, Beijing 100083, China

<sup>d</sup>Division of Science, National Astronomical Observatory of Japan (NAOJ), and SOKENDAI, 2-21-1 Osawa, Mitaka, Tokyo 181-8588, Japan

<sup>e</sup>Theory Center, IPNS, and QUP (WPI), KEK, 1-1 Oho, Tsukuba, Ibaraki 305-0801, Japan

<sup>f</sup>Kavli IPMU (WPI), UTIAS, The University of Tokyo, Kashiwa, Chiba 277-8583, Japan

E-mail: [lijunpeng@ihep.ac.cn](mailto:lijunpeng@ihep.ac.cn), [wangsai@ihep.ac.cn](mailto:wangsai@ihep.ac.cn), [zhaozc@cau.edu.cn](mailto:zhaozc@cau.edu.cn), [kazunori.kohri@gmail.com](mailto:kazunori.kohri@gmail.com)

## Abstract.

Investigation of primordial non-Gaussianity holds immense importance in testing the inflation paradigm and shedding light on the physics of the early Universe. In this study, we conduct the complete analysis of scalar-induced gravitational waves (SIGWs) by incorporating the local-type non-Gaussianity  $f_{\text{NL}}$  and  $g_{\text{NL}}$ . We develop Feynman-like diagrammatic technique and derive semi-analytic formulas for both the energy-density fraction spectrum and the angular power spectrum. For the energy-density fraction spectrum, we analyze all the relevant Feynman-like diagrams, determining their contributions to the spectrum in an order-by-order fashion. As for the angular power spectrum, our focus lies on the initial inhomogeneities, giving rise to anisotropies in SIGWs, that arise from the coupling between short- and long-wavelength modes due to primordial non-Gaussianity. Our analysis reveals that this spectrum exhibits a typical multipole dependence, characterized by  $\tilde{C}_\ell \propto [\ell(\ell+1)]^{-1}$ , which plays a crucial role in distinguishing between different sources of gravitational waves. Depending on model parameters, significant anisotropies can be achieved. We also show that the degeneracies in model parameters can be broken. The findings of our study underscore the angular power spectrum as a robust probe for investigating primordial non-Gaussianity and the physics of the early Universe. Moreover, our theoretical predictions can be tested using space-borne gravitational-wave detectors and pulsar timing arrays.

---

<sup>1</sup>Corresponding author

---

## Contents

<b>1</b>	<b>Introduction</b>	<b>1</b>
<b>2</b>	<b>Energy-density fraction spectrum</b>	<b>3</b>
2.1	Feynman-like Rules and Diagrams	6
2.2	Formulae for Energy-Density Fraction Spectrum	10
2.3	Nine Families of Integrals	11
2.4	Numerical Results	14
<b>3</b>	<b>Angular power spectrum</b>	<b>18</b>
3.1	Feynman-like Rules and Diagrams	21
3.2	Formulae for Angular Power Spectrum	23
3.3	Numerical Results	24
<b>4</b>	<b>Discussion and Conclusion</b>	<b>30</b>
<b>A</b>	<b>Equation of Motion</b>	<b>32</b>
<b>B</b>	<b>Numerical integrals</b>	<b>33</b>
<b>C</b>	<b>Boltzmann equation</b>	<b>36</b>

---

## 1 Introduction

Studying primordial non-Gaussianity is essential for testing the inflationary paradigm and gaining insights into the physics of the early Universe [1–7]. Primordial non-Gaussianity refers to deviations from Gaussian statistics in the distribution of primordial perturbations that arise during inflation. In the standard inflationary scenario, these perturbations are assumed to be Gaussian, with their statistics fully described by the power spectrum [8]. However, there are scenarios where these perturbations can exhibit non-Gaussian behavior, providing valuable insights into early-Universe physics [9, 10]. Primordial non-Gaussianity involves higher-order correlations and statistical properties of the primordial perturbations [1]. Different inflationary models can lead to varying levels and types of non-Gaussianity, which can be characterized by non-linear parameters such as  $f_{\text{NL}}$  and  $g_{\text{NL}}$ . Observations of the cosmic microwave background (CMB) [11] and large-scale structures (LSS) [12, 13] have been used for constraining these parameters on the largest observational scales. Such constraints provide valuable information about the physics of inflation and aid in distinguishing between different inflationary models.

The scalar-induced gravitational waves (SIGWs) [14–20] provide a powerful tool for investigating primordial non-Gaussianity, particularly on scales that are beyond the reach of measurements from CMB and LSS. These gravitational waves (GWs) arise from the nonlinear interactions of linear cosmological curvature perturbations in the early Universe. Unlike photons, gravitons can freely propagate once generated, as the Universe is transparent to GWs [21, 22]. As a result, the study of gravitational waves offers the potential to probe physical processes that occurred during the extremely early epochs of the Universe, corresponding to physics at incredibly small scales.

Primordial non-Gaussianity has significant effects on the energy-density fraction spectrum of SIGWs. Regarding to local-type non-Gaussianity  $f_{\text{NL}}$ , complete analysis presented in Refs. [23–26] show that this spectrum can be substantially enhanced, potentially reaching up to two orders of magnitude larger than the Gaussian scenario, depending on the levels of  $f_{\text{NL}}$ . Other works related with the effects of primordial non-Gaussianity (e.g.,  $f_{\text{NL}}$  and  $g_{\text{NL}}$ ) on SIGWs have been shown in Refs. [27–42]. Moreover, the presence of primordial non-Gaussianity can also impact the formation of primordial black holes (PBHs) that coexist with SIGWs. The distribution of PBH masses is influenced by the non-Gaussian features [37, 38, 43–68]. Experimental tests of these theoretical predictions can be conducted through multi-band GW observations. Notably, pulsar timing array (PTA) experiments [69–72] have provided compelling evidence for the existence of a gravitational-wave background (GWB), which is speculated to originate from SIGWs [73–105]. They provide an avenue for testing and validating the presence of SIGWs and their associated non-Gaussian features.

Studies have demonstrated that the non-Gaussianity  $f_{\text{NL}}$  can induce significant inhomogeneities and anisotropies in SIGWs [25, 106]. Unlike CMB, where the angular power spectrum is determined by the two-point correlators of linear curvature perturbations, the angular power spectrum of SIGWs is determined by the four-point correlators of these perturbations, inherently incorporating the effects of primordial non-Gaussianity  $f_{\text{NL}}$ . This implies that the energy density of SIGWs produced by short-wavelength modes is redistributed by long-wavelength modes due to the coupling between these modes. The parameter  $f_{\text{NL}}$  was initially investigated as a means to explore this possibility in Refs. [106], and subsequently, a comprehensive analysis on this topic was conducted for the first time in Ref. [25]. Other relevant works can be found in Refs. [60, 107–115]. In particular, Ref. [78] showed that if the PTA signal originates from scalar-induced gravitational waves, it can be tested using the Square Kilometre Array (SKA) [116–119] by measuring the corresponding angular power spectrum. Furthermore, the angular power spectrum was found to break degeneracies in cosmological parameters for the energy-density fraction spectrum [25], making it a powerful tool for probing primordial non-Gaussianity and exploring physics in the early Universe. However, to our knowledge, there are not works extending to consider the non-Gaussianity  $g_{\text{NL}}$ .

In this study, we present the first complete analysis of SIGWs, specifically examining both the energy-density fraction spectrum and the angular power spectrum, by incorporating the local-type primordial non-Gaussianity, specifically the parameters  $f_{\text{NL}}$  and  $g_{\text{NL}}$ . This work builds upon our previous research [25] and extends it to include a broader scope. To begin, we investigate the energy-density fraction spectrum of SIGWs at a homogeneous and isotropic level using a Feynman-like diagrammatic approach. We derive semi-analytic formulas for this spectrum and analyze the impact of non-Gaussianity on its behavior. As part of a comprehensive analysis, we establish a systematic classification of Feynman-like diagrams and develop a dictionary that relates these diagrams to their corresponding integrals. Subsequently, we focus on studying the angular power spectrum of SIGWs, which is influenced by both the initial inhomogeneities and the propagation effects. While the propagation effects are similar to those observed in CMB, the analysis of initial inhomogeneities requires an extension of the Feynman-like diagrammatic technique. This is because practical calculations involve a large number of Feynman-like diagrams, making it challenging to straightforwardly expand the multi-point correlators using Wick’s theorem. To address this, we develop a systematic method for evaluating the integrals associated with these Feynman-like diagrams, enabling a comprehensive analysis of the angular power spectrum. We derive

semi-analytic formulas for the angular power spectrum, which can be expressed as a combination of the Feynman-like diagrams in our established dictionary. Furthermore, we perform numerical studies to explore the implications of the angular power spectrum for primordial non-Gaussianity. We also demonstrate how our theoretical results can be tested through future multi-band GW observations. Overall, this work presents a thorough analysis of both the energy-density fraction spectrum and the angular power spectrum of SIGWs, incorporating the effects of primordial non-Gaussianity  $f_{\text{NL}}$  and  $g_{\text{NL}}$ . It provides semi-analytic formulas and numerical results that contribute to our understanding of the implications of non-Gaussianity in the early Universe and suggests potential avenues for experimental validation through GW observations.

The paper is structured as follows. In Section 2, we investigate the energy-density fraction spectra of homogeneous SIGWs at the background level. In Section 3, we analyze the angular power spectrum of anisotropic SIGWs, considering the contributions from both the initial inhomogeneities and the propagation effects at the perturbation level. In Section 4, we provide a discussion and conclusion of our findings. The supplemental materials, including additional details on the theoretical basics, numerical integration techniques, and the Boltzmann equation, are summarized in Appendices A to C, respectively.

## 2 Energy-density fraction spectrum

In this section, we initially disregard the presence of large-scale inhomogeneities in SIGWs, but we will address them in the next section. Therefore, in this section, we treat SIGWs as a homogeneous and isotropic GWB on large scales. However, small-scale inhomogeneities can still exist within SIGWs. Nevertheless, due to the angular resolution limitations of gravitational wave detectors, the observed signal along a line-of-sight is a combination of SIGWs originating from numerous small-scale regions. Consequently, the observed signal represents an ensemble average over these regions, resulting in identical signals along different line-of-sights. This perspective simplifies the evaluation of the energy-density fraction spectrum. By assuming the small-scale regions to be identical (either isotropic or anisotropic, although we adopt isotropy for simplicity), we can effectively obtain the spectrum by evaluating it in any one region. These regions can be viewed as the Hubble horizons at the time of SIGW production. We carry out this evaluation in the subsequent analysis.

The energy-density fraction spectrum  $\bar{\Omega}_{\text{GW}}(\eta, q)$  for SIGWs on subhorizon scales is defined as follows [120]

$$\bar{\rho}_{\text{gw}}(\eta) = \rho_c(\eta) \int d \ln q \bar{\Omega}_{\text{gw}}(\eta, q) , \quad (2.1)$$

where  $\rho_c = 3\mathcal{H}^2 m_{\text{Pl}}^2$  denotes the critical energy density of the Universe,  $m_{\text{Pl}} = 1/\sqrt{8\pi G}$  is the Planck mass,  $\mathcal{H}(\eta)$  stands for the conformal Hubble parameter at conformal time  $\eta$ , and the overbar signifies physical quantities at the background level. Here and hereinafter, the wavenumber  $q$  is denoted as the magnitude of the 3-momentum  $\mathbf{q}$ , namely,  $q = |\mathbf{q}|$ . The energy density of SIGWs is defined as follows [120]

$$\bar{\rho}_{\text{gw}}(\eta) = \frac{m_{\text{Pl}}^2}{16a^2(\eta)} \langle \overline{\partial_l h_{ij}(\eta, \mathbf{x}) \partial_l h_{ij}(\eta, \mathbf{x})} \rangle , \quad (2.2)$$

where  $a(\eta)$  is the scale factor of the Universe, the long overbar labels a temporal average over oscillations, and the angle brackets stand for the ensemble average. It is useful to expand

SIGWs in Fourier mode as follows

$$h_{ij}(\eta, \mathbf{x}) = \sum_{\lambda=+, \times} \int \frac{d^3 \mathbf{q}}{(2\pi)^{3/2}} e^{i\mathbf{q} \cdot \mathbf{x}} \epsilon_{ij}^\lambda(\mathbf{q}) h_\lambda(\eta, \mathbf{q}) , \quad (2.3)$$

where the polarization tensors are defined as  $\epsilon_{ij}^+(\mathbf{q}) = [\epsilon_i(\mathbf{q})\epsilon_j(\mathbf{q}) - \bar{\epsilon}_i(\mathbf{q})\bar{\epsilon}_j(\mathbf{q})]/\sqrt{2}$  and  $\epsilon_{ij}^\times(\mathbf{q}) = [\epsilon_i(\mathbf{q})\bar{\epsilon}_j(\mathbf{q}) + \bar{\epsilon}_i(\mathbf{q})\epsilon_j(\mathbf{q})]/\sqrt{2}$ , with  $\epsilon_i(\mathbf{q})$  and  $\bar{\epsilon}_i(\mathbf{q})$  being a set of orthonormal basis vectors that are perpendicular to the wavevector  $\mathbf{q}$ . This definition implies that we have  $\epsilon_{ij}^\lambda \epsilon_{ij}^{\lambda'} = \delta^{\lambda\lambda'}$  and  $\epsilon_{ij}^\lambda(\mathbf{q})$  are transverse to  $\mathbf{q}$ . The power spectrum of  $h_\lambda$  is defined as

$$\langle h_\lambda(\eta, \mathbf{q}) h_{\lambda'}(\eta, \mathbf{q}') \rangle = \delta_{\lambda\lambda'} \delta^{(3)}(\mathbf{q} + \mathbf{q}') P_{h_\lambda}(\eta, q) . \quad (2.4)$$

Combining the above formulae, the energy-density fraction spectrum is expressed in terms of the power spectrum of SIGWs, namely, [121]

$$\bar{\Omega}_{\text{gw}}(\eta, q) = \frac{q^5}{96\pi^2 \mathcal{H}^2} \overline{P_h(\eta, q)} , \quad (2.5)$$

where we introduce  $P_h = \sum_{\lambda=+, \times} P_{h_\lambda}$  for convenience.

The equation of motion for SIGWs was originally derived in the literature [14, 15]. Semi-analytic derivations can be found in Refs. [16, 17]. We provide a brief overview of the derivation results in Appendix A, following the conventions of Ref. [25]. We have a solution to the equation of motion of SIGWs on subhorizon scales, given by

$$h_\lambda(\eta, \mathbf{q}) = 4 \int \frac{d^3 \mathbf{q}_a}{(2\pi)^{3/2}} \zeta(\mathbf{q}_a) \zeta(\mathbf{q} - \mathbf{q}_a) Q_\lambda(\mathbf{q}, \mathbf{q}_a) \hat{I}(|\mathbf{q} - \mathbf{q}_a|, q, \eta) , \quad (2.6)$$

where  $\zeta(\mathbf{q})$  denotes the linear primordial curvature perturbations,  $Q_\lambda(\mathbf{q}, \mathbf{q}_a)$  denotes the projection factor as shown in Eq. (A.11), and  $\hat{I}(|\mathbf{q} - \mathbf{q}_a|, q, \eta)$  represents the kernel function as shown in Eqs. (B.11) and (B.12).

In a schematic manner, the equations above, Eqs. (2.3), (2.4), (2.5), and (2.6), suggest that  $\bar{\Omega}_{\text{gw}} \sim \langle \zeta^4 \rangle$ . To be more specific, we find

$$\begin{aligned} \langle h_{ij}(\eta, \mathbf{q}) h_{ij}(\eta, \mathbf{q}') \rangle &= 16 \int \frac{d^3 \mathbf{q}_1}{(2\pi)^{3/2}} \frac{d^3 \mathbf{q}_2}{(2\pi)^{3/2}} \langle \zeta(\mathbf{q}_1) \zeta(\mathbf{q} - \mathbf{q}_1) \zeta(\mathbf{q}_2) \zeta(\mathbf{q}' - \mathbf{q}_2) \rangle \\ &\times \sum_{\lambda, \lambda'} \epsilon_{ij}^\lambda \epsilon_{ij}^{\lambda'} Q_\lambda(\mathbf{q}, \mathbf{q}_1) \hat{I}(|\mathbf{q} - \mathbf{q}_1|, q_1, \eta) Q_{\lambda'}(\mathbf{q}', \mathbf{q}_2) \hat{I}(|\mathbf{q}' - \mathbf{q}_2|, q_2, \eta) . \end{aligned} \quad (2.7)$$

This result indicates the necessity to handle the four-point correlators of  $\zeta$ . The evaluation of this correlator will be discussed in detail in the remaining part of this section.

The nature of primordial curvature perturbations, such as non-Gaussianity, introduces complexity in calculating these correlators. By adopting the Feynman-like diagrammatic technique, the four-point correlator of Gaussian curvature perturbations can be described by a single diagram [16, 17]. However, in the case of non-Gaussianity with a parameter  $f_{\text{NL}}$ , the derivation process becomes significantly more involved, requiring the evaluation of a total of seven diagrams to calculate the four-point correlator of linear curvature perturbations [23–26]. The first complete analysis of this calculation can be found in Ref. [23], and other relevant works on this topic can be found in Refs. [24–30, 35, 38]. Furthermore, relevant works on the primordial non-Gaussian parameter  $g_{\text{NL}}$  can be found in Refs. [26, 31–33, 38].

In this study, we employ the diagrammatic approach, which has been extensively utilized in the literature [23–26], to investigate the local-type primordial non-Gaussianity, parameterized by  $f_{\text{NL}}$  and  $g_{\text{NL}}$ , of curvature perturbations within the theoretical framework of SIGWs. This work serves as a natural extension of our previous research [25], which focused solely on  $f_{\text{NL}}$ . The primary objective of our study is to derive the formulas for the angular power spectrum of anisotropic SIGWs. Additionally, it is crucial to independently derive the formulas for  $\bar{\Omega}_{\text{gw}}$  using the diagrammatic approach. Guided by these objectives, we conduct a comprehensive analysis of SIGWs, incorporating both  $f_{\text{NL}}$  and  $g_{\text{NL}}$ . We provide formulae for the energy-density fraction spectrum and the angular power spectrum, and systematically compare our results with those presented in numerous pioneering papers. Our work can serve as a valuable resource for readers interested in the same topic, akin to a dictionary of sorts.

By incorporating the local-type primordial non-Gaussianity parameterized by  $f_{\text{NL}}$  and  $g_{\text{NL}}$ , we express the linear curvature perturbations  $\zeta$  in terms of their Gaussian components, denoted as  $\zeta_g$ , as follows [122]

$$\zeta(\mathbf{x}) = \zeta_g(\mathbf{x}) + \frac{3}{5}f_{\text{NL}} \left[ \zeta_g^2(\mathbf{x}) - \langle \zeta_g^2(\mathbf{x}) \rangle \right] + \frac{9}{25}g_{\text{NL}}\zeta_g^3(\mathbf{x}) . \quad (2.8)$$

Furthermore, it is customary to decompose  $\zeta_g$  into short-wavelength modes  $\zeta_{gS}$  and long-wavelength modes  $\zeta_{gL}$ , i.e., [123]

$$\zeta_g = \zeta_{gS} + \zeta_{gL} . \quad (2.9)$$

As demonstrated in Refs. [25, 78, 106], the short-wavelength modes induce a GWB, contributing to the homogeneous and isotropic energy density. On the other hand, the long-wavelength modes redistribute the energy density spatially, resulting in inhomogeneities and anisotropies within this GWB. In this section, we will focus on studying the former, while the latter will be examined in the subsequent section.

Since  $\zeta_{gS}$  (as well as  $\zeta_{gL}$ ) is Gaussian, it is sufficient to determine its power spectrum, defined as

$$\langle \zeta_{gS}(\mathbf{q})\zeta_{gS}(\mathbf{q}') \rangle = \delta^{(3)}(\mathbf{q} + \mathbf{q}')P_{gS}(q) , \quad (2.10)$$

where the dimensionless power spectrum is defined as

$$\Delta_S^2(q) = \frac{q^3}{2\pi^2}P_{gS}(q) . \quad (2.11)$$

Similarly, we define  $\Delta_L^2(q)$  as the power spectrum of  $\zeta_{gL}$ . In this study, we assume  $\Delta_S^2$  to follow a normal distribution with respect to  $\ln q$ , given by

$$\Delta_S^2(q) = \frac{A_S}{\sqrt{2\pi}\sigma^2} \exp \left[ -\frac{\ln^2(q/q_*)}{2\sigma^2} \right] , \quad (2.12)$$

where  $\sigma$  represents the spectral width, and  $A_S$  is the spectral amplitude at the peak wavenumber  $q_*$ . The wavenumber  $q$  can be directly converted into the frequency  $\nu$ , i.e.,  $q = 2\pi\nu$ . In this study, we consider a range of spectral amplitudes  $A_S$  on the order of  $10^{-4}$  to  $10^{-1}$ , which is particularly relevant in the context of PBH formation scenarios (see reviews in Refs. [59–61, 124] and references therein). For simplicity, we set  $\sigma$  to unity, but it can be easily generalized to other values. It is important to note that perturbativity imposes the conditions  $1 > 3|f_{\text{NL}}|\sqrt{A_S}/5 + 9|g_{\text{NL}}|A_S/25$  and  $3|f_{\text{NL}}|\sqrt{A_S}/5 > 9|g_{\text{NL}}|A_S/25$ . One should note that some of the most extreme value, such as  $(3|f_{\text{NL}}|\sqrt{A_S}/5 + 9|g_{\text{NL}}|A_S/25) \rightarrow 1$ , may already exceed the reliable range of perturbativity. In the next section, we will also consider  $\Delta_L^2 \simeq 2.1 \times 10^{-9}$  on the largest observable scales [125].

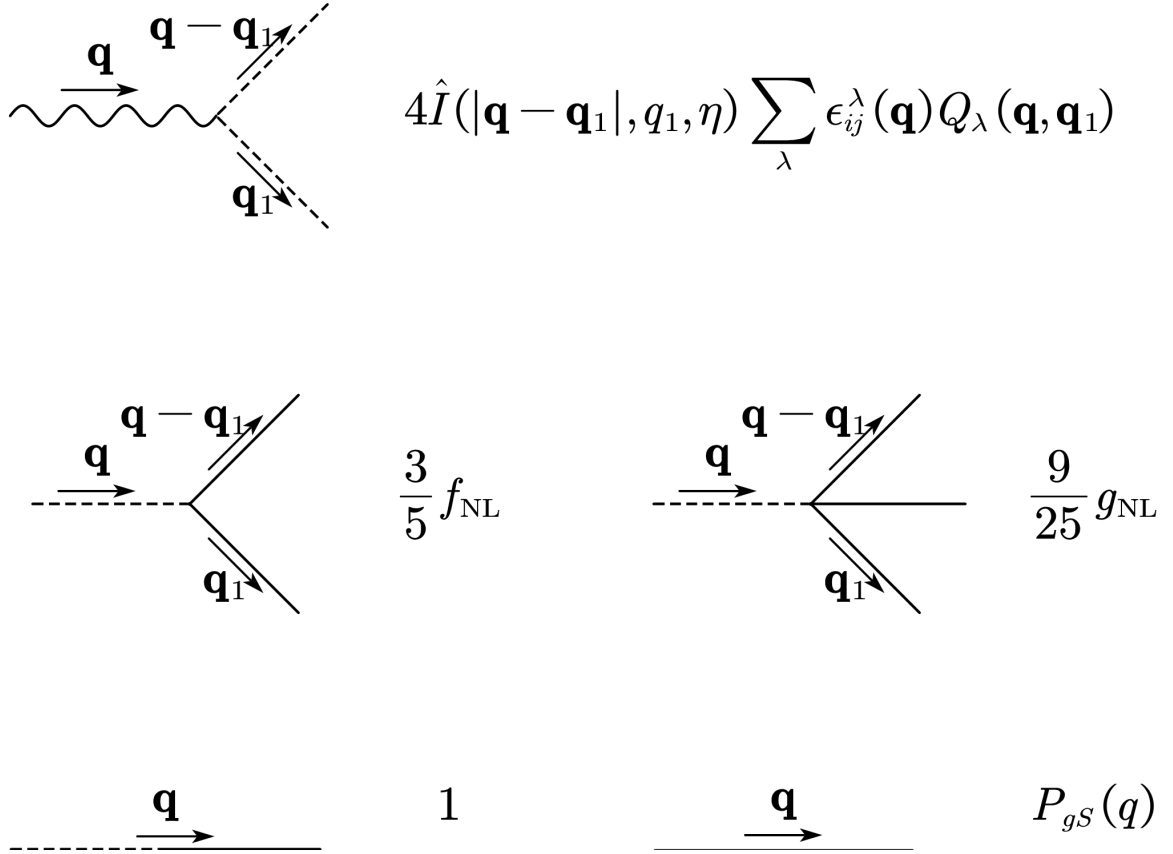


**Figure 1:** The Feynman-like rules for evaluation of Eq. (2.7) by incorporating Eq. (2.8). Wavy lines represent GWs, dashed lines denote the transfer functions, and solid lines stand for the primordial curvature power spectra. Arrows indicate the flow of comoving 3-momenta, which are conserved at each vertex. The total 3-momentum vanishes for each individual diagram, and all the loop 3-momenta should be integrated over.

## 2.1 Feynman-like Rules and Diagrams

By substituting Eq. (2.8) into the four-point correlator  $\langle \zeta^4 \rangle$  in Eq. (2.7), we can expand this correlator as a series of two-point correlators involving  $\zeta_{gS}$ . When studying Gaussian curvature perturbations, Wick's theorem is a valuable tool for such expansions [14–17]. However, when considering non-Gaussianity, we encounter challenges in conducting such expansions due to the involvement of a large number of two-point correlators. This difficulty is particularly pronounced when studying the angular power spectrum, as it requires consideration of multi-point correlators.

In this work, we employ the Feynman-like diagrammatic technique to efficiently and accurately evaluate the multi-point correlators. The diagrammatic technique has been widely used in quantum field theory and cosmology. Recently, it has been applied to calculate the energy-density fraction spectrum of SIGWs [23, 24, 26], as well as the angular power spectrum [25, 106]. This technique has the potential to overcome the challenges encountered when expanding multi-point correlators using Wick's theorem. By utilizing this method, we can more easily evaluate the energy-density fraction spectrum and, in particular, the angular





**Figure 2:** The Feynman-like diagrams for evaluating Eq. (2.7) by incorporating Eq. (2.8). The shadow square should be replaced with the panels of Figure 3.

power spectrum.

To evaluate Eq. (2.7) by incorporating Eq. (2.8), we establish a set of Feynman-like rules, which are summarized in Figure 1. The vertices in Figure 1 are labeled as the  $h$ -vertex<sup>1</sup> (upper panel),  $f_{\text{NL}}$ -vertex (middle left panel),  $g_{\text{NL}}$ -vertex (middle right panel), and Gaussian-vertex (bottom left panel), respectively. The propagator is shown in the bottom right panel.

By incorporating the primordial non-Gaussianity defined in Eq. (2.8), we can express the power spectrum of Eq. (2.7) as a series of Feynman-like diagrams, once the Feynman-like rules are known. These diagrams are thoroughly displayed in Figure 2 and Figure 3. To obtain an individual diagram, we replace the shaded square in Figure 2 with a panel from Figure 3. For the sake of brevity, we have omitted the momenta flows in each panel of Figure 3, as they can be straightforwardly deduced from momentum conservation at each vertex. In total, there are 49 Feynman-like diagrams that need to be considered in this work.

For a given Feynman-like diagram, we can immediately determine its contribution to the power spectrum in Eq. (2.7) using the Feynman-like rules. Let's consider a diagram labeled with  $X$  ( $X \in G, Gl, \dots, PN$ ), denoted as Diagram- $X$ . Its contribution can be formally expressed as

$$P_h^X = \text{Integral} \times \text{Vertices} \times \text{S.F.} , \quad (2.13)$$

where we provide the details of the “Integral”, “Vertices”, and “S.F.” in Table 1. The “Integral” represents the integrals involving the propagators and  $h$ -vertices. We have classified these integrals into 9 families, which will be explained in Subsection 2.3 along with the introduction of  $\mathcal{P}_X^{[\dots]}$ . The “Vertices” term involves the powers of  $f_{\text{NL}}$  and  $g_{\text{NL}}$  associated with the Gaussian-vertex,  $f_{\text{NL}}$ -vertex, and  $g_{\text{NL}}$ -vertex. Finally, the “S.F.” stands for the symmetric factor.

<sup>1</sup>Notably, we have included the sum of polarization modes in the  $h$ -vertex in this study. This convention differs slightly from that in our existing paper [25]. Nevertheless, this difference would not affect our results, but would simplify subsequent calculations, since the power spectra of the two polarization modes are the same, i.e.,  $P_{h+}(\eta, q) = P_{h\times}(\eta, q)$ , in this work.



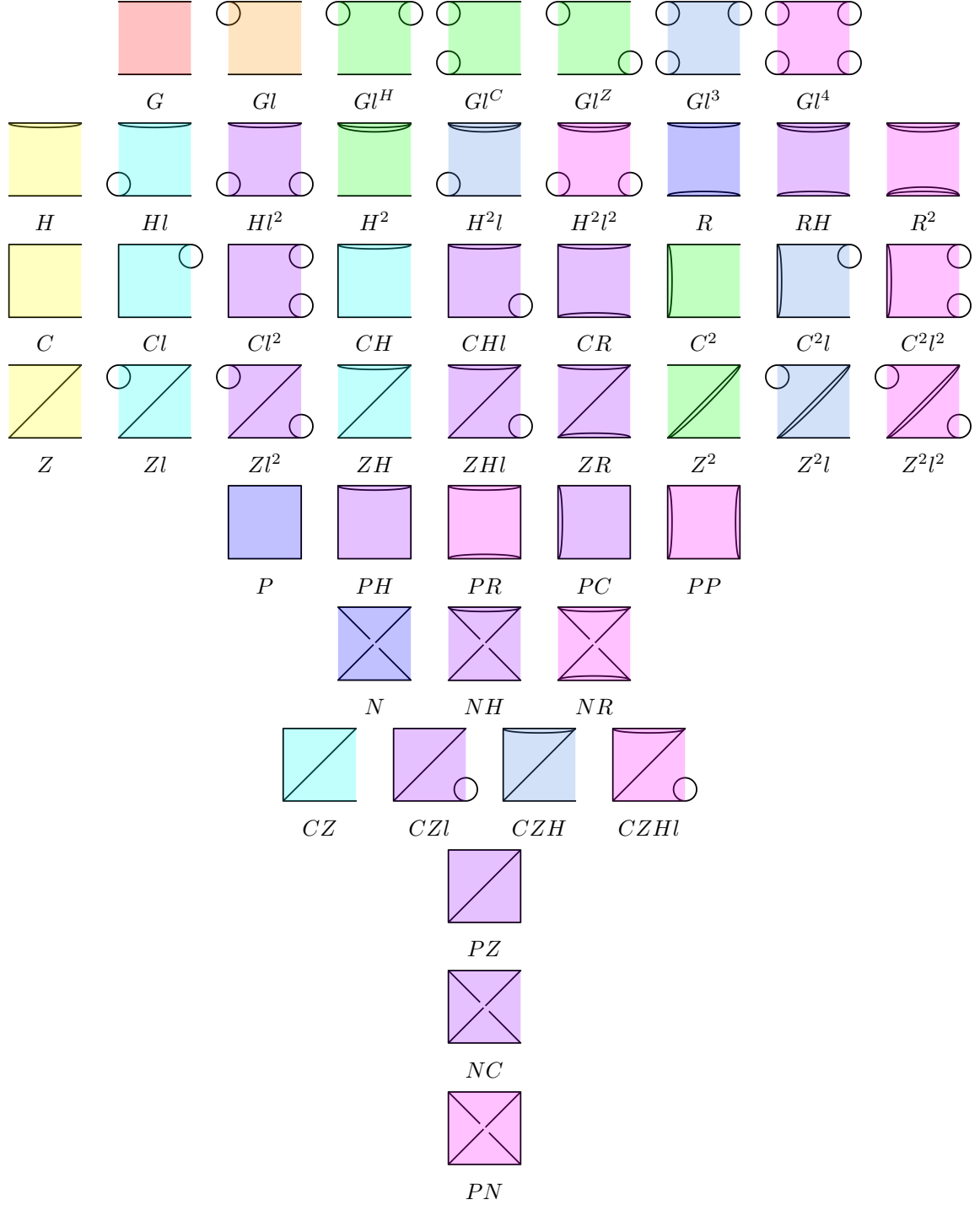


**Figure 3:** Diagrams to replace the shaded square(s) in Figure 2 (10). Panels labeled with the same color are classified into the same category (see Table 2 for the category classification). Panels in the same row are classified into the same family (see Table 3 for the family classification). Here, momenta flows along propagators are omitted for the sake of brevity.

$P_h^X$	Integral	Vertices	S.F.	continued			
$P_h^G$	$\mathcal{P}_G^{[1,1]}$	1	2	$P_h^X$	Integral	Vertices	S.F.
$P_h^{Gl}$	$A_S \mathcal{P}_G^{[1,1]}$	$\left(\frac{3}{5}\right)^2 g_{\text{NL}}$	24	$P_h^Z$	$\mathcal{P}_Z^{[1,1;1]}$	$\left(\frac{3}{5}\right)^2 f_{\text{NL}}^2$	16
$P_h^{Gl^H}$	$A_S^2 \mathcal{P}_G^{[1,1]}$	$\left(\frac{3}{5}\right)^4 g_{\text{NL}}^2$	36	$P_h^{Zl}$	$A_S \mathcal{P}_Z^{[1,1;1]}$	$\left(\frac{3}{5}\right)^4 f_{\text{NL}}^2 g_{\text{NL}}$	96
$P_h^{Gl^C}$	$A_S^2 \mathcal{P}_G^{[1,1]}$	$\left(\frac{3}{5}\right)^4 g_{\text{NL}}^2$	36	$P_h^{Zl^2}$	$A_S^2 \mathcal{P}_Z^{[1,1;1]}$	$\left(\frac{3}{5}\right)^6 f_{\text{NL}}^2 g_{\text{NL}}^2$	144
$P_h^{Gl^Z}$	$A_S^2 \mathcal{P}_G^{[1,1]}$	$\left(\frac{3}{5}\right)^4 g_{\text{NL}}^2$	36	$P_h^{Z^H}$	$\mathcal{P}_Z^{[1,2;1]}$	$\left(\frac{3}{5}\right)^4 f_{\text{NL}}^2 g_{\text{NL}}$	96
$P_h^{Gl^3}$	$A_S^3 \mathcal{P}_G^{[1,1]}$	$\left(\frac{3}{5}\right)^6 g_{\text{NL}}^3$	216	$P_h^{Z^Hl}$	$A_S \mathcal{P}_Z^{[1,2;1]}$	$\left(\frac{3}{5}\right)^6 f_{\text{NL}}^2 g_{\text{NL}}^2$	288
$P_h^{Gl^4}$	$A_S^4 \mathcal{P}_G^{[1,1]}$	$\left(\frac{3}{5}\right)^8 g_{\text{NL}}^4$	162	$P_h^{Z^R}$	$\mathcal{P}_Z^{[2,2;1]}$	$\left(\frac{3}{5}\right)^6 f_{\text{NL}}^2 g_{\text{NL}}^2$	144
$P_h^H$	$\mathcal{P}_G^{[1,2]}$	$\left(\frac{3}{5}\right)^2 f_{\text{NL}}^2$	8	$P_h^{Z^2}$	$\mathcal{P}_Z^{[1,1;2]}$	$\left(\frac{3}{5}\right)^4 g_{\text{NL}}^2$	72
$P_h^{Hl}$	$A_S \mathcal{P}_G^{[1,2]}$	$\left(\frac{3}{5}\right)^4 f_{\text{NL}}^2 g_{\text{NL}}$	48	$P_h^{Z^2l}$	$A_S \mathcal{P}_Z^{[1,1;2]}$	$\left(\frac{3}{5}\right)^6 g_{\text{NL}}^3$	432
$P_h^{Hl^2}$	$A_S^2 \mathcal{P}_G^{[1,2]}$	$\left(\frac{3}{5}\right)^6 f_{\text{NL}}^2 g_{\text{NL}}^2$	72	$P_h^{Z^2l^2}$	$A_S^2 \mathcal{P}_Z^{[1,1;2]}$	$\left(\frac{3}{5}\right)^8 g_{\text{NL}}^4$	648
$P_h^{H^2}$	$\mathcal{P}_G^{[1,3]}$	$\left(\frac{3}{5}\right)^4 g_{\text{NL}}^2$	24	$P_h^P$	$\mathcal{P}_P^{[1,1;1,1]}$	$\left(\frac{3}{5}\right)^4 f_{\text{NL}}^4$	32
$P_h^{H^2l}$	$A_S \mathcal{P}_G^{[1,3]}$	$\left(\frac{3}{5}\right)^6 g_{\text{NL}}^3$	144	$P_h^{PH}$	$\mathcal{P}_P^{[1,2;1,1]}$	$\left(\frac{3}{5}\right)^6 f_{\text{NL}}^2 g_{\text{NL}}^2$	288
$P_h^{H^2l^2}$	$A_S^2 \mathcal{P}_G^{[1,3]}$	$\left(\frac{3}{5}\right)^8 g_{\text{NL}}^4$	216	$P_h^{PR}$	$\mathcal{P}_P^{[2,2;1,1]}$	$\left(\frac{3}{5}\right)^8 g_{\text{NL}}^4$	648
$P_h^R$	$\mathcal{P}_G^{[2,2]}$	$\left(\frac{3}{5}\right)^4 f_{\text{NL}}^4$	8	$P_h^{PC}$	$\mathcal{P}_P^{[1,1;2,1]}$	$\left(\frac{3}{5}\right)^6 f_{\text{NL}}^2 g_{\text{NL}}^2$	288
$P_h^{RH}$	$\mathcal{P}_G^{[2,3]}$	$\left(\frac{3}{5}\right)^6 f_{\text{NL}}^2 g_{\text{NL}}^2$	48	$P_h^{PP}$	$\mathcal{P}_P^{[1,1;2,2]}$	$\left(\frac{3}{5}\right)^8 g_{\text{NL}}^4$	648
$P_h^{R^2}$	$\mathcal{P}_G^{[3,3]}$	$\left(\frac{3}{5}\right)^8 g_{\text{NL}}^4$	72	$P_h^N$	$\mathcal{P}_N^{[1,1,1,1]}$	$\left(\frac{3}{5}\right)^4 f_{\text{NL}}^4$	16
$P_h^C$	$\mathcal{P}_C^{[1,1;1]}$	$\left(\frac{3}{5}\right)^2 f_{\text{NL}}^2$	16	$P_h^{NH}$	$\mathcal{P}_N^{[2,1,1,1]}$	$\left(\frac{3}{5}\right)^6 f_{\text{NL}}^2 g_{\text{NL}}^2$	288
$P_h^{Cl}$	$A_S \mathcal{P}_C^{[1,1;1]}$	$\left(\frac{3}{5}\right)^4 f_{\text{NL}}^2 g_{\text{NL}}$	96	$P_h^{NR}$	$\mathcal{P}_N^{[2,2,1,1]}$	$\left(\frac{3}{5}\right)^8 g_{\text{NL}}^4$	648
$P_h^{Cl^2}$	$A_S^2 \mathcal{P}_C^{[1,1;1]}$	$\left(\frac{3}{5}\right)^6 f_{\text{NL}}^2 g_{\text{NL}}^2$	144	$P_h^{CZ}$	$\mathcal{P}_{CZ}^{[1]}$	$\left(\frac{3}{5}\right)^4 f_{\text{NL}}^2 g_{\text{NL}}$	192
$P_h^{CH}$	$\mathcal{P}_C^{[1,2;1]}$	$\left(\frac{3}{5}\right)^4 f_{\text{NL}}^2 g_{\text{NL}}$	96	$P_h^{CZl}$	$A_S \mathcal{P}_{CZ}^{[1]}$	$\left(\frac{3}{5}\right)^6 f_{\text{NL}}^2 g_{\text{NL}}^2$	576
$P_h^{CHl}$	$A_S \mathcal{P}_C^{[1,2;1]}$	$\left(\frac{3}{5}\right)^6 f_{\text{NL}}^2 g_{\text{NL}}^2$	288	$P_h^{CZH}$	$\mathcal{P}_{CZ}^{[2]}$	$\left(\frac{3}{5}\right)^6 g_{\text{NL}}^3$	864
$P_h^{C^R}$	$\mathcal{P}_C^{[2,2;1]}$	$\left(\frac{3}{5}\right)^6 f_{\text{NL}}^2 g_{\text{NL}}^2$	144	$P_h^{CZHl}$	$A_S \mathcal{P}_{CZ}^{[2]}$	$\left(\frac{3}{5}\right)^8 g_{\text{NL}}^4$	2592
$P_h^{C^2}$	$\mathcal{P}_C^{[1,1;2]}$	$\left(\frac{3}{5}\right)^4 g_{\text{NL}}^2$	72	$P_h^{PZ}$	$\mathcal{P}_{PZ}$	$\left(\frac{3}{5}\right)^6 f_{\text{NL}}^2 g_{\text{NL}}^2$	576
$P_h^{C^2l}$	$A_S \mathcal{P}_C^{[1,1;2]}$	$\left(\frac{3}{5}\right)^6 g_{\text{NL}}^3$	432	$P_h^{NC}$	$\mathcal{P}_{NC}$	$\left(\frac{3}{5}\right)^6 f_{\text{NL}}^2 g_{\text{NL}}^2$	288
$P_h^{C^2l^2}$	$A_S^2 \mathcal{P}_C^{[1,1;2]}$	$\left(\frac{3}{5}\right)^8 g_{\text{NL}}^4$	648	$P_h^{PN}$	$\mathcal{P}_{PN}$	$\left(\frac{3}{5}\right)^8 g_{\text{NL}}^4$	1296

**Table 1:** Table for illustration of the contribution from Diagram- $X$ , as shown in Fig. 3, to the power spectrum in Eq. (2.7).

$\bar{\Omega}_{\text{gw}}^{(a,b)}$	$\left(\frac{3}{5}\right)^{2(a+b)} f_{\text{NL}}^{2a} g_{\text{NL}}^b A_S^{a+b+2}$	Diagram-X
(0,0)	$A_S^2$	$G$
(0,1)	$\left(\frac{3}{5}\right)^2 g_{\text{NL}} A_S^3$	$Gl$
(1,0)	$\left(\frac{3}{5}\right)^2 f_{\text{NL}}^2 A_S^3$	$H, C, Z$
(0,2)	$\left(\frac{3}{5}\right)^4 g_{\text{NL}}^2 A_S^4$	$Gl^H, Gl^C, Gl^Z, H^2, C^2, Z^2$
(1,1)	$\left(\frac{3}{5}\right)^4 f_{\text{NL}}^2 g_{\text{NL}} A_S^4$	$Hl, Cl, Zl, CH, ZH, CZ$
(2,0)	$\left(\frac{3}{5}\right)^4 f_{\text{NL}}^4 A_S^4$	$R, P, N$
(0,3)	$\left(\frac{3}{5}\right)^6 g_{\text{NL}}^3 A_S^5$	$Gl^3, H^2l, C^2l, Z^2l, CZH$
(1,2)	$\left(\frac{3}{5}\right)^6 f_{\text{NL}}^2 g_{\text{NL}}^2 A_S^5$	$Hl^2, Cl^2, Zl^2, CHl, ZHl, CZl, RH,$ $CR, ZR, PH, PC, PZ, NH, NC$
(0,4)	$\left(\frac{3}{5}\right)^8 g_{\text{NL}}^4 A_S^6$	$Gl^4, H^2l^2, R^2, C^2l^2, Z^2l^2, PR, PP, NR, CZHl, PN$

**Table 2:** Table for illustration of the category classification. The Feynman-like diagrams of each category have the same powers in  $f_{\text{NL}}$  and  $g_{\text{NL}}$ .

## 2.2 Formulae for Energy-Density Fraction Spectrum

By following Eq. (2.5), we can determine the contribution from the Feynman-like diagram labeled with  $X$  to the energy-density fraction spectrum as

$$\bar{\Omega}_{\text{gw}}^X = \frac{q^5}{96\pi^2 \mathcal{H}^2} \bar{P}_h^X. \quad (2.14)$$

After performing the oscillation average, we can rewrite it as a series of numerically favorable integrals, as shown in Appendix B. These integrals can be computed numerically using the publicly available **vegas** package [126].

Based on the information provided in the “Vertices” column of Table 1, we classify the total of 49 Feynman-like diagrams into 9 categories, as shown in Table 2. The diagrams within each category have the same powers in  $f_{\text{NL}}$  and  $g_{\text{NL}}$ , as well as the same powers in  $A_S$ . Consequently, we divide the energy-density fraction spectrum into 9 components, denoted as  $\bar{\Omega}_{\text{gw}}^{(a,b)}$  with powers given by  $(3/5)^{2(a+b)} f_{\text{NL}}^{2a} g_{\text{NL}}^b A_S^{a+b}$ . To be more specific, these components

can be expressed as follows

$$\bar{\Omega}_{\text{gw}}^{(0,0)} = \bar{\Omega}_{\text{gw}}^G, \quad (2.15a)$$

$$\bar{\Omega}_{\text{gw}}^{(0,1)} = \bar{\Omega}_{\text{gw}}^{Gl}, \quad (2.15b)$$

$$\bar{\Omega}_{\text{gw}}^{(1,0)} = \bar{\Omega}_{\text{gw}}^H + \bar{\Omega}_{\text{gw}}^C + \bar{\Omega}_{\text{gw}}^Z, \quad (2.15c)$$

$$\bar{\Omega}_{\text{gw}}^{(0,2)} = \bar{\Omega}_{\text{gw}}^{Gl^H} + \bar{\Omega}_{\text{gw}}^{Gl^C} + \bar{\Omega}_{\text{gw}}^{Gl^Z} + \bar{\Omega}_{\text{gw}}^{H^2} + \bar{\Omega}_{\text{gw}}^{C^2} + \bar{\Omega}_{\text{gw}}^{Z^2}, \quad (2.15d)$$

$$\bar{\Omega}_{\text{gw}}^{(1,1)} = \bar{\Omega}_{\text{gw}}^{Hl} + \bar{\Omega}_{\text{gw}}^{Cl} + \bar{\Omega}_{\text{gw}}^{Zl} + \bar{\Omega}_{\text{gw}}^{CH} + \bar{\Omega}_{\text{gw}}^{ZH} + \bar{\Omega}_{\text{gw}}^{CZ}, \quad (2.15e)$$

$$\bar{\Omega}_{\text{gw}}^{(2,0)} = \bar{\Omega}_{\text{gw}}^R + \bar{\Omega}_{\text{gw}}^P + \bar{\Omega}_{\text{gw}}^N, \quad (2.15f)$$

$$\bar{\Omega}_{\text{gw}}^{(0,3)} = \bar{\Omega}_{\text{gw}}^{Gl^3} + \bar{\Omega}_{\text{gw}}^{H^2l} + \bar{\Omega}_{\text{gw}}^{C^2l} + \bar{\Omega}_{\text{gw}}^{Z^2l} + \bar{\Omega}_{\text{gw}}^{CZH}, \quad (2.15g)$$

$$\begin{aligned} \bar{\Omega}_{\text{gw}}^{(1,2)} = & \bar{\Omega}_{\text{gw}}^{Hl^2} + \bar{\Omega}_{\text{gw}}^{Cl^2} + \bar{\Omega}_{\text{gw}}^{Zl^2} + \bar{\Omega}_{\text{gw}}^{CHl} + \bar{\Omega}_{\text{gw}}^{Zhl} + \bar{\Omega}_{\text{gw}}^{CZl} + \bar{\Omega}_{\text{gw}}^{RH} + \bar{\Omega}_{\text{gw}}^{CR} + \bar{\Omega}_{\text{gw}}^{ZR} \\ & + \bar{\Omega}_{\text{gw}}^{PH} + \bar{\Omega}_{\text{gw}}^{PC} + \bar{\Omega}_{\text{gw}}^{PZ} + \bar{\Omega}_{\text{gw}}^{NH} + \bar{\Omega}_{\text{gw}}^{NC}, \end{aligned} \quad (2.15h)$$

$$\begin{aligned} \bar{\Omega}_{\text{gw}}^{(0,4)} = & \bar{\Omega}_{\text{gw}}^{Gl^4} + \bar{\Omega}_{\text{gw}}^{H^2l^2} + \bar{\Omega}_{\text{gw}}^{R^2} + \bar{\Omega}_{\text{gw}}^{C^2l^2} + \bar{\Omega}_{\text{gw}}^{Z^2l^2} + \bar{\Omega}_{\text{gw}}^{PR} + \bar{\Omega}_{\text{gw}}^{PP} \\ & + \bar{\Omega}_{\text{gw}}^{NR} + \bar{\Omega}_{\text{gw}}^{CZHl} + \bar{\Omega}_{\text{gw}}^{PN}. \end{aligned} \quad (2.15i)$$

As a result, the total energy-density spectrum can be expressed as the sum of  $\bar{\Omega}_{\text{gw}}^{(a,b)}$ , i.e.,

$$\bar{\Omega}_{\text{gw}} = \bar{\Omega}_{\text{gw}}^{(0,0)} + \bar{\Omega}_{\text{gw}}^{(0,1)} + \bar{\Omega}_{\text{gw}}^{(1,0)} + \bar{\Omega}_{\text{gw}}^{(0,2)} + \bar{\Omega}_{\text{gw}}^{(1,1)} + \bar{\Omega}_{\text{gw}}^{(2,0)} + \bar{\Omega}_{\text{gw}}^{(0,3)} + \bar{\Omega}_{\text{gw}}^{(1,2)} + \bar{\Omega}_{\text{gw}}^{(0,4)}. \quad (2.16)$$

In particular, it should be noted that  $\bar{\Omega}_{\text{gw}}^{(0,0)}$  represents the energy-density fraction spectrum of SIGWs under the assumption of Gaussianity, as demonstrated by the semi-analytic calculation in Refs. [16, 17]. There are a lot of works considering the local-type primordial non-Gaussianities. Specifically, Ref. [27, 35, 38] focused on the  $f_{\text{NL}}$  contributions denoted as  $G$ ,  $H$ , and  $R$ . Ref. [30] conducted a similar analysis, considering a specific model and scale-dependent non-Gaussianity. Ref. [28] expanded the analysis to include other  $f_{\text{NL}}$  contributions, except for the one labeled as  $Z$ , which was first considered in Ref. [29]. However, confusion arose between the contributions labeled as “walnut” in Ref. [28] and Ref. [29], respectively, due to an incomplete definition of Feynman-like rules. Specifically, the contribution referred to as “walnut” in Ref. [28] corresponds to  $C$ , while in Ref. [29], it corresponds to  $Z$ . The complete analysis, including the formulation of Feynman-like rules and diagrams, was originally provided by Ref. [23] and reexamined in Refs. [24, 25]. Furthermore, Refs. [31, 38] evaluated contributions from the non-Gaussianity of the  $g_{\text{NL}}$  order to the energy-density fraction spectrum of SIGWs, via focusing on terms belonging to the  $G$ -like contributions. In a recent work (arXiv:2308.07155v1), the analysis was extended to include more diagrams. Our current study goes further by considering two additional diagrams, specifically referred to as  $CZH$  and  $CZHl$ . In Ref. [26], the Feynman-like diagrammatic technique was employed to investigate the contributions arising from series-expandable non-Gaussianity, via calculating the energy-density fraction spectrum up to  $\mathcal{O}(A_S^4)$  order.

### 2.3 Nine Families of Integrals

In Table 1 of Subsection 2.1, we mentioned that the classification of integrals into 9 families facilitates subsequent calculations. In this subsection, we will provide a comprehensive explanation of the criteria used for this classification and introduce  $\mathcal{P}_X^{[\dots]}$ . Quick readers can skip this subsection for now and return to it later if they need more details.

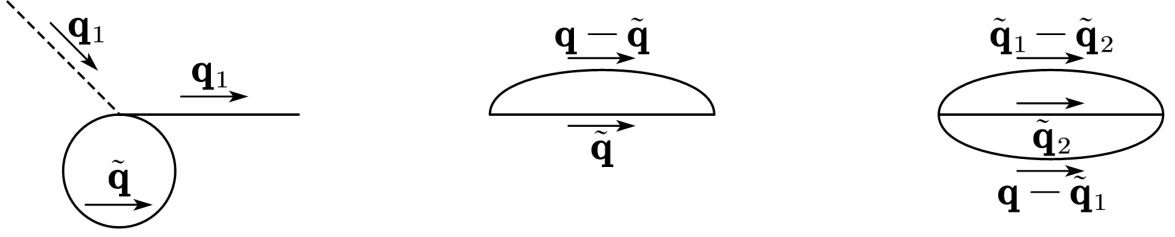


**Figure 4:** Loop integrals precomputed in advance.

Let's begin by clarifying two conventions that will simplify our subsequent calculations. The first convention pertains to the loop integral associated with an individual  $g_{\text{NL}}$ -vertex, as depicted in the left panel of Figure 4. The contribution to  $\bar{\Omega}_{\text{gw}}$  from this loop integral is solely determined by  $g_{\text{NL}}$  and  $A_S$ , specifically,

$$3 \times \frac{9}{25} g_{\text{NL}} \int \frac{d^3 \tilde{\mathbf{q}}}{(2\pi)^3} P^{[1]}(\tilde{q}) = 3 \times \left(\frac{3}{5}\right)^2 g_{\text{NL}} A_S , \quad (2.17)$$

In this expression, the number 3 represents the symmetric factor,  $(3/5)^2 g_{\text{NL}}$  arises from the  $g_{\text{NL}}$ -vertex, and  $A_S$  is associated with the loop integral. The second convention concerns the multi-propagators between two different vertices, as depicted in the middle and right panels of Figure 4. By performing the integration over loop momenta in advance, we can reduce the dimensions of the multi-variate integration. For convenience, we introduce quantities of the form

$$P^{[1]}(q) = P_{gS}(q) , \quad (2.18a)$$

$$P^{[2]}(q) = \int \frac{d^3 \tilde{\mathbf{q}}}{(2\pi)^3} P^{[1]}(\tilde{q}) P^{[1]}(|\mathbf{q} - \tilde{\mathbf{q}}|) , \quad (2.18b)$$

$$P^{[3]}(q) = \int \frac{d^3 \tilde{\mathbf{q}}}{(2\pi)^3} P^{[2]}(\tilde{q}) P^{[1]}(|\mathbf{q} - \tilde{\mathbf{q}}|) . \quad (2.18c)$$

By clarifying the aforementioned two conventions, we can immediately determine the integrals modulo these two types of loop integrals. Based on this, we classify them into a total of 9 families, namely “ $G$ -like”, “ $C$ -like”, “ $Z$ -like”, “ $P$ -like”, “ $N$ -like”, “ $CZ$ -like”, “ $PZ$ -like”, “ $NC$ -like” and “ $PN$ -like” families. The panels in the first two rows of Figure 3 belong to the “ $G$ -like” family, while the panels in each subsequent row belong to the same family. To be more specific, we summarize these families in Table 3. One advantage of our classification is that the integrals associated with the same family share the same form, except for their subscripts [...], as demonstrated below.

The integrals belonging to the “ $G$ -like” family can be expressed explicitly as follows

$$\mathcal{P}_G^{[\alpha, \beta]}(\eta, q) = 2^4 \int \frac{d^3 \mathbf{q}_1}{(2\pi)^3} P^{[\alpha]}(q_1) P^{[\beta]}(|\mathbf{q} - \mathbf{q}_1|) \sum_{\lambda=+, \times} Q_\lambda^2(\mathbf{q}, \mathbf{q}_1) \hat{I}^2(|\mathbf{q} - \mathbf{q}_1|, q_1, \eta) \quad (2.19)$$

where we take  $\alpha$  and  $\beta$  to be values from 1 to 3, with  $\alpha$  less than or equal to  $\beta$ . The integrals associated with the “ $C$ -like” family can be expressed as follows

$$\begin{aligned} \mathcal{P}_C^{[\alpha, \beta; \gamma]}(\eta, q) &= 2^4 \int \frac{d^3 \mathbf{q}_1}{(2\pi)^3} \frac{d^3 \mathbf{q}_2}{(2\pi)^3} P^{[\alpha]}(q_2) P^{[\beta]}(|\mathbf{q} - \mathbf{q}_2|) P^{[\gamma]}(|\mathbf{q}_1 - \mathbf{q}_2|) \\ &\times \sum_{\lambda=+, \times} Q_\lambda(\mathbf{q}, \mathbf{q}_1) \hat{I}(|\mathbf{q} - \mathbf{q}_1|, q_1, \eta) Q_\lambda(\mathbf{q}, \mathbf{q}_2) \hat{I}(|\mathbf{q} - \mathbf{q}_2|, q_2, \eta) , \end{aligned} \quad (2.20)$$

Family	Diagram-X
<i>G</i> -like	$G, Gl, Gl^H, Gl^C, Gl^Z, Gl^3, Gl^4,$ $H, Hl, Hl^2, H^2, H^2l, H^2l^2, R, RH, R^2$
<i>C</i> -like	$C, Cl, Cl^2, CH, CHl, CR, C^2, C^2l, C^2l^2$
<i>Z</i> -like	$Z, Zl, Zl^2, ZH, ZHl, ZR, Z^2, Z^2l, Z^2l^2$
<i>P</i> -like	$P, PH, PR, PC, PP$
<i>N</i> -like	$N, NH, NR$
<i>CZ</i> -like	$CZ, CZl, CZH, CZHl$
<i>PZ</i> -like	$PZ$
<i>NC</i> -like	$NC$
<i>PN</i> -like	$PN$

**Table 3:** Table for illustration of the family classification. The integrals associated with the Feynman-like diagrams of each family share the same form.

where we take  $\alpha, \beta$ , and  $\gamma$  to be values from 1 to 2, with  $\alpha$  less than or equal to  $\beta$ . However,  $\beta$  and  $\gamma$  cannot both be equal to 2 simultaneously. The integrals associated with the “*Z*-like” family can be expressed as follows

$$\begin{aligned} \mathcal{P}_Z^{[\alpha, \beta; \gamma]}(\eta, q) = & 2^4 \int \frac{d^3 \mathbf{q}_1}{(2\pi)^3} \frac{d^3 \mathbf{q}_2}{(2\pi)^3} P^{[\alpha]}(q_2) P^{[\beta]}(|\mathbf{q} - \mathbf{q}_1|) P^{[\gamma]}(|\mathbf{q}_1 - \mathbf{q}_2|) \\ & \times \sum_{\lambda=+, \times} Q_\lambda(\mathbf{q}, \mathbf{q}_1) \hat{I}(|\mathbf{q} - \mathbf{q}_1|, q_1, \eta) Q_\lambda(\mathbf{q}, \mathbf{q}_2) \hat{I}(|\mathbf{q} - \mathbf{q}_2|, q_2, \eta) , \end{aligned} \quad (2.21)$$

where we consider  $\alpha, \beta$ , and  $\gamma$  as values from 1 to 2, with  $\alpha$  less than or equal to  $\beta$ . However, it is not possible for both  $\beta$  and  $\gamma$  to be equal to 2 at the same time. The integrals associated with the “*P*-like” family can be expressed as follows

$$\begin{aligned} \mathcal{P}_P^{[\alpha, \beta; \gamma, \delta]}(\eta, q) = & 2^4 \int \frac{d^3 \mathbf{q}_1}{(2\pi)^3} \frac{d^3 \mathbf{q}_2}{(2\pi)^3} \frac{d^3 \mathbf{q}_3}{(2\pi)^3} P^{[\alpha]}(q_3) P^{[\beta]}(|\mathbf{q} - \mathbf{q}_3|) P^{[\gamma]}(|\mathbf{q}_1 - \mathbf{q}_3|) \\ & \times P^{[\delta]}(|\mathbf{q}_2 - \mathbf{q}_3|) \\ & \times \sum_{\lambda=+, \times} Q_\lambda(\mathbf{q}, \mathbf{q}_1) \hat{I}(|\mathbf{q} - \mathbf{q}_1|, q_1, \eta) Q_\lambda(\mathbf{q}, \mathbf{q}_2) \hat{I}(|\mathbf{q} - \mathbf{q}_2|, q_2, \eta) , \end{aligned} \quad (2.22)$$

where we consider  $\alpha, \beta, \gamma$ , and  $\delta$  as values from 1 to 2, with  $\alpha$  less than or equal to  $\beta$ , and  $\gamma$  greater than or equal to  $\delta$ . However, it is not possible for both  $\beta$  and  $\gamma$  to be equal to 2 at

the same time. The integrals associated with the “ $N$ -like” family can be expressed as follows

$$\begin{aligned} \mathcal{P}_N^{[\alpha, \beta; 1, 1]}(\eta, q) = & 2^4 \int \frac{d^3 \mathbf{q}_1}{(2\pi)^3} \frac{d^3 \mathbf{q}_2}{(2\pi)^3} \frac{d^3 \mathbf{q}_3}{(2\pi)^3} P^{[\alpha]}(|\mathbf{q} - \mathbf{q}_3|) P^{[\beta]}(|\mathbf{q}_1 + \mathbf{q}_2 - \mathbf{q}_3|) \\ & \times P^{[1]}(|\mathbf{q}_1 - \mathbf{q}_3|) P^{[1]}(|\mathbf{q}_2 - \mathbf{q}_3|) \\ & \times \sum_{\lambda=+, \times} Q_\lambda(\mathbf{q}, \mathbf{q}_1) \hat{I}(|\mathbf{q} - \mathbf{q}_1|, q_1, \eta) Q_\lambda(\mathbf{q}, \mathbf{q}_2) \hat{I}(|\mathbf{q} - \mathbf{q}_2|, q_2, \eta) , \end{aligned} \quad (2.23)$$

where we consider  $\alpha$  and  $\beta$  as values from 1 to 2, with  $\alpha$  greater than or equal to  $\beta$ . The integrals associated with the “ $CZ$ -like” family can be expressed as follows

$$\begin{aligned} \mathcal{P}_{CZ}^{[\alpha]}(\eta, q) = & 2^4 \int \frac{d^3 \mathbf{q}_1}{(2\pi)^3} \frac{d^3 \mathbf{q}_2}{(2\pi)^3} \frac{d^3 \mathbf{q}_3}{(2\pi)^3} P^{[1]}(q_2) P^{[\alpha]}(|\mathbf{q} - \mathbf{q}_3|) P^{[1]}(|\mathbf{q}_1 - \mathbf{q}_3|) \\ & \times P^{[1]}(|\mathbf{q}_2 - \mathbf{q}_3|) \\ & \times \sum_{\lambda=+, \times} Q_\lambda(\mathbf{q}, \mathbf{q}_1) \hat{I}(|\mathbf{q} - \mathbf{q}_1|, q_1, \eta) Q_\lambda(\mathbf{q}, \mathbf{q}_2) \hat{I}(|\mathbf{q} - \mathbf{q}_2|, q_2, \eta) , \end{aligned} \quad (2.24)$$

where we consider  $\alpha$  to be either 1 or 2. Since each of the “ $PZ$ -like”, “ $NC$ -like”, and “ $PN$ -like” families consists of only one diagram, we omit their superscripts for brevity. The associated integrals can be expressed as follows

$$\begin{aligned} \mathcal{P}_{PZ}(\eta, q) = & 2^4 \int \frac{d^3 \mathbf{q}_1}{(2\pi)^3} \frac{d^3 \mathbf{q}_2}{(2\pi)^3} \frac{d^3 \mathbf{q}_3}{(2\pi)^3} \frac{d^3 \mathbf{q}_4}{(2\pi)^3} P^{[1]}(q_4) P^{[1]}(|\mathbf{q} - \mathbf{q}_3|) P^{[1]}(|\mathbf{q}_1 - \mathbf{q}_3|) \\ & \times P^{[1]}(|\mathbf{q}_2 - \mathbf{q}_4|) P^{[1]}(|\mathbf{q}_3 - \mathbf{q}_4|) \\ & \times \sum_{\lambda=+, \times} Q_\lambda(\mathbf{q}, \mathbf{q}_1) \hat{I}(|\mathbf{q} - \mathbf{q}_1|, q_1, \eta) Q_\lambda(\mathbf{q}, \mathbf{q}_2) \hat{I}(|\mathbf{q} - \mathbf{q}_2|, q_2, \eta) , \end{aligned} \quad (2.25)$$

$$\begin{aligned} \mathcal{P}_{NC}(\eta, q) = & 2^4 \int \frac{d^3 \mathbf{q}_1}{(2\pi)^3} \frac{d^3 \mathbf{q}_2}{(2\pi)^3} \frac{d^3 \mathbf{q}_3}{(2\pi)^3} \frac{d^3 \mathbf{q}_4}{(2\pi)^3} P^{[1]}(q_3) P^{[1]}(|\mathbf{q} - \mathbf{q}_4|) P^{[1]}(|\mathbf{q}_2 - \mathbf{q}_3|) \\ & \times P^{[1]}(|\mathbf{q}_2 - \mathbf{q}_4|) P^{[1]}(|\mathbf{q}_1 + \mathbf{q}_3 - \mathbf{q}_4|) \\ & \times \sum_{\lambda=+, \times} Q_\lambda(\mathbf{q}, \mathbf{q}_1) \hat{I}(|\mathbf{q} - \mathbf{q}_1|, q_1, \eta) Q_\lambda(\mathbf{q}, \mathbf{q}_2) \hat{I}(|\mathbf{q} - \mathbf{q}_2|, q_2, \eta) , \end{aligned} \quad (2.26)$$

$$\begin{aligned} \mathcal{P}_{PN}(\eta, q) = & 2^4 \int \frac{d^3 \mathbf{q}_1}{(2\pi)^3} \frac{d^3 \mathbf{q}_2}{(2\pi)^3} \frac{d^3 \mathbf{q}_3}{(2\pi)^3} \frac{d^3 \mathbf{q}_4}{(2\pi)^3} \frac{d^3 \mathbf{q}_5}{(2\pi)^3} P^{[1]}(q_3) P^{[1]}(|\mathbf{q} - \mathbf{q}_4|) P^{[1]}(|\mathbf{q}_2 - \mathbf{q}_5|) \\ & \times P^{[1]}(|\mathbf{q}_3 - \mathbf{q}_5|) P^{[1]}(|\mathbf{q}_4 - \mathbf{q}_5|) P^{[1]}(|\mathbf{q}_1 + \mathbf{q}_3 - \mathbf{q}_4|) \\ & \times \sum_{\lambda=+, \times} Q_\lambda(\mathbf{q}, \mathbf{q}_1) \hat{I}(|\mathbf{q} - \mathbf{q}_1|, q_1, \eta) Q_\lambda(\mathbf{q}, \mathbf{q}_2) \hat{I}(|\mathbf{q} - \mathbf{q}_2|, q_2, \eta) . \end{aligned} \quad (2.27)$$

## 2.4 Numerical Results

In this analysis, we highlight the significant effects of  $f_{\text{NL}}$  and  $g_{\text{NL}}$  on the energy-density fraction spectrum of SIGWs. Additionally, we illustrate the presence of significant degeneracies in the model parameters for the spectrum, which pose challenges in accurately probing  $f_{\text{NL}}$  and  $g_{\text{NL}}$  using the spectrum alone.

To evaluate Eq. (2.15) numerically for the SIGWs generated during the radiation-dominated phase of the early Universe, we set  $\sigma = 1$ . The results of the unscaled energy-density fraction spectra  $[(3/5)^{2(a+b)} f_{\text{NL}}^{2a} g_{\text{NL}}^b A_S^{a+b+2}]^{-1} \bar{\Omega}_{\text{gw}}^{(a,b)}(\eta, q)$  are shown in Figure 5. By scaling these unscaled spectra and summing them up, we obtain the total spectrum  $\bar{\Omega}_{\text{gw}}(\eta, q)$



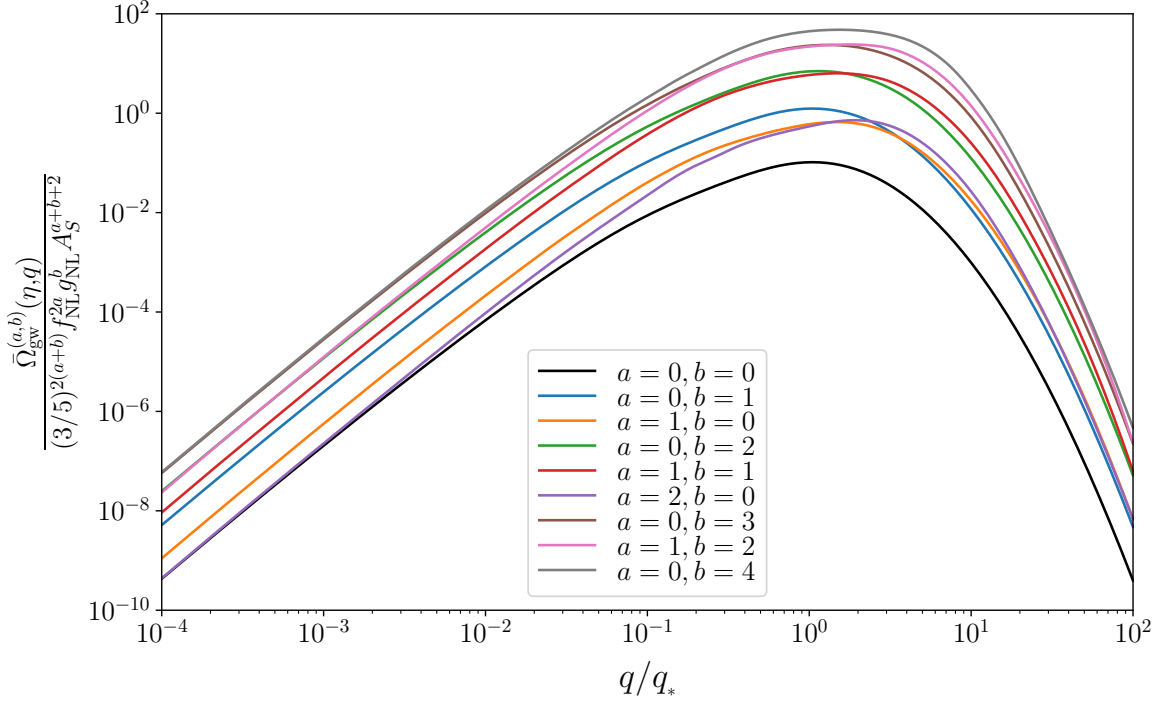


**Figure 5:** Unscaled (or equivalently,  $A_S = 1$ ,  $3f_{\text{NL}}/5 = 1$  and  $9g_{\text{NL}}/25 = 1$ ) components of the energy-density fraction spectra of SIGWs in powers of the primordial non-Gaussian parameters  $f_{\text{NL}}$  and  $g_{\text{NL}}$ .

as  $\bar{\Omega}_{\text{gw}}(\eta, q) = \sum_{(a,b)} \bar{\Omega}_{\text{gw}}^{(a,b)}(\eta, q)$ , as given in Eq. (2.16). It is worth noting that generalizations for studying other values of  $\sigma$  and different epochs of the early Universe can be carried out relatively easily.

We are also interested in studying the physical energy-density fraction spectrum of SIGWs in the present Universe, specifically at the conformal time  $\eta_0$ . This spectrum is related to the total spectrum at the production time  $\eta$  in the following manner [127]

$$h^2 \bar{\Omega}_{\text{gw},0}(\nu) = h^2 \Omega_{\text{rad},0} \left[ \frac{g_{*,\rho}(T)}{g_{*,\rho}(T_{\text{eq}})} \right] \left[ \frac{g_{*,s}(T_{\text{eq}})}{g_{*,s}(T)} \right]^{4/3} \bar{\Omega}_{\text{gw}}(\eta, q), \quad (2.28)$$

where  $h$  represents the dimensionless Hubble constant, and  $h^2 \Omega_{\text{rad},0} = 4.2 \times 10^{-5}$  denotes the physical energy-density fraction of radiation in the present Universe [125]. The temperature  $T$  (and  $T_{\text{eq}}$ ) corresponds to the cosmic temperature at the production time (and the epoch of matter-radiation equality), while  $\nu$  refers to the gravitational-wave frequency. Furthermore, it should be noted that  $\nu$  is determined by  $T$ , meaning that there is a relationship between the two, i.e., [128]

$$\frac{\nu}{\text{nHz}} = 26.5 \left( \frac{T}{\text{GeV}} \right) \left( \frac{g_{*,\rho}(T)}{106.75} \right)^{1/2} \left( \frac{g_{*,s}(T)}{106.75} \right)^{-1/3}, \quad (2.29)$$

where  $g_{*,\rho}$  and  $g_{*,s}$  are quantities associated with the number of relativistic species, and they are tabulated functions of the temperature  $T$ . These tabulated functions can be found in Ref. [124].

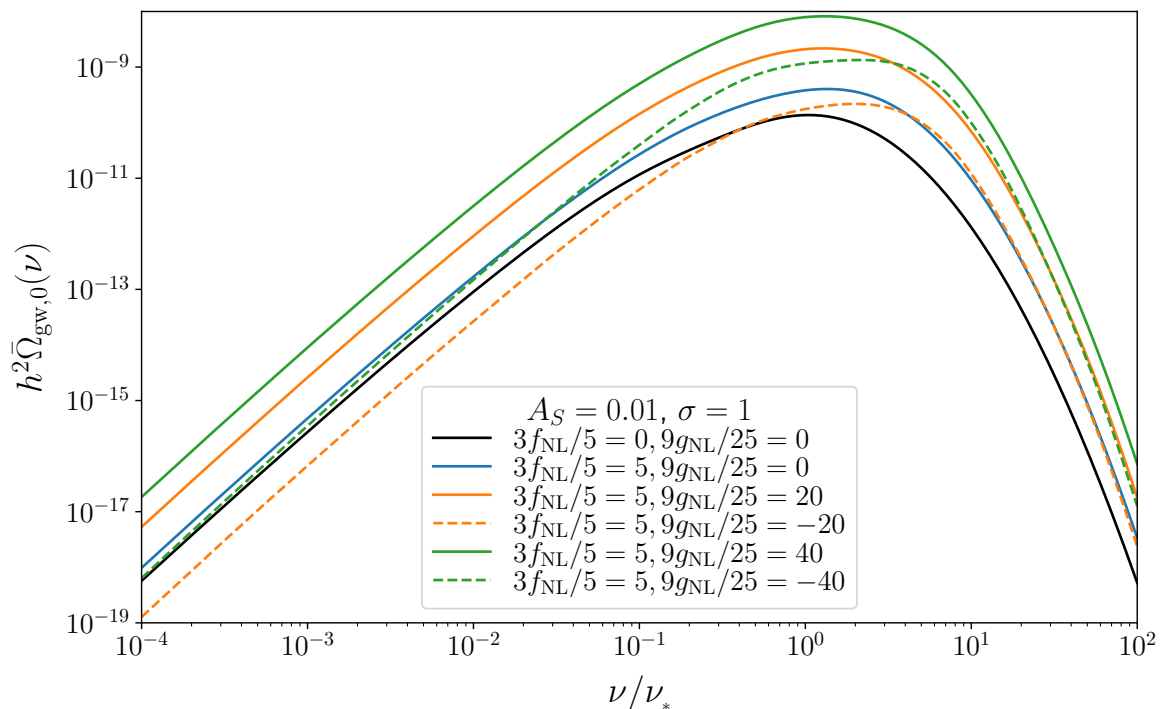


**Figure 6:** Energy-density fraction spectra of SIGWs in the present Universe.

Figure 6 illustrates the contributions of both  $f_{\text{NL}}$  and  $g_{\text{NL}}$  to the energy-density fraction spectrum of SIGWs in the present Universe. By combining Figure 5 with Figure 6, we observe that the contributions from  $f_{\text{NL}}$  are always positive, while those from  $g_{\text{NL}}$  depend not only on its sign but also on its amplitude. This behavior arises because the unscaled energy-density fraction spectrum  $\bar{\Omega}_{\text{gw}}^{(a,b)}$  is explicitly proportional to  $f_{\text{NL}}^{2a}$  and  $g_{\text{NL}}^b$ , where  $a = 0, 1, 2$  and  $b = 0, 1, 2, 3, 4$ . It is evident that there is a sign degeneracy for  $f_{\text{NL}}$  in  $\bar{\Omega}_{\text{gw}}^{(a,b)}$ , but not for  $g_{\text{NL}}$ . When  $g_{\text{NL}}$  is positive (represented by solid curves), the contributions from it to  $\bar{\Omega}_{\text{gw}}^{(a,b)}$  are always positive. On the other hand, when  $g_{\text{NL}}$  is negative (indicated by dashed curves), the contributions are positive for even values of  $b$  and negative for odd values of  $b$ . Furthermore, the contributions to  $\bar{\Omega}_{\text{gw}}$  also depend on the absolute value of  $g_{\text{NL}}$  (more precisely, on the combinations  $f_{\text{NL}}^{2a} g_{\text{NL}}^b A_S^{a+b+2}$ ).

The aforementioned observations are visually demonstrated in Figure 6. When comparing the scenario with Gaussianity, we observe that the inclusion of  $f_{\text{NL}}$  and positive  $g_{\text{NL}}$  consistently enhances the overall energy-density fraction spectrum for a fixed value of  $A_S$ . Conversely, a small negative  $g_{\text{NL}}$  can suppress this spectrum, especially in the low-frequency range, compared to a positive one. In fact, the suppression can be substantial to the extent that the suppressed spectrum falls below the level of the Gaussian spectrum.

To comprehensively illustrate the dependence of the SIGW energy-density fraction spectrum on  $f_{\text{NL}}$  and  $g_{\text{NL}}$ , we present an array of contour plots in Figure 7. The contour plots depict the energy-density fraction spectrum in the present Universe with  $f_{\text{NL}}$  and  $g_{\text{NL}}$  as variables. The value of  $A_S$  remains constant within each column, and  $\nu/\nu_*$  is fixed within each row. The same position on each panel corresponds to specific values of  $f_{\text{NL}}\sqrt{A_S}$  and  $g_{\text{NL}}A_S$ . Each panel is divided into four triangular regions by dotted lines. The left and right regions

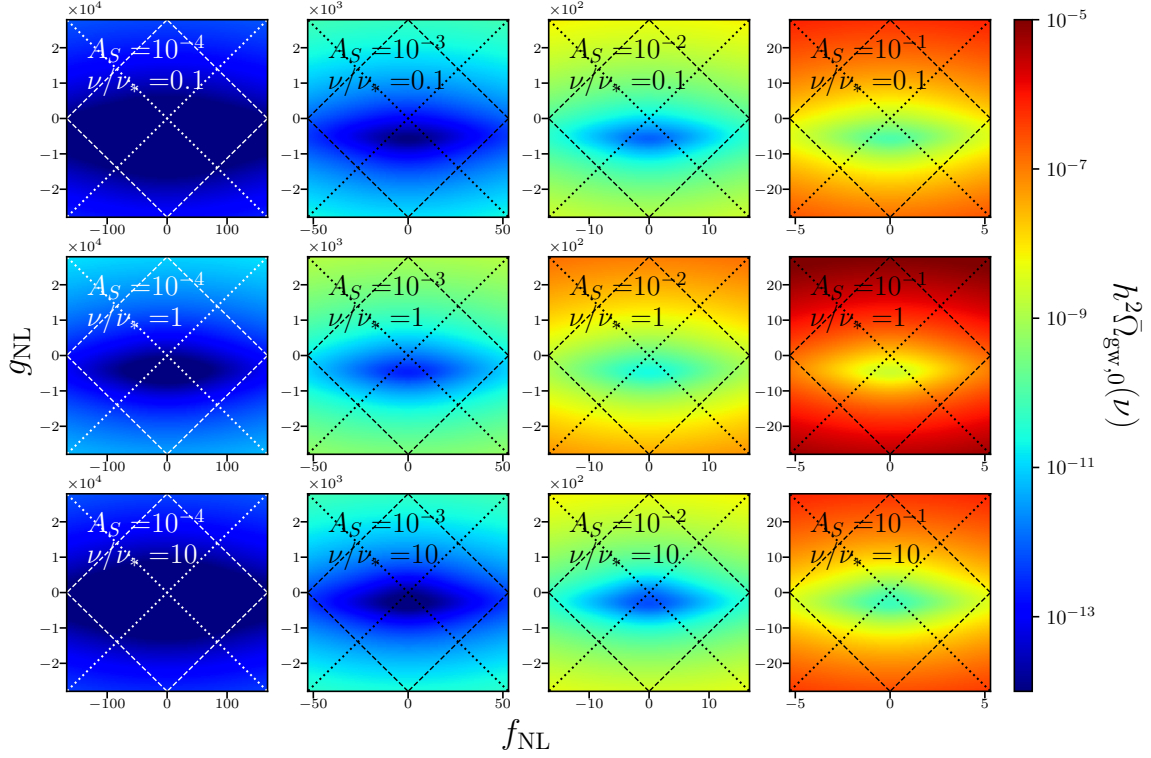


**Figure 7:** The present-day energy-density fraction spectrum of SIGWs with respect to the primordial non-Gaussian parameters  $f_{\text{NL}}$  and  $g_{\text{NL}}$ . Dotted lines represent  $g_{\text{NL}} = \pm 5f_{\text{NL}}/(3\sqrt{A_S})$ , which signify that the contribution from  $f_{\text{NL}}$  to  $\zeta$  is equal to that from  $g_{\text{NL}}$ . Dashed lines represent  $3|f_{\text{NL}}|\sqrt{A_S}/5 + 9|g_{\text{NL}}|A_S/25 = 1$ , which signify that the contribution from non-Gaussian terms to  $\zeta$  is equal to that from the Gaussian term.

represent the contribution of the  $g_{\text{NL}}$  term being smaller than that of the  $f_{\text{NL}}$  term, ensuring perturbativity, while the top and bottom regions represent the opposite. The square regions surrounded by dashed lines represent the contributions of the primordial non-Gaussian terms being greater than that of the Gaussian term. In each panel, it is evident that  $h^2 \bar{\Omega}_{\text{gw},0}(\nu)$  is more sensitive to  $9g_{\text{NL}}A_S/25$  than  $3f_{\text{NL}}\sqrt{A_S}/5$ . Additionally, increasing  $A_S$  consistently enhances the spectral amplitudes as expected. Although large non-Gaussianity typically leads to large spectral amplitudes in each panel, the position of minimal amplitude consistently appears in the regions of zero  $f_{\text{NL}}$  and small negative  $g_{\text{NL}}$ .

Our theoretical predictions are expected to be tested using space-borne gravitational-wave detectors and detector networks such as Taiji [135, 136], Tianqin [137–139], LISA [110, 140], BBO [133, 141], DECIGO [132, 142], and others. In Figure 8, we compare a range of theoretical results with the sensitivity curves of the latter three detectors. We consider parameter regimes that may be relevant to scenarios involving PBHs [60, 143]. For PBHs within mass ranges detectable by space-borne detectors for SIGWs [128, 144, 145], they are considered as potential candidates for cold dark matter. Therefore, it is crucial to investigate the significant impact of primordial non-Gaussianity on the abundance of PBHs [38, 44–46, 55, 56, 58, 146]. From Figure 8, we observe that these detectors have the potential to shed light on this question in the future.

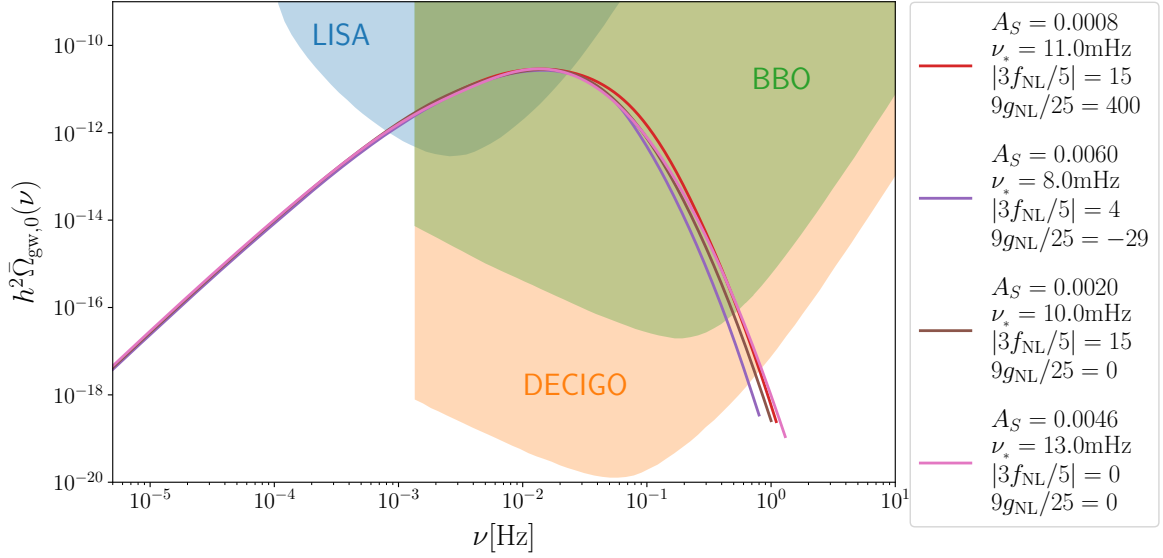


**Figure 8:** Energy-density fraction spectra of SIGW in the present Universe compared with the sensitivity curves of LISA (blue shaded region) [129, 130], DECIGO (orange shaded region) [131, 132], and BBO (green shaded region) [133, 134]. For all the cases,  $\sigma = 1$  is assumed for the spectra.

However, it is important to note that there exist significant degeneracies among the model parameters affecting the energy-density fraction spectra. In Figure 8, the four spectra appear to closely overlap, yet they correspond to entirely different parameter combinations. Breaking these degeneracies is crucial, and therefore, we propose a new approach to address this issue in Section 3.

### 3 Angular power spectrum

In this section, we extend our analysis to include the effects of large-scale inhomogeneities, which were previously neglected in Section 2. For the first time, we comprehensively investigate the inhomogeneities and anisotropies in SIGWs by incorporating both  $f_{\text{NL}}$  and  $g_{\text{NL}}$ . We develop systematic formulas to calculate the angular power spectrum, allowing us to study the spatial variations of SIGWs on large scales. Similar to the observations of temperature anisotropies in CMB, the study of SIGWs as a form of GWB is expected to reveal inhomogeneities and anisotropies. These inhomogeneities can provide valuable insights into the nature of our Universe, similar to how the CMB has led to precise measurements of six fundamental parameters in the concordance model of cosmology.

In the existing literature, there have been three relevant works addressing the same topic. In Ref. [106], the authors examined the angular power spectrum of SIGWs by incorporating  $f_{\text{NL}}$  for the first time. Subsequently, we conducted the first comprehensive analysis of the angular power spectrum by incorporating  $f_{\text{NL}}$  in our previous works [25, 78]. Compared to the former work, the latter studies considered all contributions of  $f_{\text{NL}}$ . In this current work, we extend our previous investigations by including all contributions of  $g_{\text{NL}}$  in the analysis of the angular power spectrum of SIGWs.

The presence of large-scale inhomogeneities in SIGWs can be attributed to two main factors, as discussed in Refs. [25, 78, 106]. Firstly, the initial inhomogeneities arise due to the coupling between long-wavelength and short-wavelength modes. The long-wavelength modes redistribute the energy density of gravitational waves induced by the short-wavelength modes, resulting in the formation of initial inhomogeneities on large scales. Secondly, similar to the analysis of CMB, inhomogeneities can also arise from propagation effects caused by the presence of long-wavelength gravitational potentials, such as the Sachs-Wolfe (SW) effect [147]. In our analysis, we consider both of these factors. It is important to note that our evaluation adopts the cosmological principle, which assumes statistical homogeneity and isotropy on large scales.

Similar to the measurement of temperature fluctuations in relic photons [148], the large-scale inhomogeneities in SIGWs within an observed region centered at position  $\mathbf{x}$  and conformal time  $\eta'$  can be quantified using the density contrast  $\delta_{\text{gw}}$ . This density contrast is defined as follows

$$\delta_{\text{gw}}(\eta', \mathbf{x}, \mathbf{q}) = 4\pi \frac{\omega_{\text{gw}}(\eta', \mathbf{x}, \mathbf{q})}{\Omega_{\text{gw}}(\eta', q)} - 1. \quad (3.1)$$

By averaging over a large number of such regions, the resulting averaged energy-density fraction spectrum can be expressed as

$$\bar{\Omega}_{\text{gw}}(\eta', q) = 4\pi \langle \omega_{\text{gw}}(\eta', \mathbf{x}, \mathbf{q}) \rangle, \quad (3.2)$$

which yields results that are identical to those obtained in Section 2. Similarly, we find that  $\langle \delta_{\text{gw}}(\eta', \mathbf{x}, \mathbf{q}) \rangle = 0$ , indicating that, on average, the density contrast is zero. The energy-density full spectrum  $\omega_{\text{gw}}(\eta', \mathbf{x}, \mathbf{q})$  is defined in relation to the energy density  $\rho_{\text{gw}}(\eta', \mathbf{x})$  as follows [120]

$$\rho_{\text{gw}}(\eta', \mathbf{x}) = \rho_{\text{c}}(\eta') \int d \ln q d^2 \hat{\mathbf{q}} \omega_{\text{gw}}(\eta', \mathbf{x}, \mathbf{q}), \quad (3.3)$$

where the symbol  $\hat{\mathbf{q}}$  represents the unit directional vector, given by  $\hat{\mathbf{q}} = \mathbf{q}/q$ . Additionally, the energy density of the inhomogeneous SIGWs is defined as

$$\rho_{\text{gw}}(\eta, \mathbf{x}) = \frac{m_{\text{Pl}}^2}{16a^2(\eta)} \overline{\partial_l h_{ij}(\eta, \mathbf{x}) \partial_l h_{ij}(\eta, \mathbf{x})}. \quad (3.4)$$

Hence, we can express the initial energy-density full spectrum  $\omega_{\text{gw}}(\eta, \mathbf{x}, \mathbf{q})$  in the following manner

$$\omega_{\text{gw}}(\eta, \mathbf{x}, \mathbf{q}) = -\frac{q^3}{48\mathcal{H}^2} \int \frac{d^3 \mathbf{k}}{(2\pi)^3} e^{i\mathbf{k} \cdot \mathbf{x}} [(\mathbf{k} - \mathbf{q}) \cdot \mathbf{q}] \overline{h_{ij}(\eta, \mathbf{k} - \mathbf{q}) h_{ij}(\eta, \mathbf{q})}, \quad (3.5)$$

which depends not only on the magnitude of  $q$  but also on the unit directional vector  $\hat{\mathbf{q}}$ . In the given equations,  $\mathbf{q}$  represents the comoving momentum of SIGWs associated with short wavelengths, while  $\mathbf{k}$  is associated with a Fourier mode of the inhomogeneities in SIGWs, corresponding to long wavelengths. Hence, in the subsequent analysis, we will consider the regime where  $q \gtrsim \mathcal{H}^{-1} \gg k$ .

The evolution of the density contrast is described by the Boltzmann equation [149]. In the context of relic photons, this equation has been solved using the line-of-sight approach [148]. More recently, the same approach has been applied to the study of general GWBs [150]. Subsequently, it has been used to investigate two-point and three-point correlators for cosmological GWBs [151, 152]. In the context of anisotropies in SIGWs, the authors of

Refs. [25, 78, 106] have explored the significant influence of  $f_{\text{NL}}$ . Other relevant works can be found in Refs. [60, 107–115].

Based on the line-of-sight solution to the Boltzmann equation, as derived in Appendix C, we demonstrate that the present density contrast  $\delta_{\text{gw},0}(\mathbf{q}) = \delta_{\text{gw}}(\eta_0, \mathbf{x}_0, \mathbf{q})$  incorporates both the initial inhomogeneities and the effects of propagation, i.e., [25, 78, 106]

$$\delta_{\text{gw},0}(\mathbf{q}) = \delta_{\text{gw}}(\eta, \mathbf{x}, \mathbf{q}) + [4 - n_{\text{gw}}(\nu)] \Phi(\eta, \mathbf{x}) , \quad (3.6)$$

where the value of  $q$  is given by the equation  $q = 2\pi\nu$ , with  $\nu$  representing the frequency, and the determination of the index of the energy-density fraction spectrum is based on

$$n_{\text{gw}}(\nu) = \frac{\partial \ln \bar{\Omega}_{\text{gw},0}(\nu)}{\partial \ln \nu} \simeq \frac{\partial \ln \bar{\Omega}_{\text{gw}}(\eta, q)}{\partial \ln q} \Big|_{q=2\pi\nu} . \quad (3.7)$$

The first term on the right-hand side of Eq. (3.6) represents the initial inhomogeneities, while the second term corresponds to the SW effect [147]. Furthermore, the integrated Sachs-Wolfe (ISW) effect [147], as shown in Ref. [106], is found to be less significant compared to the SW effect. In this study, we disregard the ISW effect, but it can be easily accounted for if necessary. When considering the long-wavelength modes that reentered the Hubble horizon during matter domination, we characterize the SW effect using the Bardeen potential on large scales, i.e.,

$$\Phi(\eta, \mathbf{x}) = \frac{3}{5} \int \frac{d^3\mathbf{k}}{(2\pi)^{3/2}} e^{i\mathbf{k}\cdot\mathbf{x}} \zeta_{gL}(\mathbf{k}) , \quad (3.8)$$

where  $\zeta_{gL}$  represents the primordial curvature perturbations of long-wavelength as introduced in Eq. (2.9). One of the remaining tasks is to assess the initial inhomogeneities  $\delta_{\text{gw}}(\eta, \mathbf{x}, \mathbf{q})$ . This will be addressed in the upcoming subsection.

Now, it is imperative to provide some insights into the physical implications of Eq. (3.6), or more broadly, Eq. (C.12). Firstly, let us consider the propagation effects, namely the SW and ISW effects. It has been established that these effects are identical for both the CMB and GWBs, as massless photons and gravitons follow the same perturbed geodesics [150–152]. Moreover, it is crucial to note that the second comment pertains to the initial inhomogeneities, which differ for the CMB and GWBs. If any initial inhomogeneities existed in the CMB, they have been completely wiped out due to frequent scatterings between photons and electrons in the early Universe [149]. In contrast, the initial inhomogeneities in GWBs persist, as the early Universe is transparent to GWs [21, 22]. Consequently, GWBs have the potential to serve as powerful probes of early-Universe physics.

The reduced angular power spectrum is widely used to describe the statistical properties of the anisotropies in SIGWs. This spectrum is defined by the two-point correlator of the present density contrast, namely,

$$\langle \delta_{\text{gw},0,\ell m}(2\pi\nu) \delta_{\text{gw},0,\ell' m'}^*(2\pi\nu) \rangle = \delta_{\ell\ell'} \delta_{mm'} \tilde{C}_\ell(\nu) , \quad (3.9)$$

where  $\delta_{\text{GW},0}(\mathbf{q})$ , defined in Eq. (3.6), is expanded using spherical harmonics, that is,

$$\delta_{\text{gw},0}(\mathbf{q}) = \sum_{\ell m} \delta_{\text{gw},0,\ell m}(q) Y_{\ell m}(\hat{\mathbf{q}}) . \quad (3.10)$$

By inserting Eq. (3.6) into Eq. (3.10) and subsequently Eq. (3.9), the reduced angular power spectrum for SIGWs can be readily obtained.

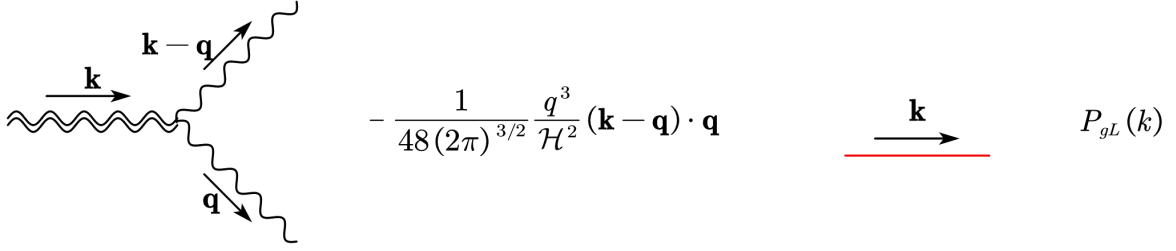


**Figure 9:** The Feynman-like rules complementary to those of Figure 1. Left panel represents the  $\omega$ -vertex, for which double wavy lines denote  $\omega_{\text{gw}}$ . Right panel shows the primordial power spectrum of long-wavelength modes in red solid line.

Practically, evaluating the terms that involve only the propagation effects, such as the SW effect shown in Eq. (3.8), is somewhat straightforward. However, when we consider the initial inhomogeneities, which are related to Eq. (3.5), we need to evaluate the multi-point correlator  $\langle h^4 \rangle \sim \langle \zeta^8 \rangle$ . This involves, at most, the 24-point correlator of the form  $\langle \zeta_g^{24} \rangle$ . Expanding these correlators straightforwardly using Wick's theorem proves to be particularly challenging. Therefore, we also adopt a Feynman-like diagrammatic technique to simplify the evaluation in the following.

### 3.1 Feynman-like Rules and Diagrams

In this section, we exclusively concentrate on the initial inhomogeneities at large scales, arising from the spatial modulation of energy density caused by the long-wavelength modes.

By substituting Eqs. (2.8) and (2.9) into Eq. (3.5), we can approximately express the effect of long-wavelength modulation as follows

$$\omega_{\text{gw}}(\eta, \mathbf{x}, \mathbf{q}) \sim \langle \zeta^4 \rangle_{\mathbf{x}} \sim \langle \zeta_S^4 \rangle_{\mathbf{x}} + \mathcal{O}(\zeta_{gL}) f_{\text{NL}} \langle \zeta_S \zeta_S^3 \rangle_{\mathbf{x}} + \mathcal{O}(\zeta_{gL}) g_{\text{NL}} \langle \zeta_S^2 \zeta_S^3 \rangle_{\mathbf{x}}, \quad (3.11)$$

where  $\zeta_S$  represents the short-wavelength modes associated with the primordial non-Gaussianity, and the subscript  $\mathbf{x}$  denotes an ensemble average within the observed region centered at  $\mathbf{x}$ . The term  $\langle \zeta_S^4 \rangle_{\mathbf{x}}$  represents the monopole, denoted as  $\bar{\Omega}(\eta, q)$ , while the last two terms capture the effects of long-wavelength modulation, indicating that  $\delta_{\text{gw}}(\eta, \mathbf{x}, \mathbf{q}) \sim \zeta_{gL}$  as defined in Eq. (3.1). In this analysis, we have neglected higher-order terms in  $\zeta_{gL}$  due to the negligible dimensionless power spectrum of long-wavelength modes compared to that of short-wavelength modes, specifically  $\Delta_L^2 \ll \Delta_S^2$ . Therefore, at the linear order in  $\Delta_L^2 \sim \langle \zeta_{gL}^2 \rangle$ , we obtain the angular power spectrum defined in Eq. (3.9) as follows

$$\langle \delta_{\text{gw}}(\eta, \mathbf{x}, \mathbf{q}) \delta_{\text{gw}}(\eta, \mathbf{x}', \mathbf{q}') \rangle \sim \langle \omega_{\text{gw}}(\eta, \mathbf{x}, \mathbf{q}) \omega_{\text{gw}}(\eta, \mathbf{x}', \mathbf{q}') \rangle^{\mathcal{O}(\Delta_L^2)} \sim \Delta_L^2 \langle \dots \rangle_{\mathbf{x}} \langle \dots \rangle_{\mathbf{x}'}, \quad (3.12)$$

where  $\langle \dots \rangle_{\mathbf{x}}$  represents the combination of angle brackets in the last two terms of Eq. (3.11). In fact, it is more convenient to use  $\langle \omega_{\text{gw}}(\eta, \mathbf{x}, \mathbf{q}) \omega_{\text{gw}}(\eta, \mathbf{x}', \mathbf{q}') \rangle$  when establishing the Feynman-like rules.

Analogous to the Feynman-like diagrammatic technique utilized in Section 2, we reformulate the expression  $\langle \omega_{\text{gw}}(\eta, \mathbf{x}, \mathbf{q}) \omega_{\text{gw}}(\eta, \mathbf{x}', \mathbf{q}') \rangle$  as a series of Feynman-like diagrams. Previous studies that have employed this technique to analyze the angular power spectrum for SIGWs can be found in Refs [25, 78, 106]. By substituting Eqs. (3.5) into the two-point correlator and incorporating Eqs. (2.8) and (2.9), we can explicitly introduce two additional



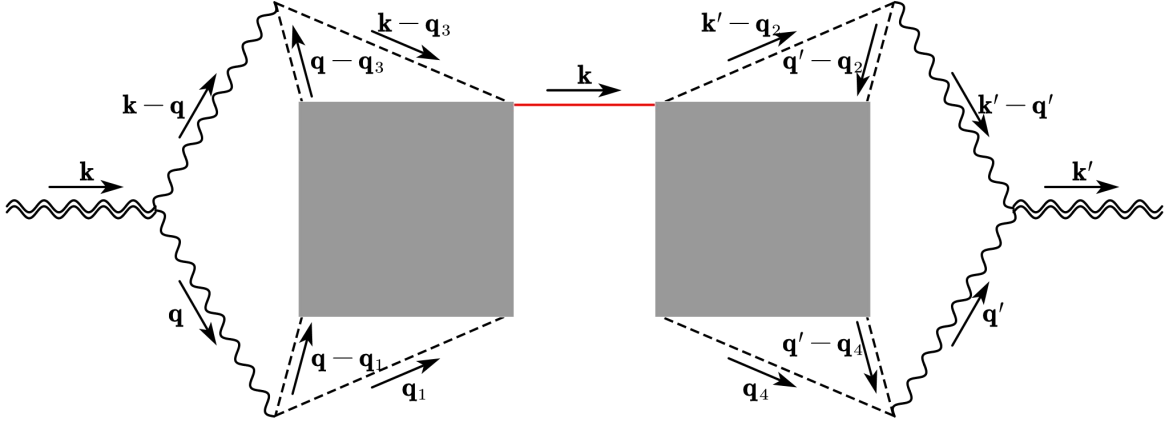


**Figure 10:** The Feynman-like diagram of the angular power spectrum of SIGWs. The shadow squares should be replaced with the panels in Fig. 3.

Feynman-like rules, as summarized in Figure 9. The left panel represents the  $\omega$ -vertex, while the right panel depicts the propagator of the long-wavelength modes. These supplementary Feynman-like rules complement those shown in Figure 1 in Section 2. It is important to note that the Feynman-like rules for the vertices in Figure 1 remain unchanged, irrespective of the colors of the solid lines. This indicates that these vertices are independent of the propagators of the short-wavelength and long-wavelength modes.

Corresponding to Eq. (3.12), the Feynman-like diagrams are fully depicted in Figure 10 and Figure 3. To obtain an individual diagram, we need to replace the two shaded squares in Figure 10 with the panels from Figure 3, respectively. Here, we have neglected the disconnected diagrams, which correspond to the monopole  $\bar{\Omega}_{\text{gw}}(\eta, q)$ , and the diagrams of higher order in  $\Delta_L^2$ . For a given Feynman-like diagram, there is a single “non-Gaussian bridge”, represented by the red line in Figure 10, that connects the initial inhomogeneities located at two different positions separated by a large distance. The contribution of this diagram to the two-point correlator is proportional to  $\bar{\Omega}_{\text{gw}}^X \langle \zeta_{gL} \zeta_{gL} \rangle \bar{\Omega}_{\text{gw}}^{X'}$ . This can be equivalently expressed as a correlator between  $\bar{\Omega}_{\text{gw}}^X \zeta_{gL}$  and  $\bar{\Omega}_{\text{gw}}^{X'} \zeta_{gL}$ , which represent the contributions of long-wavelength modulation to  $\omega_{\text{gw}}(\eta, \mathbf{x}, \mathbf{q})$ . By summing over all the Feynman-like diagrams, we obtain the total effect of long-wavelength modulation on  $\omega_{\text{gw}}(\eta, \mathbf{x}, \mathbf{q})$ , which is analogous to the last two terms in Eq. (3.11).

Precisely speaking, we can reformulate Eq. (3.11) into a novel expression of the following form

$$\omega_{\text{gw}}(\eta, \mathbf{x}, \mathbf{q}) = \frac{\bar{\Omega}_{\text{gw}}(\eta, q)}{4\pi} + \frac{\Omega_{\text{ng}}(\eta, q)}{4\pi} \int \frac{d^3\mathbf{k}}{(2\pi)^{3/2}} e^{i\mathbf{k} \cdot \mathbf{x}} \zeta_{gL}(\mathbf{k}) , \quad (3.13)$$

where for the sake of convenience, we introduce a new quantity  $\Omega_{\text{ng}}(\eta, q)$  that follows the form

$$\begin{aligned} \Omega_{\text{ng}}(\eta, q) = & \frac{6f_{\text{NL}}}{5} \left( 4\bar{\Omega}_{\text{gw}}^{(0,0)} + 3\bar{\Omega}_{\text{gw}}^{(0,1)} + 2\bar{\Omega}_{\text{gw}}^{(1,0)} + 2\bar{\Omega}_{\text{gw}}^{(0,2)} + \bar{\Omega}_{\text{gw}}^{(1,1)} + \bar{\Omega}_{\text{gw}}^{(0,3)} \right) \\ & + \frac{9g_{\text{NL}}}{5f_{\text{NL}}} \left( 2\bar{\Omega}_{\text{gw}}^{(1,0)} + 2\bar{\Omega}_{\text{gw}}^{(1,1)} + 4\bar{\Omega}_{\text{gw}}^{(2,0)} + 2\bar{\Omega}_{\text{gw}}^{(1,2)} \right) . \end{aligned} \quad (3.14)$$

The next crucial step is to derive the aforementioned equation.

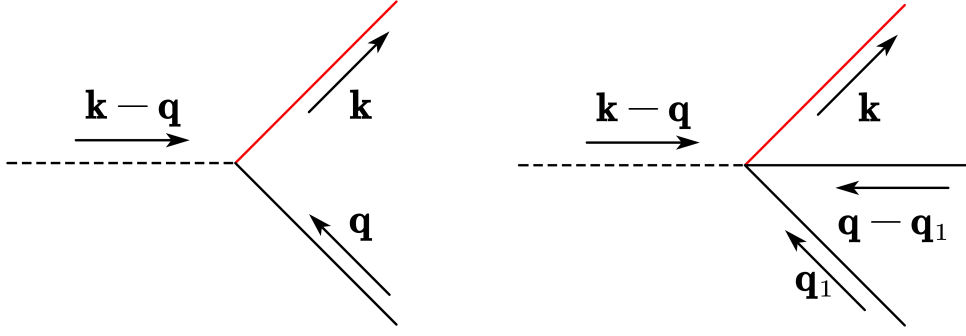


**Figure 11:** Vertices involved in the non-Gaussian bridge.

To simplify the process, we adopt a diagrammatic approach to derive Eq. (3.14). This approach is equivalent to the traditional expansion outlined in Eq. (3.11), utilizing Wick's theorem. As illustrated in the left panel of Figure 11, the inclusion of the non-Gaussian bridge leads to the transformation of the Gaussian vertex into the  $f_{\text{NL}}$ -vertex. This transformation also results in a doubling of the symmetric factor, leading to an additional factor of 2. In this case, the contribution from Diagram- $X$  to  $\Omega_{\text{ng}}$  is given by  $2N_{\text{Gau}}^X [(3f_{\text{NL}}/5)/1] \bar{\Omega}_{\text{gw}}^X$ , where  $N_{\text{Gau}}^X$  represents the number of Gaussian vertices. As shown in the right panel of Figure 11, the inclusion of the non-Gaussian bridge converts the  $f_{\text{NL}}$ -vertex into the  $g_{\text{NL}}$ -vertex. This transformation also triples the symmetric factor, resulting in an additional factor of 3. In this scenario, the contribution from Diagram- $X$  to  $\Omega_{\text{ng}}$  is given by  $3N_{f_{\text{NL}}}^X [(9g_{\text{NL}}/25)/(3f_{\text{NL}}/5)] \bar{\Omega}_{\text{gw}}^X$ , where  $N_{f_{\text{NL}}}^X$  represents the number of  $f_{\text{NL}}$ -vertices. The count of various vertices is determined by the category associated with Diagram- $X$ , which implies  $N_{\text{Gau}}^X = 4 - 2a - b$  and  $N_{f_{\text{NL}}}^X = 2a$ . By employing Table 2 as a dictionary, we can readily obtain Eq. (3.14). It is worth noting that the ten diagrams of the (0, 4)-category do not contribute to  $\Omega_{\text{ng}}$ , as we are considering non-Gaussianity up to the order of  $g_{\text{NL}}$ . This suggests a decoupling of modes with short-wavelength and long-wavelength for these diagrams. Please note that we have revised the definition of  $\Omega_{\text{ng}}$  compared to our previous works [25, 78], where we only considered  $f_{\text{NL}}$ . When  $g_{\text{NL}}$  is zero, our new definition of  $\Omega_{\text{ng}}$  reverts back to the old definition if we divide the new definition by  $(3f_{\text{NL}}/5)$ .

### 3.2 Formulae for Angular Power Spectrum

Based on the aforementioned findings, it is now necessary to derive the equation for the angular power spectrum of SIGWs, as defined in Eq. (3.9). By substituting Eq. (3.13) into Eq. (3.1), we obtain the initial density contrast, denoted as  $\delta(\mathbf{k})$ , which can be expressed as

$$\delta_{\text{gw}}(\eta, \mathbf{x}, \mathbf{q}) = \frac{\Omega_{\text{ng}}(\eta, q)}{\bar{\Omega}_{\text{gw}}(\eta, q)} \int \frac{d^3 \mathbf{k}}{(2\pi)^{3/2}} e^{i\mathbf{k} \cdot \mathbf{x}} \zeta_{gL}(\mathbf{k}). \quad (3.15)$$

Subsequently, by further substituting Eq. (3.8) and Eq. (3.15) into Eq. (3.6), we can derive the present density contrast, i.e.,

$$\delta_{\text{gw},0}(\mathbf{q}) = \left\{ \frac{\Omega_{\text{ng}}(\eta, 2\pi\nu)}{\bar{\Omega}_{\text{gw}}(\eta, 2\pi\nu)} + \frac{3}{5} [4 - n_{\text{gw}}(\nu)] \right\} \int \frac{d^3 \mathbf{k}}{(2\pi)^{3/2}} e^{i\mathbf{k} \cdot \mathbf{x}} \zeta_{gL}(\mathbf{k}), \quad (3.16)$$

where the expression for  $\Omega_{\text{ng}}$  is given in Eq. (3.14). Ultimately, by substituting Eq. (3.16) into Eq. (3.10) and subsequently Eq. (3.9), we derive the fundamental equation of this study

for the reduced angular power spectrum, i.e.,

$$\tilde{C}_\ell(\nu) = \frac{2\pi\Delta_L^2}{\ell(\ell+1)} \left\{ \frac{\Omega_{\text{ng}}(\eta, 2\pi\nu)}{\bar{\Omega}_{\text{gw}}(\eta, 2\pi\nu)} + \frac{3}{5} [4 - n_{\text{gw}}(\nu)] \right\}^2, \quad (3.17)$$

which can be further reformulated as the angular power spectrum, i.e.,

$$C_\ell(\nu) = \left[ \frac{\bar{\Omega}_{\text{gw},0}(\nu)}{4\pi} \right]^2 \tilde{C}_\ell(\nu). \quad (3.18)$$

Eq. (3.17) demonstrates that the angular power spectrum is influenced by the initial inhomogeneities, propagation effects, and their intersections. Similar to the analysis of CMB, we can define the root-mean-squared (rms) energy density for the anisotropies in SIGWs as  $[\ell(\ell+1)C_\ell(\nu)/2\pi]^{1/2}$ . This quantity is independent of the angular multipoles  $\ell$ , but varies with the frequencies of SIGW.

We would like to provide further comments regarding the multipole dependence of the reduced angular power spectrum, as illustrated by Eq. (3.17). It is worth noting that we have observed a distinctive multipole dependence, where  $C_\ell \propto [\ell(\ell+1)]^{-1}$ , for SIGWs. This behavior has also been reported in the literature [25, 78, 106, 153]. In contrast, for GWBs generated by binary black holes (BBHs), the multipole dependence has been found to be roughly proportional to  $(\ell+1/2)^{-1}$  [150, 154–164]. On the other hand, for a GWB originating from cosmic string loops, the multipole dependence has been shown to be proportional to  $\ell^0$  [165–167]. Therefore, the multipole dependence plays a crucial role in differentiating SIGWs from these other sources of GWBs (for reviews, see Ref. [109]). It is important to note that there are other cosmological sources of gravitational waves, such as inflation [108, 115, 168–170], domain walls [171], first-order phase transitions [172–178], and preheating [179, 180], which predict angular power spectra with a similar  $\tilde{C}_\ell \sim \ell^{-2}$  dependence as SIGWs. To distinguish SIGWs from these sources, cross-correlation studies between GWBs and various observables, such as CMB [108, 112, 153, 154, 181–186], LSS [154, 187–193], and 21cm lines [194, 195], have been proposed. Furthermore, it is worth mentioning that apart from the information contained in the characteristic energy density  $\bar{\Omega}_{\text{gw}}$ , there is additional information embedded in the frequency dependence of  $C_\ell$ . This frequency dependence could potentially serve as a valuable tool for further distinguishing between different sources of GWs [25, 113, 153, 196]. We will now proceed to demonstrate this frequency dependence in the following discussion.

### 3.3 Numerical Results

We present numerical results illustrating the impact of both  $f_{\text{NL}}$  and  $g_{\text{NL}}$  on the angular power spectrum of SIGWs. By studying this spectrum, we are able to reexamine the issue of degeneracies in the model parameters, which can be effectively resolved.

During the radiation-dominated era of the early Universe, we investigate the reduced angular power spectrum of SIGWs. This spectrum is defined in Eq. (3.17). We keep  $A_S = 10^{-4}$  and  $\sigma = 1$  fixed, while varying the values of  $f_{\text{NL}}$  and  $g_{\text{NL}}$ . Throughout this work, we let  $\sigma = 1$  for the simplicity. Variations of  $\sigma$  may change the following numerical results, but do not change our conclusions. To visually represent our numerical results, we present the plot of  $\ell(\ell+1)\tilde{C}_\ell(\nu)$  as a function of  $\nu/\nu_*$  in Figure 12. The black solid curve corresponds to the results in the Gaussian case, where the contributions are solely due to the propagation

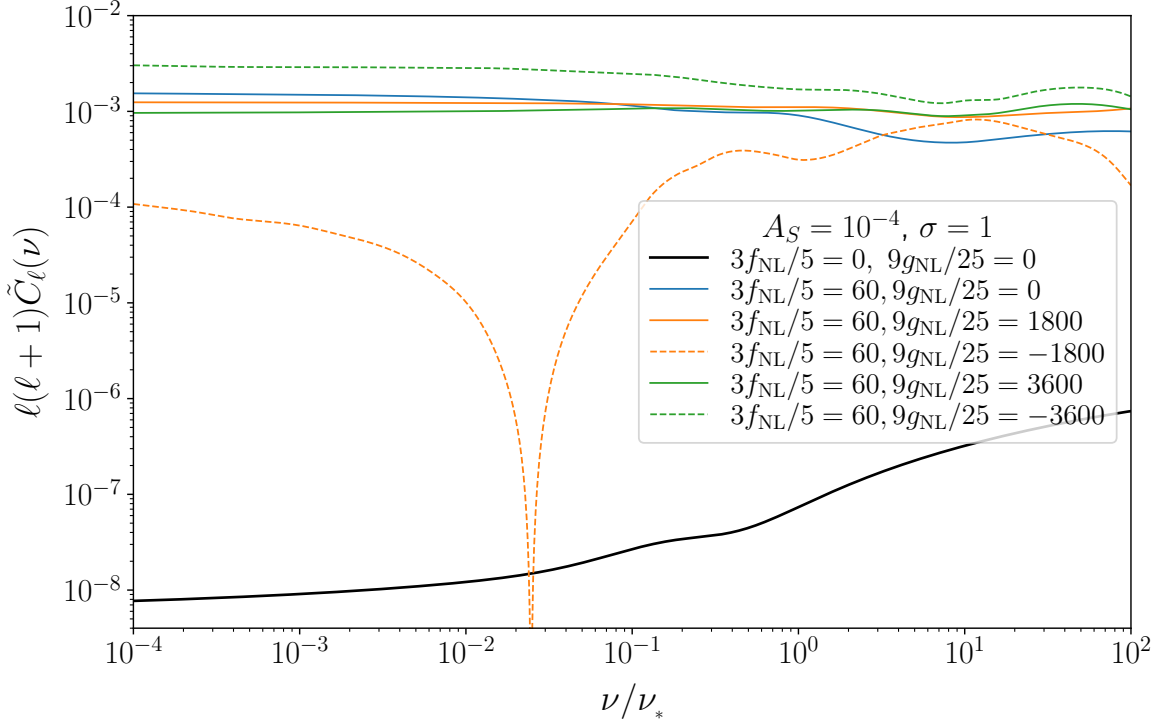


**Figure 12:** Reduced angular power spectrum for the anisotropies in SIGWs.

effects. The colored curves indicate the additional contributions from the primordial non-Gaussianity. We observe that such non-Gaussianity can generate significant anisotropies, with the spectral amplitude reaching values as high as  $\sim 10^{-3}$ . Notably, this amplitude already exceeds that of the GWBs generated by inspiralling BBHs in the LISA band, where  $\tilde{C}_\ell \lesssim \mathcal{O}(10^{-4})$  [156, 161, 197]. This suggests that the anticipated signal is comparable to these astrophysical foregrounds. Furthermore, we find that the resulting enhancement, when compared to the Gaussian case, is five orders of magnitude. In this study, we specifically focus on the parameter  $g_{\text{NL}}$ , as the parameter  $f_{\text{NL}}$  has already been extensively investigated in our previous works [25, 78]. To illustrate our findings, we fix  $3f_{\text{NL}}/5 = 60$  and vary  $g_{\text{NL}}$ . We observe that the sign of  $g_{\text{NL}}$  can significantly impact both the spectral amplitude and the spectral index.

We assess the angular power spectrum, as defined in Eq. (3.18), and present the numerical outcomes of  $\ell(\ell+1)C_\ell(\nu)$  in relation to  $\nu$  in Figure 13. We employ the same set of model parameters as depicted in Figure 6. When compared to the Gaussian scenario, the presence of primordial non-Gaussianity consistently amplifies the spectral amplitude. In this analysis, we specifically focus on  $g_{\text{NL}}$  while keeping  $3f_{\text{NL}}/5 = 5$  fixed. As demonstrated in Figure 13, the spectral amplitude for positive values of  $g_{\text{NL}}$  consistently surpasses that for negative values of  $g_{\text{NL}}$ . Furthermore, in comparison to the case of  $g_{\text{NL}} = 0$ , the spectral amplitude is suppressed (enhanced) when  $g_{\text{NL}}$  is negative but possesses a small (large) absolute value. When  $g_{\text{NL}}$  is positive, the spectral amplitude is always enhanced relative to the  $g_{\text{NL}} = 0$  scenario. Moreover, the degree of enhancement becomes more pronounced as the positive  $g_{\text{NL}}$  value increases.

As demonstrated in Refs. [25, 78], the degeneracies in the model parameters of the

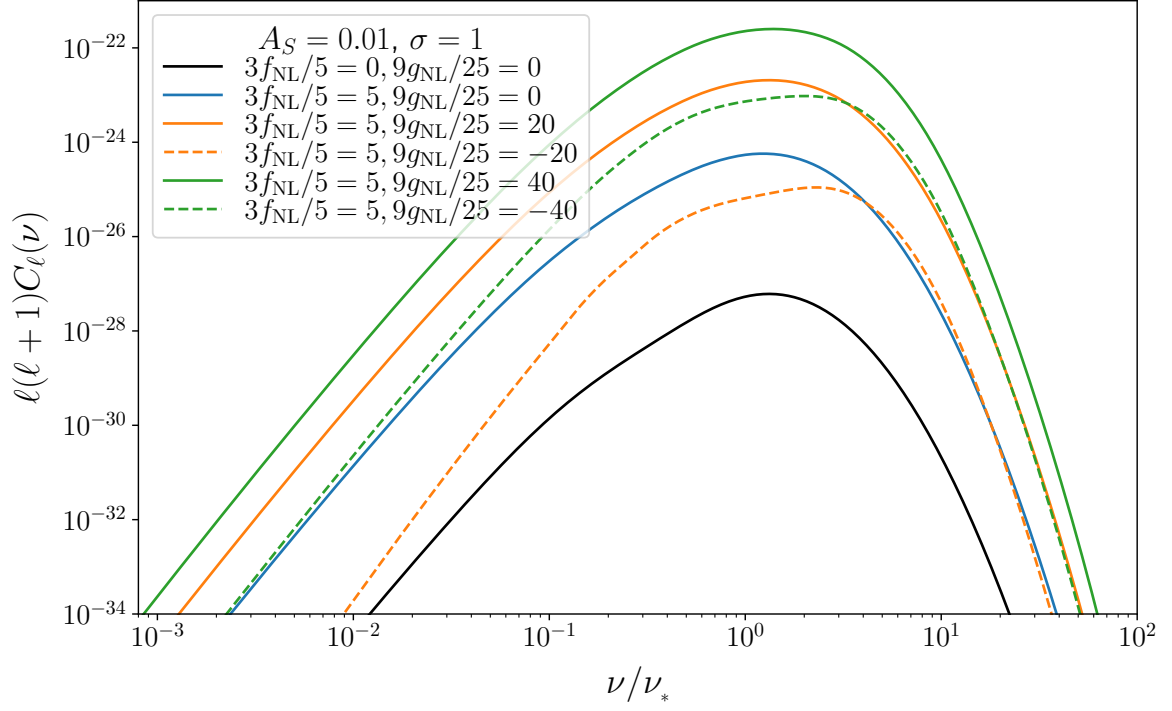


**Figure 13:** Angular power spectrum for the anisotropies in SIGWs. We use the same sets of model parameter as those of Figure 6.

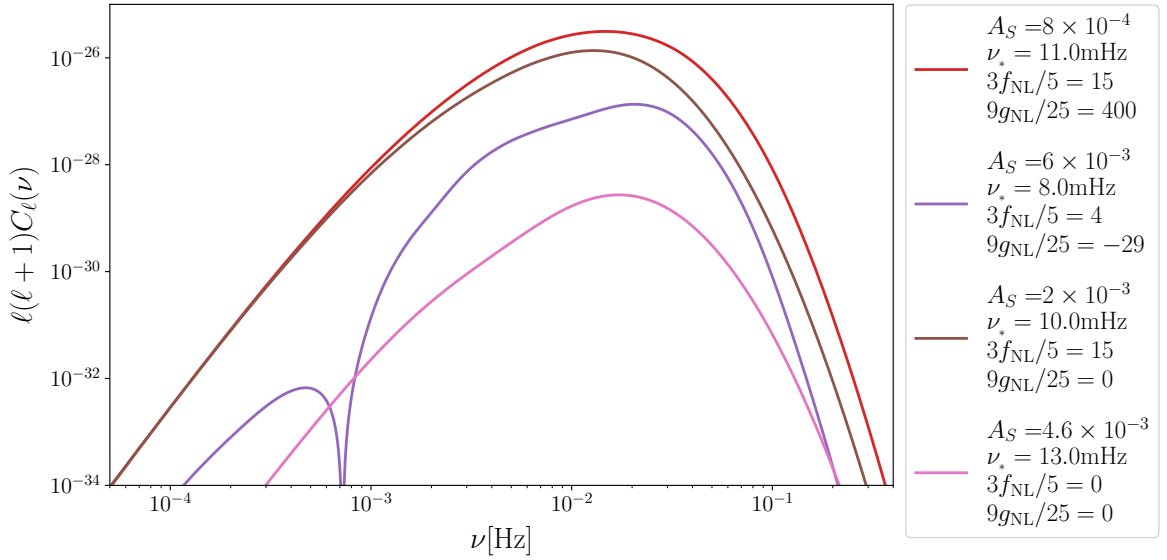


**Figure 14:** Degeneracies in the model parameters are broken by the angular power spectrum. Here, we adopt the same model parameters as those of Fig. 8, where they are shown to be degenerate for the energy-density fraction spectrum.

energy-density fraction spectrum can be overcome by considering the angular power spectrum. Figure 8 illustrates these degeneracies, as the energy-density fraction spectra appear nearly identical for four different sets of model parameters. However, Figure 14 displays the corresponding angular power spectra for the same sets of model parameters, revealing noticeable differences in both spectral amplitudes and profiles. Consequently, these previously mentioned degeneracies are explicitly broken. Thus, the angular power spectrum can be employed to determine the model parameters that cannot be individually determined based solely on the energy-density fraction spectrum.

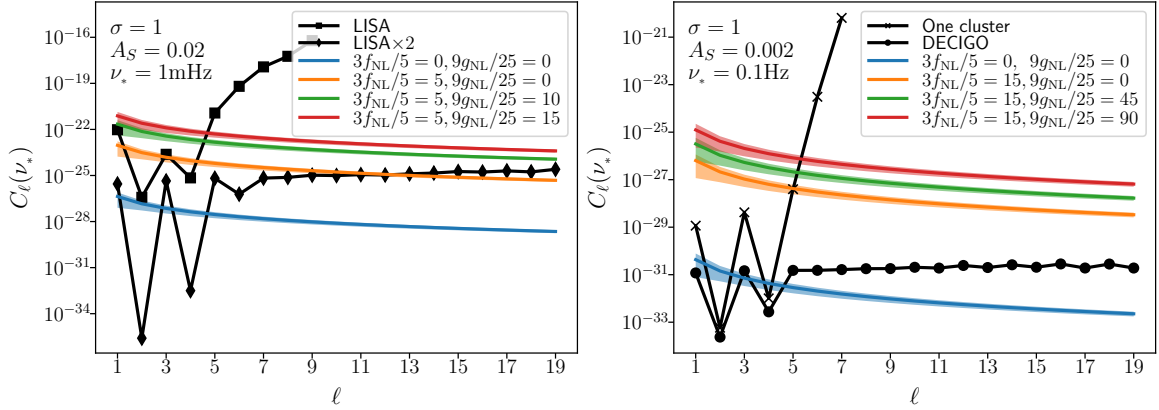


**Figure 15:** Comparison between the theoretical angular power spectra and the noise angular power spectra of LISA at the 1 milli-Hz band (left panel) [197] and DECIGO at the deci-Hz band (right panel) [197]. Shaded regions represent the uncertainties (68% confidence level) due to the cosmic variance, i.e.,  $\Delta C_\ell/C_\ell = \sqrt{2/(2\ell+1)}$ .

Our theoretical predictions regarding the angular power spectrum can potentially be tested using future GW detectors. In Figure 15, we compare the sensitivity curves of the LISA and DECIGO detectors [197] with the expected angular power spectra for values of  $A_S$  that are relevant in the context of scenarios involving the formation of PBHs (see reviews, e.g., in Ref. [60]). The frequency ranges of the SIGWs corresponding to these detectors correspond to the mass ranges of PBHs, within which PBHs could potentially account for the abundance of cold dark matter in the present Universe. Consistent with our previous work [25], we find that detector networks exhibit superior sensitivities compared to individual detectors.

We further investigate the angular power spectrum of SIGWs within the frequency band of PTA. In Figure 16, the black solid curve represents the model parameters derived from the NANOGrav 15-year (NG15) data release [74], which only considered the Gaussian case. It is noteworthy that this curve overlaps with the other two colored solid curves, which include the effects of primordial non-Gaussianity. This implies that all three sets of model parameters can be used for interpreting the observed signal [69–72]. To obtain a more precise estimation of the model parameters, we calculate the rms energy densities of SIGWs for these three sets of parameters and compare them (dashed curves) with the sensitivity curve of the Square Kilometre Array (SKA) [198] in Figure 16. Notably, there are noticeable differences in the spectral amplitudes of the rms energy densities, suggesting the potential for determining the underlying theory and model parameters accurately. Similar results can also be found in Ref. [78].

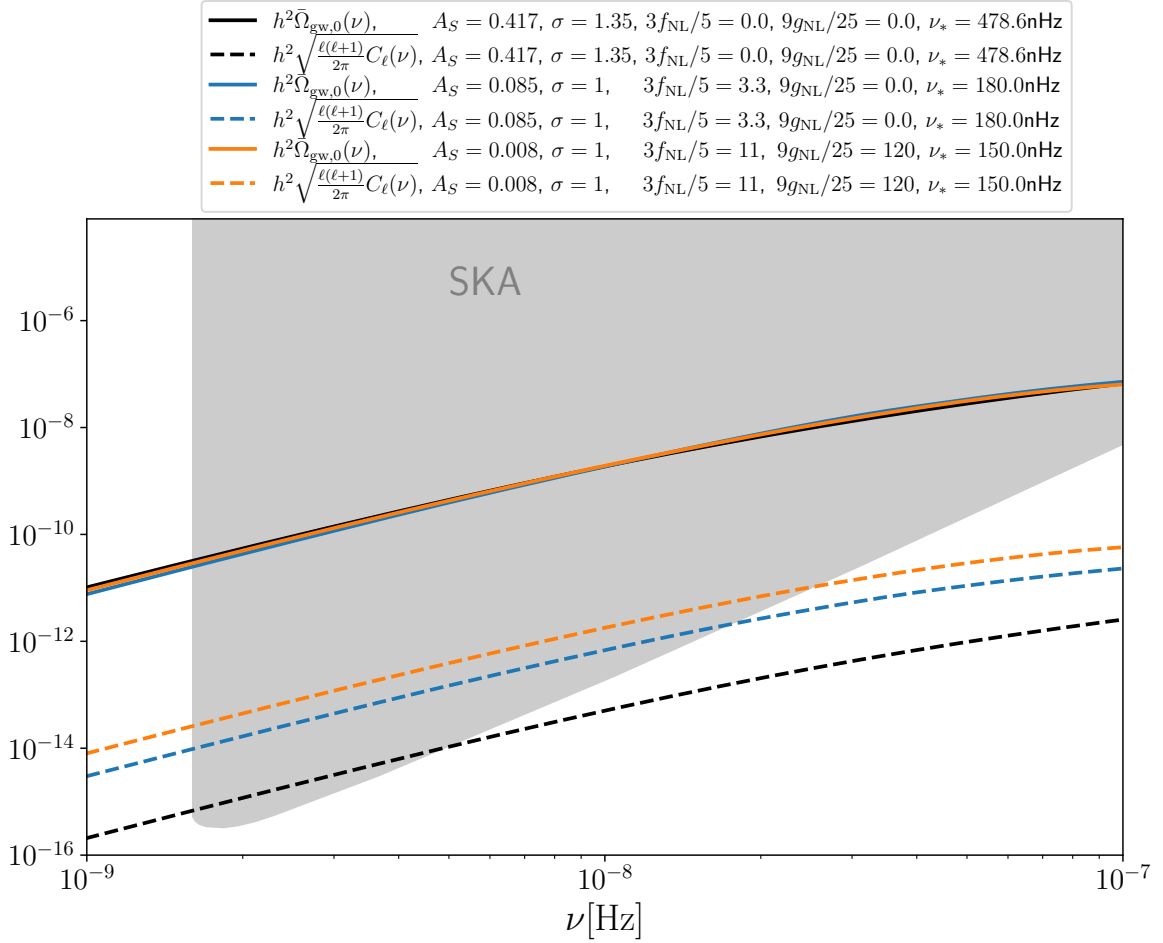


**Figure 16:** The root-mean-squared energy density for the anisotropies in SIGWs in the PTA band. Energy-density fraction spectra are displayed to compare with the NANOGrav 15-year best-fit result. Shaded region can be explored with SKA.

We also present an array of contour plots for  $\ell(\ell+1)\tilde{C}_\ell(\nu)$  in Figure 17, arranged identically to Figure 7. The dependence of the SIGW angular power spectrum on  $f_{\text{NL}}$  and  $g_{\text{NL}}$  can be easily observed from this array. It is noted that the magnitude of the reduced angular power spectrum decreases with an increase in  $A_S$ . For the case of  $A_S \leq 10^{-3}$ , when  $f_{\text{NL}}$  takes a nearly-zero value regardless of the value of  $g_{\text{NL}}$ , or when  $g_{\text{NL}}$  takes a small value with minus sign regardless of the value of  $f_{\text{NL}}$ ,  $\tilde{C}_\ell(\nu)$  reaches the minimum value of 0, which implies that the anisotropies in SIGW vanish at the corresponding frequency band. Moreover, each panel for such a value of  $A_S$  reveals that the SIGW anisotropies are more significant for a large negative  $g_{\text{NL}}$  than a positive one. Otherwise, if  $A_S$  takes a larger value, the magnitude of  $\tilde{C}_\ell(\nu)$  becomes larger when the signs of  $f_{\text{NL}}$  and  $g_{\text{NL}}$  are the same, especially in the high-frequency range.

Additional information about the anisotropies in SIGWs may be concealed within the cross-correlated angular power spectrum. This spectrum, defined as  $\langle \delta_{\text{gw},0,\ell m}(2\pi\nu) \delta_{\text{gw},0,\ell' m'}^*(2\pi\nu') \rangle = \delta_{\ell\ell'} \delta_{mm'} \tilde{C}_\ell(\nu, \nu')$ , describes the correlation between two different frequency bands. However, this definition is somewhat redundant. Therefore, we propose a redefinition of the cross-



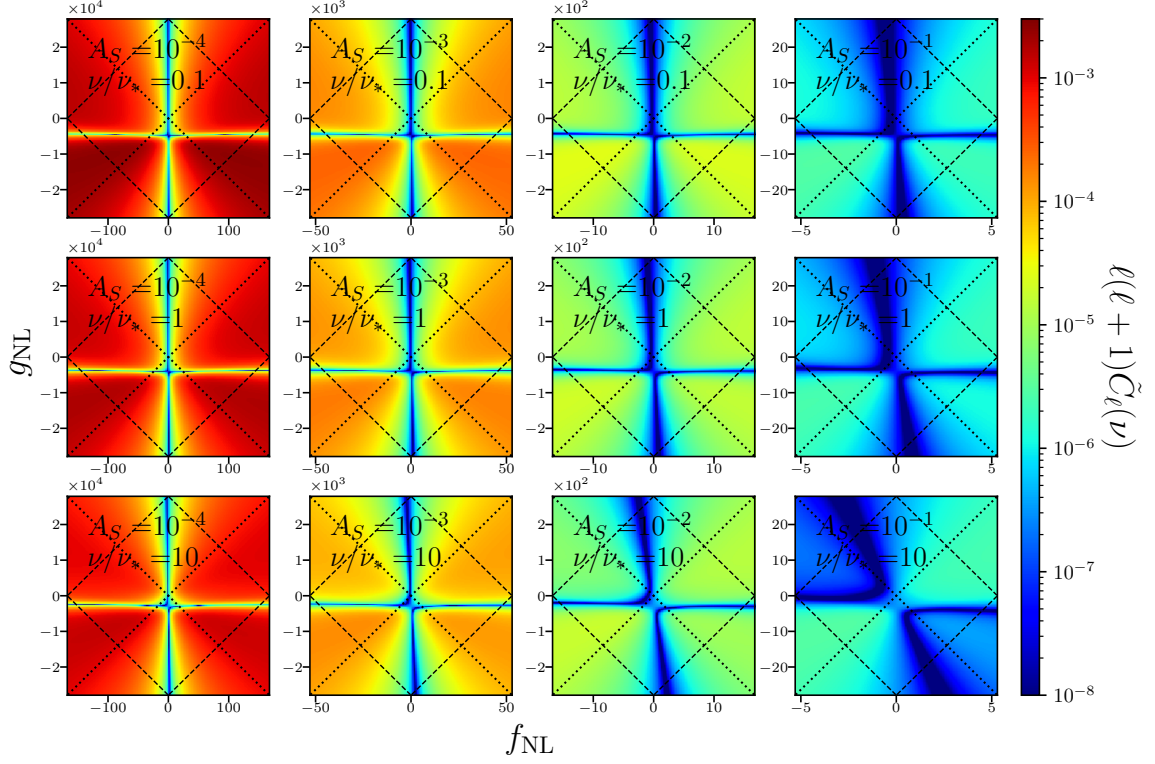


**Figure 17:** Reduced angular power spectrum of SIGWs with respect to the primordial non-Gaussian parameters  $f_{\text{NL}}$  and  $g_{\text{NL}}$ . The conventions for the dotted and dashed lines are the same as those in Figure 7.

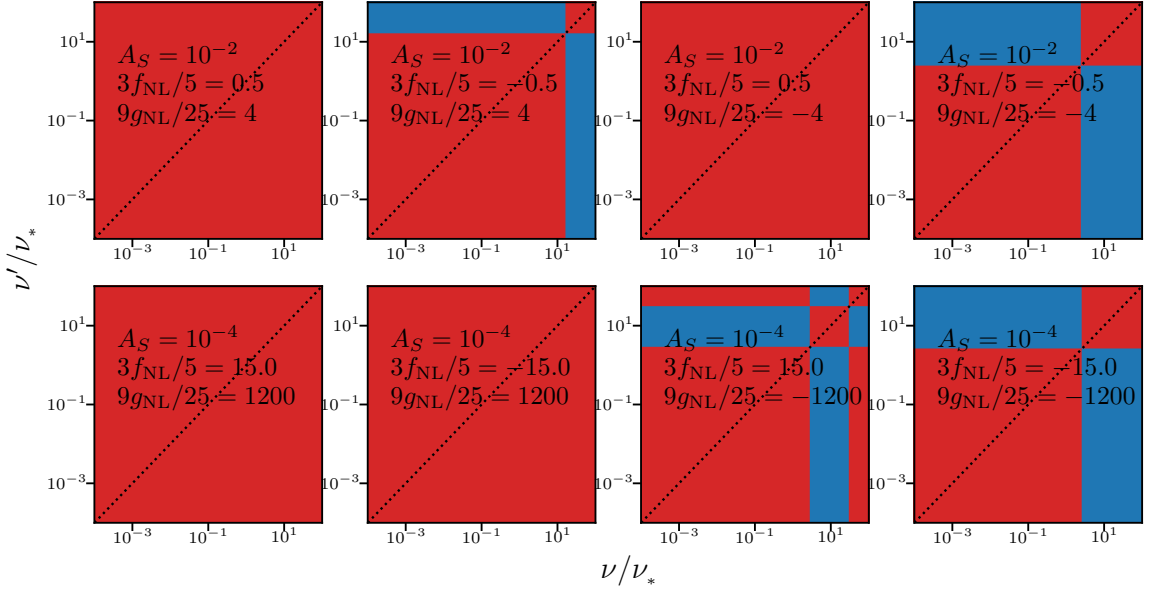


**Figure 18:** Correlation factor in red color for  $r_\ell(\nu, \nu') = +1$  and blue color for  $r_\ell(\nu, \nu') = -1$ .

correlation as a correlation factor,  $r_\ell(\nu, \nu') = \tilde{C}_\ell(\nu, \nu') / \sqrt{\tilde{C}_\ell(\nu)\tilde{C}_\ell(\nu')}$ , where  $\pm 1$  represents the sign depending on the frequency bands. In Figure 18, we illustrate the impact of primordial non-Gaussianity on  $r_\ell(\nu, \nu')$  in the  $\nu - \nu'$  plane. The red shaded regions indicate  $r_\ell = +1$ , while the blue shaded regions represent  $r_\ell = -1$ .

## 4 Discussion and Conclusion

In this study, we have undertaken the first complete analysis of the energy-density fraction spectrum and the angular power spectrum of SIGWs. Notably, we have incorporated the local-type primordial non-Gaussianity parameterized by  $f_{\text{NL}}$  and  $g_{\text{NL}}$  simultaneously, marking a significant advancement in our understanding of these phenomena.

By utilizing a Feynman-like diagrammatic technique, we have delved into the noteworthy effects of  $f_{\text{NL}}$  and  $g_{\text{NL}}$  on the energy-density fraction spectrum of SIGWs. Through a thorough consideration of all relevant Feynman-like diagrams, we have established a comprehensive dictionary that correlates each diagram with its corresponding contribution to this spectrum. For the first time, we have successfully derived semi-analytic formulas for the energy-density fraction spectrum by systematically evaluating the contributions from these diagrams in a hierarchical manner. Our numerical analysis reveals that non-Gaussianity has a significant impact on both the amplitude and shape of the SIGWs spectrum, contingent upon the specific levels and functional forms of the non-Gaussianity. This arises from the fact that the non-Gaussianity of the primordial curvature perturbations introduces additional contributions to the energy-density fraction spectrum.

We have anticipated that the energy-density fraction spectrum of SIGWs can be experimentally tested in the future using space-borne GW detector networks and PTA experiments. In particular, we have shown that the recent strong evidence for GWB reported by PTA collaborations can be explained by this theory. Furthermore, we have demonstrated the significant degeneracies in the model parameters, specifically the non-Gaussian parameters  $f_{\text{NL}}$  and  $g_{\text{NL}}$ , which pose notable challenges in determining these parameters.

For the first time, we have conducted a comprehensive analysis of the inhomogeneities and anisotropies in SIGWs, incorporating both the  $f_{\text{NL}}$  and  $g_{\text{NL}}$  effects. The presence of primordial non-Gaussianity can induce anisotropies in SIGWs. In this study, we have taken into account both the initial inhomogeneities and the propagation effects. Interestingly, we have found that the propagation effects in SIGWs are identical to those observed in CMB. However, while the initial inhomogeneities vanish for the CMB, they persist for SIGWs and reach the Earth in the present day. To explore the properties of the initial inhomogeneities, we employed a Feynman-like diagrammatic technique, which involved dealing with a multitude of complex diagrams. Nevertheless, we have developed systematic approaches to simplify our analytic evaluation. Specifically, we have identified all the Feynman-like diagrams that allow for the modulation of energy densities. In other words, we have focused on the diagrams that involve couplings between short-wavelength and long-wavelength modes when evaluating the initial inhomogeneities.

We have successfully derived the formulae for the angular power spectrum of SIGWs. From our analysis, we have discovered a universal characteristic of this spectrum, namely, the multipole dependence of the form  $C_\ell \propto [\ell(\ell + 1)]^{-1}$ . This multipole dependence has the potential to distinguish SIGWs from other sources of GWBs, which may exhibit distinct multipole dependencies. Our numerical results have revealed significant influences of  $f_{\text{NL}}$  and  $g_{\text{NL}}$  on the angular power spectrum. In particular, we have observed enhancements of the

spectral amplitude by several orders of magnitude. Furthermore, we have found that large anisotropies in SIGWs can be generated. This suggests promising prospects for detection and potential differentiation from other sources of GWBs. The sign of  $g_{\text{NL}}$  has been shown to have a significant impact on both the spectral amplitude and index. Moreover, we have demonstrated that the angular power spectrum can explicitly break the degeneracies in the model parameters. This exciting result highlights the potential of the angular power spectrum as a powerful probe of the early-Universe physics that would otherwise remain unexplored.

We anticipate that the angular power spectrum predictions will undergo testing through space-borne GW detector networks [129–139, 197, 199] and PTA detectors [116–119, 200–205]. Such tests would not only provide new insights into the early-Universe physics but also into the nature of dark matter. For example, SIGWs of the LISA band could be a potential probe of scenarios involving asteroid-mass PBHs, which have the potential to account for all cold dark matter. Future measurements of the angular power spectrum in the PTA band, such as those from the SKA program, are expected to reveal the origins of the recent PTA signal. This would be particularly promising in terms of identifying the underlying theory, such as the theory of SIGWs, and its relevant parameters.

Our investigation of SIGWs also has significant implications for exploring scenarios involving PBHs, which are hypothesized to be a possible candidate for cold dark matter and a potential source of the individual GW events observed by the LIGO, Virgo, and KAGRA [206–210]. In fact, the presence of primordial non-Gaussianity has a notable impact on the abundance and mass distribution of PBHs, as the threshold for their formation can be influenced by the levels and specific forms of these non-Gaussianity. Furthermore, due to the coupling between short-wavelength and long-wavelength modes, they can induce a more clustered distribution of PBHs compared to the Gaussian case. This clustering effect could enhance the rate of binary PBH formation, resulting in a higher local merger rate that can potentially explain the observed individual GW events.

Overall, the existence of primordial non-Gaussianity can have significant implications for both the energy-density fraction spectrum and the angular power spectrum of SIGWs. Conversely, a thorough examination of the two spectra can provide valuable insights into the primordial curvature perturbations, the nature of PBH dark matter, and the physics of the early Universe, particularly the inflation models. Moreover, by employing the Feynman-like diagrammatic technique, it becomes straightforward to verify the correctness of the findings presented in this paper and make comparisons with results from other studies.

Finally, we highlight that our research approach can be easily extended to study contributions of primordial non-Gaussianity to the angular bispectrum and trispectrum of SIGWs, which have been comprehensively analyzed in Ref. [211]. Furthermore, it can be straightforwardly generalized to investigate impacts of higher-order non-Gaussianity on SIGWs, which are left to our future works.

## Acknowledgments

We acknowledge Profs. Bin Gong, Tao Liu, Yi Wang, and Mr. Yan-Heng Yu for helpful discussion. S.W. and J.P.L. are partially supported by the National Natural Science Foundation of China (Grant No. 12175243), the National Key R&D Program of China No. 2023YFC2206403, the Science Research Grants from the China Manned Space Project with No. CMS-CSST-2021-B01, and the Key Research Program of the Chinese Academy of Sciences (Grant No. XDPB15). Z.C.Z. is supported by the National Key Research and De-

velopment Program of China Grant No. 2021YFC2203001 and the National Natural Science Foundation of China (Grant NO. 12005016). K.K. is supported by KAKENHI Grant No. JP22H05270.

## A Equation of Motion

We consider the perturbed spatially-flat Friedmann-Robertson-Walker (FRW) spacetime in the conformal Newtonian gauge. The metric thus reads

$$ds^2 = a^2(\eta) \left\{ -(1 + 2\Phi)d\eta^2 + \left[ (1 - 2\Phi)\delta_{ij} + \frac{1}{2}h_{ij} \right] dx^i dx^j \right\}, \quad (\text{A.1})$$

where  $\Phi(\eta, \mathbf{x})$  denotes the linear scalar perturbations, and  $h_{ij}(\eta, \mathbf{x})$  stands for the transverse-traceless tensor perturbations induced by  $\Phi(\eta, \mathbf{x})$ , i.e., the SIGWs. The conformal Hubble parameter  $\mathcal{H}(\eta)$  is defined as  $\mathcal{H}(\eta) = \partial_\eta a/a$ , which equals to  $1/\eta$  during radiation domination especially.

The evolution of  $\Phi(\eta, \mathbf{q})$  is governed by a master equation derived from the first-order Einstein's equation. In the absence of entropy perturbations, the explicit form of the master equation reads [212]

$$\partial_\eta^2 \Phi + 3\mathcal{H} \left( 1 + c_s^2 \right) \partial_\eta \Phi + 3 \left( c_s^2 - w \right) \mathcal{H}^2 \Phi + c_s^2 q^2 \Phi = 0, \quad (\text{A.2})$$

where  $c_s^2$  denotes the speed of sound. For the above linear differential equation,  $\Phi(\eta, \mathbf{q})$  can be connected to the primordial (comoving) curvature perturbations  $\zeta(\mathbf{q})$  through the scalar transfer function  $T(q\eta)$ , i.e.,

$$\Phi(\eta, \mathbf{q}) = \left( \frac{3 + 3w}{5 + 3w} \right) T(q\eta) \zeta(\mathbf{q}), \quad (\text{A.3})$$

where  $w$  is the equation-of-state parameter of the Universe. In the case of radiation domination with  $w = c_s^2 = 1/3$ , the master equation can be solved to obtain the transfer function  $T(q\eta)$ . By substituting Eq. (A.3) into Eq. (A.2), we get the solution for  $T(q\eta)$ , i.e.,

$$T(x) = \frac{9}{x^2} \left[ \frac{\sin(x/\sqrt{3})}{x/\sqrt{3}} - \cos(x/\sqrt{3}) \right], \quad (\text{A.4})$$

where we denote  $x = q\eta$  for brevity.

The evolution of  $h_{ij}(\eta, \mathbf{q})$  is governed by an equation of motion, which arises from the spatial components of Einstein's equation at second order, i.e., [14, 15]

$$\partial_\eta^2 h_\lambda(\eta, \mathbf{q}) + 2\mathcal{H} \partial_\eta h_\lambda(\eta, \mathbf{q}) + q^2 h_\lambda(\eta, \mathbf{q}) = 4S_\lambda(\eta, \mathbf{q}), \quad (\text{A.5})$$

where  $S_\lambda(\eta, \mathbf{q})$  represents the source term quadratic in the scalar perturbations  $\Phi$ , i.e.,

$$\begin{aligned} \mathcal{S}_\lambda(\eta, \mathbf{q}) = & \int \frac{d^3 \mathbf{q}_a}{(2\pi)^{3/2}} \epsilon_{ij}^\lambda(\mathbf{q}) q_a^i q_a^j \left\{ 2\Phi(\eta, \mathbf{q} - \mathbf{q}_a) \Phi(\eta, \mathbf{q}_a) \right. \\ & \left. + \frac{4}{3(1+w)\mathcal{H}^2} [\partial_\eta \Phi(\eta, \mathbf{q} - \mathbf{q}_a) + \mathcal{H} \Phi(\eta, \mathbf{q} - \mathbf{q}_a)] [\partial_\eta \Phi(\eta, \mathbf{q}_a) + \mathcal{H} \Phi(\eta, \mathbf{q}_a)] \right\}. \end{aligned} \quad (\text{A.6})$$

Following the Green's function method [16, 17], the solution to Eq. (A.5) is formally given by

$$a(\eta) h_\lambda(\eta, \mathbf{q}) = 4 \int^\eta d\eta' G_{\mathbf{q}}(\eta, \eta') a(\eta') \mathcal{S}_\lambda(\eta', \mathbf{q}). \quad (\text{A.7})$$

Here, the Green's function  $G_{\mathbf{q}}(\eta, \eta')$  satisfies the differential equation of the form

$$\partial_{\eta}^2 G_{\mathbf{q}}(\eta, \eta') + \left[ q^2 - \frac{\partial_{\eta}^2 a(\eta)}{a(\eta)} \right] G_{\mathbf{q}}(\eta, \eta') = \delta(\eta - \eta') , \quad (\text{A.8})$$

for which the solution during radiation domination is given by

$$G_{\mathbf{q}}(\eta, \eta') = \Theta(\eta - \eta') \frac{\sin[q(\eta - \eta')]}{q} , \quad (\text{A.9})$$

with  $\Theta(x)$  being the Heaviside function with variable  $x$ .

To get Eq. (2.6), we need to reformulate  $\mathcal{S}_{\lambda}(\eta, \mathbf{q})$  of Eq. (A.7). Following Eq. (A.6), we immediately get

$$\mathcal{S}_{\lambda}(\eta, \mathbf{q}) = \int \frac{d^3 \mathbf{q}_a}{(2\pi)^{3/2}} q^2 Q_{\lambda}(\mathbf{q}, \mathbf{q}_a) F(|\mathbf{q} - \mathbf{q}_a|, q_a, \eta) \zeta(\mathbf{q}_a) \zeta(\mathbf{q} - \mathbf{q}_a) , \quad (\text{A.10})$$

where Eq. (A.3) has been used. Here, we have introduced the projection factor of the form

$$Q_{\lambda}(\mathbf{q}, \mathbf{q}_i) = \epsilon_{ij}^{\lambda}(\mathbf{q}) \frac{q_a^i q_a^j}{q^2} = \frac{\sin^2 \theta}{\sqrt{2}} \times \begin{cases} \cos(2\phi_i) & \lambda = + \\ \sin(2\phi_i) & \lambda = \times \end{cases} , \quad (\text{A.11})$$

where  $\theta$  denotes the separation angle between  $\mathbf{q}$  and  $\mathbf{q}_i$ , while  $\phi_i$  is the azimuthal angle of  $\mathbf{q}_i$  when  $\mathbf{q}$  is aligned with the  $\mathbf{z}$  axis. We also have introduced a functional of the form

$$F(p_a, q_a, \eta) = \frac{4}{3} T(p_a \eta) T(q_a \eta) + \frac{4\eta^2}{9} \partial_{\eta} T(p_a \eta) \partial_{\eta} T(q_a \eta) + \frac{4\eta}{9} \partial_{\eta} [T(p_a \eta) T(q_a \eta)] , \quad (\text{A.12})$$

where we denote  $p_a = |\mathbf{q} - \mathbf{q}_a|$ . By substituting Eq. (A.10) into Eq. (A.7), and introducing a kernel function of the form

$$\hat{I}(|\mathbf{q} - \mathbf{q}_a|, q_a, \eta) = \int^{\eta} d\eta' q^2 G_{\mathbf{q}}(\eta, \eta') \frac{a(\eta')}{a(\eta)} F(|\mathbf{q} - \mathbf{q}_a|, q_a, \eta') , \quad (\text{A.13})$$

we can thus express  $h_{\lambda}$  in terms of  $Q_{\lambda}$ ,  $\hat{I}$ , and  $\zeta$ , namely,

$$\begin{aligned} h_{\lambda}(\eta, \mathbf{q}) &= 4 \int^{\eta} d\eta' G_{\mathbf{q}}(\eta, \eta') \frac{a(\eta')}{a(\eta)} \int \frac{d^3 \mathbf{q}_a}{(2\pi)^{3/2}} q^2 Q_{\lambda}(\mathbf{q}, \mathbf{q}_a) F(|\mathbf{q} - \mathbf{q}_a|, q_a, \eta) \zeta(\mathbf{q}_a) \zeta(\mathbf{q} - \mathbf{q}_a) \\ &= 4 \int \frac{d^3 \mathbf{q}_a}{(2\pi)^{3/2}} \zeta(\mathbf{q}_a) \zeta(\mathbf{q} - \mathbf{q}_a) Q_{\lambda}(\mathbf{q}, \mathbf{q}_a) \hat{I}(|\mathbf{q} - \mathbf{q}_a|, q, \eta) . \end{aligned} \quad (\text{A.14})$$

This is exactly the expression of Eq. (2.6).

## B Numerical integrals

To evaluate  $\bar{\Omega}_{\text{gw}}^X(\eta, q)$  in Eq. (2.14), we seek to rephrase the corresponding integrals in Section 2 in a form that is more amenable to numerical calculations. Here, we calculate the unscaled components of energy-density fraction spectrum, which are still labeled with  $\bar{\Omega}_{\text{gw}}^X(\eta, q)$  in this Appendix. This is equivalent to fixing the model parameters, i.e.,  $A_S = 1$ ,  $3f_{\text{NL}}/5 = 1$ , and  $9g_{\text{NL}}/25 = 1$ . Following Table 2, the eventual results can be straightforwardly recovered

via multiplying the unscaled results by  $(3/5)^{2(a+b)} f_{\text{NL}}^{2a} g_{\text{NL}}^b A_S^{a+b+2}$ , where  $a$  and  $b$  denote the powers of these components in  $f_{\text{NL}}$  and  $g_{\text{NL}}$ , respectively.

By substituting Eqs. (2.19 – 2.27) into Table 1 and further substituting the results into Eq. (2.13), we can express Eq. (2.14) as follows

$$\frac{\bar{\Omega}_{\text{gw}}^X(\eta, q)}{\text{S.F.}} = \frac{q^5 \eta^2}{16\pi^2} \left\{ \prod_i \int \frac{d^3 \mathbf{q}_i}{(2\pi)^3} \right\} \left\{ \prod P^{[\dots]} \right\} \times \left\{ \sum_{\lambda=+, \times} Q_\lambda(\mathbf{q}, \mathbf{q}_1) Q_\lambda(\mathbf{q}, \mathbf{q}_j) \hat{I}(|\mathbf{q} - \mathbf{q}_1|, q_1, \eta) \hat{I}(|\mathbf{q} - \mathbf{q}_j|, q_j, \eta) \right\}, \quad (\text{B.1})$$

where we have  $i = 1, \dots, n$  with  $n \leq 5$  being the order of integration,  $j = 1, 2$ , and  $\prod P^{[\dots]}$  stands for products of power spectra in Eqs. (2.19 – 2.27). In the following, we evaluate the terms in the three pairs of braces on the right hand side of Eq. (B.1), respectively.

For the first brace, we transform the variables of integration into five sets of new variables  $(u_i, v_i)$  with  $i = 1, 2, 3, 4, 5$ , namely,

$$v_i = \frac{q_i}{q}, \quad u_i = \frac{|\mathbf{q} - \mathbf{q}_i|}{q}. \quad (\text{B.2})$$

We further convert the integration regions into rectangle ones via introducing the variable transformation as follows

$$s_i = u_i - v_i, \quad t_i = u_i + v_i - 1. \quad (\text{B.3})$$

Hence, the first brace transforms to the following form

$$\prod_i \int \frac{d^3 \mathbf{q}_i}{(2\pi)^3} = \frac{q^3}{2(2\pi)^3} \prod_i \left( \int_0^\infty dt_i \int_{-1}^1 ds_i v_i u_i \int_0^{2\pi} d\phi_i \right), \quad (\text{B.4})$$

where  $\phi_i$  is defined below Eq. (A.11).

For the second brace, we show the expressions of  $P^{[1]}(q)$ ,  $P^{[2]}(q)$ ,  $P^{[3]}(q)$ , and the variable transformations concerned with them. Based on Eq. (2.12), we represent the unscaled  $P^{[1]}$  (or equivalently  $P_{gS}$ ) as follows

$$P^{[1]}(q) = \frac{2\pi^2}{q^3} \Delta_S^2(q) = \frac{2\pi^2}{q^3} \frac{1}{\sqrt{2\pi\sigma^2}} \exp\left(-\frac{\ln^2(q/q_*)}{2\sigma^2}\right). \quad (\text{B.5})$$

We further express the unscaled  $P^{[2]}$  and  $P^{[3]}$  as follows

$$P^{[2]}(q) = \int \frac{d^3 \tilde{\mathbf{q}}_1}{(2\pi)^3} P^{[1]}(\tilde{q}_1) P^{[1]}(|\mathbf{q} - \tilde{\mathbf{q}}_1|) = \frac{\pi^2}{2q^3} \int_0^\infty d\tilde{t}_1 \int_{-1}^1 d\tilde{s}_1 \frac{\Delta_S^2(\tilde{v}_1 q) \Delta_S^2(\tilde{u}_1 q)}{(\tilde{v}_1 \tilde{u}_1)^2}, \quad (\text{B.6})$$

$$P^{[3]}(q) = \int \frac{d^3 \tilde{\mathbf{q}}_1}{(2\pi)^3} P^{[2]}(\tilde{q}_1) P^{[1]}(|\mathbf{q} - \tilde{\mathbf{q}}_1|) = \frac{\pi^2}{8q^3} \prod_{i=1,2} \left( \int_0^\infty d\tilde{t}_i \int_{-1}^1 d\tilde{s}_i \right) \frac{\Delta_S^2(\tilde{u}_1 q) \Delta_S^2(\tilde{v}_1 \tilde{v}_2 q) \Delta_S^2(\tilde{v}_1 \tilde{u}_2 q)}{(\tilde{v}_1 \tilde{u}_1 \tilde{v}_2 \tilde{u}_2)^2}, \quad (\text{B.7})$$

where we have introduced the transformation of variables  $(\tilde{v}_1, \tilde{u}_1)$  and  $(\tilde{v}_2, \tilde{u}_2)$  of the form

$$\begin{aligned} \tilde{v}_1 &= \frac{\tilde{q}_1}{q}, & \tilde{u}_1 &= \frac{|\mathbf{q} - \tilde{\mathbf{q}}_1|}{q}, \\ \tilde{v}_2 &= \frac{\tilde{q}_2}{\tilde{q}_1}, & \tilde{u}_2 &= \frac{|\tilde{\mathbf{q}}_1 - \tilde{\mathbf{q}}_2|}{\tilde{q}_1}, \end{aligned}$$

and the transformations from  $(\tilde{u}_i, \tilde{v}_i)$  to two sets of new variables  $(\tilde{s}_i, \tilde{t}_i)$  with  $i = 1, 2$  are similar to Eq. (B.3), i.e.,  $\tilde{s}_i = \tilde{u}_i - \tilde{v}_i$ ,  $\tilde{t}_i = \tilde{u}_i + \tilde{v}_i - 1$ . Since the above integrals involve inner products of  $\mathbf{q}_i$  and  $\mathbf{q}_j$ , it is convenient to introduce a new quantity, i.e.,

$$y_{ij} = \frac{\mathbf{q}_i \cdot \mathbf{q}_j}{q^2} = \frac{\cos \varphi_{ij}}{4} \sqrt{t_i(t_i + 2)(1 - s_i^2)t_j(t_j + 2)(1 - s_j^2)} + \frac{1}{4}[1 - s_i(t_i + 1)][1 - s_j(t_j + 1)] , \quad (\text{B.8})$$

where we denote  $\varphi_{ij} = \phi_i - \phi_j$  for the sake of brevity. We further introduce two new quantities of the form

$$w_{ij} = \frac{|\mathbf{q}_i - \mathbf{q}_j|}{q} = \sqrt{v_i^2 + v_j^2 - 2y_{ij}} , \quad (\text{B.9})$$

$$w_{ijk} = \frac{|\mathbf{q}_i + \mathbf{q}_j - \mathbf{q}_k|}{q} = \sqrt{v_i^2 + v_j^2 + v_k^2 + 2y_{ij} - 2y_{ik} - 2y_{jk}} . \quad (\text{B.10})$$

Consequently, all the variables of  $P^{[\dots]}$  in Eqs. (2.19 – 2.27) can be expressed in terms of  $v_i q$ ,  $u_i q$ ,  $w_{ij} q$  or  $w_{ijk} q$ .

For the third brace, we first recast the kernel function  $\hat{I}(|\mathbf{q} - \mathbf{q}_i|, q_i, \eta)$  during radiation domination into  $I_{\text{RD}}(u_i, v_i, x)$  with  $x = q\eta$ , namely,

$$\hat{I}(|\mathbf{q} - \mathbf{q}_i|, q_i, \eta) = I_{\text{RD}}\left(\frac{|\mathbf{q} - \mathbf{q}_i|}{q}, \frac{q_i}{q}, q\eta\right) = I_{\text{RD}}(u_i, v_i, x) , \quad (\text{B.11})$$

which can be straightforwardly derived from Eq. (A.13). As demonstrated in Refs. [16, 17], the analytical formula for  $I(u_i, v_i, x)$  on subhorizon scales, i.e.,  $x \gg 1$ , can be expressed as follows

$$I_{\text{RD}}(u_i, v_i, x \gg 1) = \frac{1}{x} I_A(u_i, v_i) [I_B(u_i, v_i) \sin x - \pi I_C(u_i, v_i) \cos x] , \quad (\text{B.12a})$$

$$I_A(u_i, v_i) = \frac{3(u_i^2 + v_i^2 - 3)}{4u_i^3 v_i^3} , \quad (\text{B.12b})$$

$$I_B(u_i, v_i) = -4u_i v_i + (u_i^2 + v_i^2 - 3) \ln \left| \frac{3 - (u_i + v_i)^2}{3 - (u_i - v_i)^2} \right| , \quad (\text{B.12c})$$

$$I_C(u_i, v_i) = (u_i^2 + v_i^2 - 3) \Theta(u_i + v_i - \sqrt{3}) . \quad (\text{B.12d})$$

Moreover, the oscillation average of two kernel functions with the same  $x$  is shown as [23]

$$\overline{I_{\text{RD}}(u_i, v_i, x \gg 1) I_{\text{RD}}(u_j, v_j, x \gg 1)} = \frac{I_A(u_i, v_i) I_A(u_j, v_j)}{2x^2} \left[ I_B(u_i, v_i) I_B(u_j, v_j) + \pi^2 I_C(u_i, v_i) I_C(u_j, v_j) \right] . \quad (\text{B.13})$$

Combining the kernel function with the projection factor, we can introduce a new function for simplifying our evaluation, i.e.,

$$J(u_i, v_i, x) = \frac{x}{8} [(v_i + u_i)^2 - 1] [1 - (v_i - u_i)^2] I_{\text{RD}}(u_i, v_i, x) , \quad (\text{B.14})$$

where  $Q_\lambda(\mathbf{q}, \mathbf{q}_i)$  is shown in Eq. (A.11) and  $I_{\text{RD}}(u_i, v_i, x \gg 1)$  is shown in Eq. (B.12). After explicit computation, we get the following relations

$$\sum_\lambda Q_\lambda^2(\mathbf{q}, \mathbf{q}_1) \overline{\hat{I}^2(|\mathbf{q} - \mathbf{q}_1|, q_1, \eta)} = \frac{1}{x^2} \overline{J^2(u_1, v_1, x)} , \quad (\text{B.15})$$



$$\sum_{\lambda} Q_{\lambda}(\mathbf{q}, \mathbf{q}_1) Q_{\lambda}(\mathbf{q}, \mathbf{q}_2) \overline{\hat{I}(|\mathbf{q} - \mathbf{q}_1|, q_1, \eta) \hat{I}(|\mathbf{q} - \mathbf{q}_2|, q_2, \eta)} = \frac{\cos(2\varphi_{12})}{x^2} \overline{J(u_1, v_1, x) J(u_2, v_2, x)} . \quad (\text{B.16})$$

## C Boltzmann equation

To derive the present density contrast  $\delta_{\text{gw},0}$  in Eq. (3.6), we review the Boltzmann equation for gravitons following Refs. [150–152]. We decompose the distribution function  $f(\eta', \mathbf{x}, \mathbf{q})$  for gravitons into a background  $\bar{f}(\eta', q)$  and perturbations  $\Gamma(\eta', \mathbf{x}, \mathbf{q})$ , namely,

$$f(\eta', \mathbf{x}, \mathbf{q}) = \bar{f}(\eta', q) - q \frac{\partial \bar{f}}{\partial q} \Gamma(\eta', \mathbf{x}, \mathbf{q}) . \quad (\text{C.1})$$

The evolution of  $f(\eta', \mathbf{x}, \mathbf{q})$  follows the Boltzmann equation, i.e.,

$$\frac{df}{d\eta'} = \mathcal{I}(f) + \mathcal{C}(f) , \quad (\text{C.2})$$

where  $\mathcal{I}$  denotes the emissivity term and  $\mathcal{C}$  stands for the collision term. For gravitons, the collision term is negligible, i.e.,  $\mathcal{C} = 0$  [21, 22, 150]. For cosmological sources, the emissivity term is treated as the initial condition, implying  $\mathcal{I} = 0$  [151, 152]. Therefore, the Boltzmann equation is expressed as

$$\frac{df}{d\eta'} = \frac{\partial f}{\partial \eta'} + \frac{\partial f}{\partial x^i} \frac{dx^i}{d\eta'} + \frac{\partial f}{\partial q} \frac{dq}{d\eta'} + \frac{\partial f}{\partial n^i} \frac{dn^i}{d\eta'} = 0 . \quad (\text{C.3})$$

To calculate the Boltzmann equation up to first order, we adopt relations of  $dx^i/d\eta' = n^i$ ,  $dq/d\eta' = (\partial_{\eta'} \Phi - n^i \partial_i \Phi) q$ , and  $dn^i/d\eta' = 0$  resulted from perturbed geodesics of massless gravitons. Hence, Eq. (C.3) can be separated into a background equation and a perturbation equation, i.e.,

$$\partial_{\eta'} \bar{f} = 0 , \quad (\text{C.4})$$

$$\partial_{\eta'} \Gamma + n^i \partial_i \Gamma = \partial_{\eta'} \Phi - n^i \partial_i \Phi . \quad (\text{C.5})$$

Eq. (C.4) indicates that the background remains unchanged during process of evolution. For the perturbations, we can transform Eq. (C.5) into Fourier space, namely,

$$\partial_{\eta'} \Gamma + ik\mu \Gamma = \partial_{\eta'} \Phi - ik\mu \Phi , \quad (\text{C.6})$$

where we denote  $k\mu = \mathbf{k} \cdot \mathbf{n}$  for simplicity. Following Refs. [150–152], we can obtain the line-of-sight solution to Eq. (C.6) as follows [151, 152]

$$\Gamma(\eta_0, \mathbf{k}, \mathbf{q}) = e^{ik\mu(\eta-\eta_0)} [\Gamma(\eta, \mathbf{k}, \mathbf{q}) + \Phi(\eta, \mathbf{k})] + 2 \int_{\eta}^{\eta_0} d\eta' e^{ik\mu(\eta'-\eta_0)} \partial_{\eta'} \Phi(\eta', \mathbf{k}) , \quad (\text{C.7})$$

where we have disregarded the monopole term  $\Phi(\eta_0, \mathbf{k})$ .

The perturbations  $\Gamma$  lead to the inhomogeneities of the energy density of GWs, implying that  $\delta_{\text{gw}} \propto \Gamma$ . Exactly, we express the energy density  $\rho_{\text{gw}}(\eta', \mathbf{x})$  in terms of  $f(\eta', \mathbf{x}, \mathbf{q})$ , i.e.,

$$\rho_{\text{gw}}(\eta', \mathbf{x}) = \frac{1}{a^4} \int d^3 \mathbf{q} q f(\eta', \mathbf{x}, \mathbf{q}) . \quad (\text{C.8})$$

Hence, we establish a relation between  $f$  and the energy-density full spectrum  $\omega_{\text{gw}}(\eta', \mathbf{x}, \mathbf{q})$ , defined in Eq. (3.3), as follows

$$f(\eta', \mathbf{x}, \mathbf{q}) = \rho_c \left( \frac{a}{q} \right)^4 \omega_{\text{gw}}(\eta', \mathbf{x}, \mathbf{q}) . \quad (\text{C.9})$$

Since  $\langle \omega_{\text{gw}}(\eta', \mathbf{x}, q) \rangle = \bar{\Omega}_{\text{gw}}(\eta', q)/4\pi$  is obtained in Eq. (3.2) and  $\bar{f}(\eta', q)$  stands for the background term of  $f(\eta', \mathbf{x}, \mathbf{q})$ , we get

$$\bar{f}(\eta', q) = \frac{\rho_c}{4\pi} \left( \frac{a}{q} \right)^4 \bar{\Omega}_{\text{gw}}(\eta', q) . \quad (\text{C.10})$$

Consequently, the density contrast, as defined in Eq. (3.1), can be represented in terms of  $\Gamma(\eta', \mathbf{x}, \mathbf{q})$ , i.e., [151, 152]

$$\delta_{\text{gw}}(\eta', \mathbf{x}, \mathbf{q}) = \left[ 4 - \frac{\partial \ln \bar{\Omega}_{\text{gw}}(\eta', q)}{\partial \ln q} \right] \Gamma(\eta', \mathbf{x}, \mathbf{q}) = [4 - n_{\text{gw}}(\nu)] \Gamma(\eta', \mathbf{x}, \mathbf{q}) , \quad (\text{C.11})$$

where  $n_{\text{gw}}(\nu)$  is defined in Eq. (3.7). Considering the line-of-sight  $\mathbf{x}_0 - \mathbf{x} = (\eta_0 - \eta)\mathbf{n}_0$  and combining Eq. (C.7) with Eq. (C.11), we immediately obtain a formula for the present density contrast in configuration space, i.e., [25]

$$\begin{aligned} \delta_{\text{gw},0}(\mathbf{q}) &= \delta_{\text{gw}}(\eta, \mathbf{x}, \mathbf{q}) + [4 - n_{\text{gw}}(\nu)] \Phi(\eta, \mathbf{x}) \\ &\quad + 2 [4 - n_{\text{gw}}(\nu)] \int \frac{d^3 \mathbf{k}}{(2\pi)^{3/2}} e^{i\mathbf{k} \cdot \mathbf{x}_0} \int_{\eta}^{\eta_0} d\eta' e^{ik\mu(\eta' - \eta_0)} \partial_{\eta'} \Phi(\eta', \mathbf{k}) , \end{aligned} \quad (\text{C.12})$$

where  $\delta_{\text{gw}}(\eta, \mathbf{x}, \mathbf{q})$  represents the initial perturbations,  $\Phi(\eta, \mathbf{x})$  corresponds to the SW effect [147], and the integral signifies the ISW effect [147]. According to Ref. [106], the ISW effect is typically of less importance and can be disregarded. Finally, we obtain the formula for the present density contrast of SIGWs, as shown in Eq. (3.6).

## References

- [1] J.M. Maldacena, *Non-Gaussian features of primordial fluctuations in single field inflationary models*, *JHEP* **05** (2003) 013 [[astro-ph/0210603](#)].
- [2] N. Bartolo, E. Komatsu, S. Matarrese and A. Riotto, *Non-Gaussianity from inflation: Theory and observations*, *Phys. Rept.* **402** (2004) 103 [[astro-ph/0406398](#)].
- [3] T.J. Allen, B. Grinstein and M.B. Wise, *Nongaussian Density Perturbations in Inflationary Cosmologies*, *Phys. Lett. B* **197** (1987) 66.
- [4] N. Bartolo, S. Matarrese and A. Riotto, *Nongaussianity from inflation*, *Phys. Rev. D* **65** (2002) 103505 [[hep-ph/0112261](#)].
- [5] V. Acquaviva, N. Bartolo, S. Matarrese and A. Riotto, *Second order cosmological perturbations from inflation*, *Nucl. Phys. B* **667** (2003) 119 [[astro-ph/0209156](#)].
- [6] F. Bernardeau and J.-P. Uzan, *NonGaussianity in multifield inflation*, *Phys. Rev. D* **66** (2002) 103506 [[hep-ph/0207295](#)].
- [7] X. Chen, M.-x. Huang, S. Kachru and G. Shiu, *Observational signatures and non-Gaussianities of general single field inflation*, *JCAP* **01** (2007) 002 [[hep-th/0605045](#)].
- [8] D.H. Lyth and A. Riotto, *Particle physics models of inflation and the cosmological density perturbation*, *Phys. Rept.* **314** (1999) 1 [[hep-ph/9807278](#)].

- [9] P.D. Meerburg et al., *Primordial Non-Gaussianity*, [1903.04409](#).
- [10] M.W. Davies, P. Carrilho and D.J. Mulryne, *Non-Gaussianity in inflationary scenarios for primordial black holes*, *JCAP* **06** (2022) 019 [[2110.08189](#)].
- [11] PLANCK collaboration, *Planck 2018 results. IX. Constraints on primordial non-Gaussianity*, *Astron. Astrophys.* **641** (2020) A9 [[1905.05697](#)].
- [12] E. Castorina et al., *Redshift-weighted constraints on primordial non-Gaussianity from the clustering of the eBOSS DR14 quasars in Fourier space*, *JCAP* **09** (2019) 010 [[1904.08859](#)].
- [13] M. Biagetti, A. Cole and G. Shiu, *The Persistence of Large Scale Structures I: Primordial non-Gaussianity*, *JCAP* **04** (2021) 061 [[2009.04819](#)].
- [14] K.N. Ananda, C. Clarkson and D. Wands, *The Cosmological gravitational wave background from primordial density perturbations*, *Phys. Rev. D* **75** (2007) 123518 [[gr-qc/0612013](#)].
- [15] D. Baumann, P.J. Steinhardt, K. Takahashi and K. Ichiki, *Gravitational Wave Spectrum Induced by Primordial Scalar Perturbations*, *Phys. Rev. D* **76** (2007) 084019 [[hep-th/0703290](#)].
- [16] J.R. Espinosa, D. Racco and A. Riotto, *A Cosmological Signature of the SM Higgs Instability: Gravitational Waves*, *JCAP* **09** (2018) 012 [[1804.07732](#)].
- [17] K. Kohri and T. Terada, *Semianalytic calculation of gravitational wave spectrum nonlinearly induced from primordial curvature perturbations*, *Phys. Rev. D* **97** (2018) 123532 [[1804.08577](#)].
- [18] S. Mollerach, D. Harari and S. Matarrese, *CMB polarization from secondary vector and tensor modes*, *Phys. Rev. D* **69** (2004) 063002 [[astro-ph/0310711](#)].
- [19] H. Assadullahi and D. Wands, *Constraints on primordial density perturbations from induced gravitational waves*, *Phys. Rev. D* **81** (2010) 023527 [[0907.4073](#)].
- [20] G. Domènech, *Scalar Induced Gravitational Waves Review*, *Universe* **7** (2021) 398 [[2109.01398](#)].
- [21] N. Bartolo, A. Hoseinpour, G. Orlando, S. Matarrese and M. Zarei, *Photon-graviton scattering: A new way to detect anisotropic gravitational waves?*, *Phys. Rev. D* **98** (2018) 023518 [[1804.06298](#)].
- [22] R. Flauger and S. Weinberg, *Absorption of Gravitational Waves from Distant Sources*, *Phys. Rev. D* **99** (2019) 123030 [[1906.04853](#)].
- [23] P. Adshead, K.D. Lozanov and Z.J. Weiner, *Non-Gaussianity and the induced gravitational wave background*, *JCAP* **10** (2021) 080 [[2105.01659](#)].
- [24] H.V. Ragavendra, *Accounting for scalar non-Gaussianity in secondary gravitational waves*, *Phys. Rev. D* **105** (2022) 063533 [[2108.04193](#)].
- [25] J.-P. Li, S. Wang, Z.-C. Zhao and K. Kohri, *Primordial Non-Gaussianity and Anisotropies in Gravitational Waves induced by Scalar Perturbations*, [2305.19950](#).
- [26] K.T. Abe, R. Inui, Y. Tada and S. Yokoyama, *Primordial black holes and gravitational waves induced by exponential-tailed perturbations*, *JCAP* **05** (2023) 044 [[2209.13891](#)].
- [27] R.-g. Cai, S. Pi and M. Sasaki, *Gravitational Waves Induced by non-Gaussian Scalar Perturbations*, *Phys. Rev. Lett.* **122** (2019) 201101 [[1810.11000](#)].
- [28] C. Unal, *Imprints of Primordial Non-Gaussianity on Gravitational Wave Spectrum*, *Phys. Rev. D* **99** (2019) 041301 [[1811.09151](#)].
- [29] V. Atal and G. Domènech, *Probing non-Gaussianities with the high frequency tail of induced gravitational waves*, *JCAP* **06** (2021) 001 [[2103.01056](#)].

- [30] H.V. Ragavendra, P. Saha, L. Sriramkumar and J. Silk, *Primordial black holes and secondary gravitational waves from ultraslow roll and punctuated inflation*, *Phys. Rev. D* **103** (2021) 083510 [[2008.12202](#)].
- [31] C. Yuan and Q.-G. Huang, *Gravitational waves induced by the local-type non-Gaussian curvature perturbations*, *Phys. Lett. B* **821** (2021) 136606 [[2007.10686](#)].
- [32] C. Yuan and Q.-G. Huang, *A topic review on probing primordial black hole dark matter with scalar induced gravitational waves*, [2103.04739](#).
- [33] C. Yuan, D.-S. Meng and Q.-G. Huang, *Full analysis of the scalar-induced gravitational waves for the curvature perturbation with local-type non-Gaussianities*, [2308.07155](#).
- [34] S. Garcia-Saenz, L. Pinol, S. Renaux-Petel and D. Werth, *No-go theorem for scalar-trispectrum-induced gravitational waves*, *JCAP* **03** (2023) 057 [[2207.14267](#)].
- [35] F. Zhang, *Primordial black holes and scalar induced gravitational waves from the E model with a Gauss-Bonnet term*, *Phys. Rev. D* **105** (2022) 063539 [[2112.10516](#)].
- [36] G. Domènech and M. Sasaki, *Hamiltonian approach to second order gauge invariant cosmological perturbations*, *Phys. Rev. D* **97** (2018) 023521 [[1709.09804](#)].
- [37] J. Garcia-Bellido, M. Peloso and C. Unal, *Gravitational Wave signatures of inflationary models from Primordial Black Hole Dark Matter*, *JCAP* **09** (2017) 013 [[1707.02441](#)].
- [38] T. Nakama, J. Silk and M. Kamionkowski, *Stochastic gravitational waves associated with the formation of primordial black holes*, *Phys. Rev. D* **95** (2017) 043511 [[1612.06264](#)].
- [39] J. Lin, S. Gao, Y. Gong, Y. Lu, Z. Wang and F. Zhang, *Primordial black holes and scalar induced gravitational waves from Higgs inflation with noncanonical kinetic term*, *Phys. Rev. D* **107** (2023) 043517 [[2111.01362](#)].
- [40] L.-Y. Chen, H. Yu and P. Wu, *Primordial non-Gaussianity in inflation with gravitationally enhanced friction*, *Phys. Rev. D* **106** (2022) 063537 [[2210.05201](#)].
- [41] R.-G. Cai, S. Pi, S.-J. Wang and X.-Y. Yang, *Resonant multiple peaks in the induced gravitational waves*, *JCAP* **05** (2019) 013 [[1901.10152](#)].
- [42] R.-G. Cai, S. Pi, S.-J. Wang and X.-Y. Yang, *Pulsar Timing Array Constraints on the Induced Gravitational Waves*, *JCAP* **10** (2019) 059 [[1907.06372](#)].
- [43] J.S. Bullock and J.R. Primack, *NonGaussian fluctuations and primordial black holes from inflation*, *Phys. Rev. D* **55** (1997) 7423 [[astro-ph/9611106](#)].
- [44] C.T. Byrnes, E.J. Copeland and A.M. Green, *Primordial black holes as a tool for constraining non-Gaussianity*, *Phys. Rev. D* **86** (2012) 043512 [[1206.4188](#)].
- [45] S. Young and C.T. Byrnes, *Primordial black holes in non-Gaussian regimes*, *JCAP* **08** (2013) 052 [[1307.4995](#)].
- [46] G. Franciolini, A. Kehagias, S. Matarrese and A. Riotto, *Primordial Black Holes from Inflation and non-Gaussianity*, *JCAP* **03** (2018) 016 [[1801.09415](#)].
- [47] S. Passaglia, W. Hu and H. Motohashi, *Primordial black holes and local non-Gaussianity in canonical inflation*, *Phys. Rev. D* **99** (2019) 043536 [[1812.08243](#)].
- [48] V. Atal and C. Germani, *The role of non-gaussianities in Primordial Black Hole formation*, *Phys. Dark Univ.* **24** (2019) 100275 [[1811.07857](#)].
- [49] V. Atal, J. Garriga and A. Marcos-Caballero, *Primordial black hole formation with non-Gaussian curvature perturbations*, *JCAP* **09** (2019) 073 [[1905.13202](#)].
- [50] M. Taoso and A. Urbano, *Non-gaussianities for primordial black hole formation*, *JCAP* **08** (2021) 016 [[2102.03610](#)].

- [51] D.-S. Meng, C. Yuan and Q.-g. Huang, *One-loop correction to the enhanced curvature perturbation with local-type non-Gaussianity for the formation of primordial black holes*, *Phys. Rev. D* **106** (2022) 063508 [[2207.07668](#)].
- [52] C. Chen, A. Ghoshal, Z. Lalak, Y. Luo and A. Naskar, *Growth of curvature perturbations for PBH formation in non-minimal curvaton scenario revisited*, [2305.12325](#).
- [53] R. Kawaguchi, T. Fujita and M. Sasaki, *Highly asymmetric probability distribution from a finite-width upward step during inflation*, [2305.18140](#).
- [54] C. Fu, P. Wu and H. Yu, *Primordial black holes and oscillating gravitational waves in slow-roll and slow-climb inflation with an intermediate noninflationary phase*, *Phys. Rev. D* **102** (2020) 043527 [[2006.03768](#)].
- [55] K. Inomata, M. Kawasaki, K. Mukaida and T.T. Yanagida, *NANOGrav Results and LIGO-Virgo Primordial Black Holes in Axionlike Curvaton Models*, *Phys. Rev. Lett.* **126** (2021) 131301 [[2011.01270](#)].
- [56] S. Young, C.T. Byrnes and M. Sasaki, *Calculating the mass fraction of primordial black holes*, *JCAP* **07** (2014) 045 [[1405.7023](#)].
- [57] S. Choudhury, A. Karde, S. Panda and M. Sami, *Primordial non-Gaussianity from ultra slow-roll Galileon inflation*, [2306.12334](#).
- [58] G. Ferrante, G. Franciolini, A. Iovino, Junior. and A. Urbano, *Primordial non-Gaussianity up to all orders: Theoretical aspects and implications for primordial black hole models*, *Phys. Rev. D* **107** (2023) 043520 [[2211.01728](#)].
- [59] A.M. Green and B.J. Kavanagh, *Primordial Black Holes as a dark matter candidate*, *J. Phys. G* **48** (2021) 043001 [[2007.10722](#)].
- [60] B. Carr, K. Kohri, Y. Sendouda and J. Yokoyama, *Constraints on primordial black holes*, *Rept. Prog. Phys.* **84** (2021) 116902 [[2002.12778](#)].
- [61] A. Escrivà, F. Kuhnel and Y. Tada, *Primordial Black Holes*, [2211.05767](#).
- [62] A. Escrivà, Y. Tada, S. Yokoyama and C.-M. Yoo, *Simulation of primordial black holes with large negative non-Gaussianity*, *JCAP* **05** (2022) 012 [[2202.01028](#)].
- [63] J.M. Ezquiaga, J. García-Bellido and V. Vennin, *The exponential tail of inflationary fluctuations: consequences for primordial black holes*, *JCAP* **03** (2020) 029 [[1912.05399](#)].
- [64] A. Kehagias, I. Musco and A. Riotto, *Non-Gaussian Formation of Primordial Black Holes: Effects on the Threshold*, *JCAP* **12** (2019) 029 [[1906.07135](#)].
- [65] Y.-F. Cai, X.-H. Ma, M. Sasaki, D.-G. Wang and Z. Zhou, *One small step for an inflaton, one giant leap for inflation: A novel non-Gaussian tail and primordial black holes*, *Phys. Lett. B* **834** (2022) 137461 [[2112.13836](#)].
- [66] Y.-F. Cai, X.-H. Ma, M. Sasaki, D.-G. Wang and Z. Zhou, *Highly non-Gaussian tails and primordial black holes from single-field inflation*, *JCAP* **12** (2022) 034 [[2207.11910](#)].
- [67] Z. Yi, Q. Gao, Y. Gong and Z.-h. Zhu, *Primordial black holes and scalar-induced secondary gravitational waves from inflationary models with a noncanonical kinetic term*, *Phys. Rev. D* **103** (2021) 063534 [[2011.10606](#)].
- [68] F. Zhang, J. Lin and Y. Lu, *Double-peaked inflation model: Scalar induced gravitational waves and primordial-black-hole suppression from primordial non-Gaussianity*, *Phys. Rev. D* **104** (2021) 063515 [[2106.10792](#)].
- [69] H. Xu et al., *Searching for the Nano-Hertz Stochastic Gravitational Wave Background with the Chinese Pulsar Timing Array Data Release I*, *Res. Astron. Astrophys.* **23** (2023) 075024 [[2306.16216](#)].

- [70] EPTA, INPTA: collaboration, *The second data release from the European Pulsar Timing Array - III. Search for gravitational wave signals*, *Astron. Astrophys.* **678** (2023) A50 [[2306.16214](#)].
- [71] NANOGrav collaboration, *The NANOGrav 15-year Data Set: Evidence for a Gravitational-Wave Background*, *Astrophys. J. Lett.* **951** (2023) [[2306.16213](#)].
- [72] D.J. Reardon et al., *Search for an isotropic gravitational-wave background with the Parkes Pulsar Timing Array*, *Astrophys. J. Lett.* **951** (2023) [[2306.16215](#)].
- [73] EPTA collaboration, *The second data release from the European Pulsar Timing Array: V. Implications for massive black holes, dark matter and the early Universe*, [2306.16227](#).
- [74] NANOGrav collaboration, *The NANOGrav 15-year Data Set: Search for Signals from New Physics*, *Astrophys. J. Lett.* **951** (2023) [[2306.16219](#)].
- [75] G. Franciolini, A. Iovino, Junior., V. Vaskonen and H. Veermae, *The recent gravitational wave observation by pulsar timing arrays and primordial black holes: the importance of non-gaussianities*, [2306.17149](#).
- [76] K. Inomata, K. Kohri and T. Terada, *The Detected Stochastic Gravitational Waves and Subsolar-Mass Primordial Black Holes*, [2306.17834](#).
- [77] Y.-F. Cai, X.-C. He, X. Ma, S.-F. Yan and G.-W. Yuan, *Limits on scalar-induced gravitational waves from the stochastic background by pulsar timing array observations*, [2306.17822](#).
- [78] S. Wang, Z.-C. Zhao, J.-P. Li and Q.-H. Zhu, *Exploring the Implications of 2023 Pulsar Timing Array Datasets for Scalar-Induced Gravitational Waves and Primordial Black Holes*, [2307.00572](#).
- [79] L. Liu, Z.-C. Chen and Q.-G. Huang, *Implications for the non-Gaussianity of curvature perturbation from pulsar timing arrays*, [2307.01102](#).
- [80] K.T. Abe and Y. Tada, *Translating nano-Hertz gravitational wave background into primordial perturbations taking account of the cosmological QCD phase transition*, [2307.01653](#).
- [81] R. Ebadi, S. Kumar, A. McCune, H. Tai and L.-T. Wang, *Gravitational Waves from Stochastic Scalar Fluctuations*, [2307.01248](#).
- [82] D.G. Figueroa, M. Pieroni, A. Ricciardone and P. Simakachorn, *Cosmological Background Interpretation of Pulsar Timing Array Data*, [2307.02399](#).
- [83] Z. Yi, Q. Gao, Y. Gong, Y. Wang and F. Zhang, *The waveform of the scalar induced gravitational waves in light of Pulsar Timing Array data*, [2307.02467](#).
- [84] E. Madge, E. Morgante, C. Puchades-Ibáñez, N. Ramberg, W. Ratzinger, S. Schenk et al., *Primordial gravitational waves in the nano-Hertz regime and PTA data – towards solving the GW inverse problem*, [2306.14856](#).
- [85] H. Firouzjahi and A. Talebian, *Induced Gravitational Waves from Ultra Slow-Roll Inflation and Pulsar Timing Arrays Observations*, [2307.03164](#).
- [86] Q.-H. Zhu, Z.-C. Zhao and S. Wang, *Joint implications of BBN, CMB, and PTA Datasets for Scalar-Induced Gravitational Waves of Second and Third orders*, [2307.03095](#).
- [87] Z.-Q. You, Z. Yi and Y. Wu, *Constraints on primordial curvature power spectrum with pulsar timing arrays*, [2307.04419](#).
- [88] G. Ye and A. Silvestri, *Can gravitational wave background feel wiggles in spacetime?*, [2307.05455](#).
- [89] S.A. Hosseini Mansoori, F. Felegray, A. Talebian and M. Sami, *PBHs and GWs from  $\mathbb{T}^2$ -inflation and NANOGrav 15-year data*, [2307.06757](#).



- [90] S. Balaji, G. Domènech and G. Franciolini, *Scalar-induced gravitational wave interpretation of PTA data: the role of scalar fluctuation propagation speed*, [2307.08552](#).
- [91] B. Das, N. Jaman and M. Sami, *Gravitational Waves Background (NANOGrav) from Quintessential Inflation*, [2307.12913](#).
- [92] L. Bian, S. Ge, J. Shu, B. Wang, X.-Y. Yang and J. Zong, *Gravitational wave sources for Pulsar Timing Arrays*, [2307.02376](#).
- [93] J.-H. Jin, Z.-C. Chen, Z. Yi, Z.-Q. You, L. Liu and Y. Wu, *Confronting sound speed resonance with pulsar timing arrays*, [2307.08687](#).
- [94] Z.-C. Zhao, Q.-H. Zhu, S. Wang and X. Zhang, *Exploring the Equation of State of the Early Universe: Insights from BBN, CMB, and PTA Observations*, [2307.13574](#).
- [95] L. Liu, Z.-C. Chen and Q.-G. Huang, *Probing the equation of state of the early Universe with pulsar timing arrays*, [2307.14911](#).
- [96] Z. Yi, Z.-Q. You and Y. Wu, *Model-independent reconstruction of the primordial curvature power spectrum from PTA data*, [2308.05632](#).
- [97] L. Frosina and A. Urbano, *On the inflationary interpretation of the nHz gravitational-wave background*, [2308.06915](#).
- [98] S. Choudhury, A. Karde, S. Panda and M. Sami, *Scalar induced gravity waves from ultra slow-roll Galileon inflation*, [2308.09273](#).
- [99] J. Ellis, M. Fairbairn, G. Franciolini, G. Hütsi, A. Iovino, M. Lewicki et al., *What is the source of the PTA GW signal?*, [2308.08546](#).
- [100] M. Kawasaki and K. Murai, *Enhancement of gravitational waves at Q-ball decay including non-linear density perturbations*, [2308.13134](#).
- [101] Z. Yi, Z.-Q. You, Y. Wu, Z.-C. Chen and L. Liu, *Exploring the NANOGrav Signal and Planet-mass Primordial Black Holes through Higgs Inflation*, [2308.14688](#).
- [102] K. Harigaya, K. Inomata and T. Terada, *Induced Gravitational Waves with Kination Era for Recent Pulsar Timing Array Signals*, [2309.00228](#).
- [103] H. An, B. Su, H. Tai, L.-T. Wang and C. Yang, *Phase transition during inflation and the gravitational wave signal at pulsar timing arrays*, [2308.00070](#).
- [104] M.R. Gangopadhyay, V.V. Godithi, K. Ichiki, R. Inui, T. Kajino, A. Manusankar et al., *Is NanoGRAV signals pointing towards resonant particle creation during inflation?*, [2309.03101](#).
- [105] Z. Chang, Y.-T. Kuang, D. Wu and J.-Z. Zhou, *Scalar Induced Gravitational Waves from Finslerian Inflation and Pulsar Timing Arrays Observations*, [2309.06676](#).
- [106] N. Bartolo, D. Bertacca, V. De Luca, G. Franciolini, S. Matarrese, M. Peloso et al., *Gravitational wave anisotropies from primordial black holes*, *JCAP* **02** (2020) 028 [[1909.12619](#)].
- [107] L. Valbusa Dall’Armi, A. Ricciardone, N. Bartolo, D. Bertacca and S. Matarrese, *Imprint of relativistic particles on the anisotropies of the stochastic gravitational-wave background*, *Phys. Rev. D* **103** (2021) 023522 [[2007.01215](#)].
- [108] E. Dimastrogiovanni, M. Fasiello, A. Malhotra, P.D. Meerburg and G. Orlando, *Testing the early universe with anisotropies of the gravitational wave background*, *JCAP* **02** (2022) 040 [[2109.03077](#)].
- [109] LISA COSMOLOGY WORKING GROUP collaboration, *Probing anisotropies of the Stochastic Gravitational Wave Background with LISA*, *JCAP* **11** (2022) 009 [[2201.08782](#)].
- [110] LISA COSMOLOGY WORKING GROUP collaboration, *Cosmology with the Laser Interferometer Space Antenna*, [2204.05434](#).



- [111] C. Ünal, E.D. Kovetz and S.P. Patil, *Multimessenger probes of inflationary fluctuations and primordial black holes*, *Phys. Rev. D* **103** (2021) 063519 [[2008.11184](#)].
- [112] A. Malhotra, E. Dimastrogiovanni, M. Fasiello and M. Shiraishi, *Cross-correlations as a Diagnostic Tool for Primordial Gravitational Waves*, *JCAP* **03** (2021) 088 [[2012.03498](#)].
- [113] Y. Cui, S. Kumar, R. Sundrum and Y. Tsai, *Unraveling Cosmological Anisotropies within Stochastic Gravitational Wave Backgrounds*, [2307.10360](#).
- [114] A. Malhotra, E. Dimastrogiovanni, G. Domènech, M. Fasiello and G. Tasinato, *New universal property of cosmological gravitational wave anisotropies*, *Phys. Rev. D* **107** (2023) 103502 [[2212.10316](#)].
- [115] L. Valbusa Dall’Armi, A. Mierna, S. Matarrese and A. Ricciardone, *Adiabatic or Non-Adiabatic? Unraveling the Nature of Initial Conditions in the Cosmological Gravitational Wave Background*, [2307.11043](#).
- [116] P.E. Dewdney, P.J. Hall, R.T. Schilizzi and T.J.L.W. Lazio, *The Square Kilometre Array*, *IEEE Proceedings* **97** (2009) 1482.
- [117] A. Weltman et al., *Fundamental physics with the Square Kilometre Array*, *Publ. Astron. Soc. Austral.* **37** (2020) e002 [[1810.02680](#)].
- [118] C.J. Moore, R.H. Cole and C.P.L. Berry, *Gravitational-wave sensitivity curves*, *Class. Quant. Grav.* **32** (2015) 015014 [[1408.0740](#)].
- [119] G. Janssen et al., *Gravitational wave astronomy with the SKA*, *PoS AASKA14* (2015) 037 [[1501.00127](#)].
- [120] M. Maggiore, *Gravitational wave experiments and early universe cosmology*, *Phys. Rept.* **331** (2000) 283 [[gr-qc/9909001](#)].
- [121] K. Inomata, M. Kawasaki, K. Mukaida, Y. Tada and T.T. Yanagida, *Inflationary primordial black holes for the LIGO gravitational wave events and pulsar timing array experiments*, *Phys. Rev. D* **95** (2017) 123510 [[1611.06130](#)].
- [122] E. Komatsu and D.N. Spergel, *Acoustic signatures in the primary microwave background bispectrum*, *Phys. Rev. D* **63** (2001) 063002 [[astro-ph/0005036](#)].
- [123] Y. Tada and S. Yokoyama, *Primordial black holes as biased tracers*, *Phys. Rev. D* **91** (2015) 123534 [[1502.01124](#)].
- [124] K. Saikawa and S. Shirai, *Primordial gravitational waves, precisely: The role of thermodynamics in the Standard Model*, *JCAP* **05** (2018) 035 [[1803.01038](#)].
- [125] PLANCK collaboration, *Planck 2018 results. VI. Cosmological parameters*, *Astron. Astrophys.* **641** (2020) A6 [[1807.06209](#)].
- [126] G.P. Lepage, *Adaptive multidimensional integration: VEGAS enhanced*, *J. Comput. Phys.* **439** (2021) 110386 [[2009.05112](#)].
- [127] S. Wang, T. Terada and K. Kohri, *Prospective constraints on the primordial black hole abundance from the stochastic gravitational-wave backgrounds produced by coalescing events and curvature perturbations*, *Phys. Rev. D* **99** (2019) 103531 [[1903.05924](#)].
- [128] Z.-C. Zhao and S. Wang, *Bayesian Implications for the Primordial Black Holes from ‘NANOGrav Pulsar-Timing Data Using the Scalar-Induced Gravitational Waves*, *Universe* **9** (2023) 157 [[2211.09450](#)].
- [129] J. Baker et al., *The Laser Interferometer Space Antenna: Unveiling the Millihertz Gravitational Wave Sky*, [1907.06482](#).
- [130] T.L. Smith, T.L. Smith, R.R. Caldwell and R. Caldwell, *LISA for Cosmologists: Calculating the Signal-to-Noise Ratio for Stochastic and Deterministic Sources*, *Phys. Rev. D* **100** (2019) 104055 [[1908.00546](#)].

- [131] N. Seto, S. Kawamura and T. Nakamura, *Possibility of direct measurement of the acceleration of the universe using 0.1-Hz band laser interferometer gravitational wave antenna in space*, *Phys. Rev. Lett.* **87** (2001) 221103 [[astro-ph/0108011](#)].
- [132] S. Kawamura et al., *Current status of space gravitational wave antenna DECIGO and B-DECIGO*, *PTEP* **2021** (2021) 05A105 [[2006.13545](#)].
- [133] J. Crowder and N.J. Cornish, *Beyond LISA: Exploring future gravitational wave missions*, *Phys. Rev. D* **72** (2005) 083005 [[gr-qc/0506015](#)].
- [134] T.L. Smith and R. Caldwell, *Sensitivity to a Frequency-Dependent Circular Polarization in an Isotropic Stochastic Gravitational Wave Background*, *Phys. Rev. D* **95** (2017) 044036 [[1609.05901](#)].
- [135] W.-R. Hu and Y.-L. Wu, *The Taiji Program in Space for gravitational wave physics and the nature of gravity*, *Natl. Sci. Rev.* **4** (2017) 685.
- [136] Z. Ren, T. Zhao, Z. Cao, Z.-K. Guo, W.-B. Han, H.-B. Jin et al., *Taiji data challenge for exploring gravitational wave universe*, *Front. Phys. (Beijing)* **18** (2023) 64302 [[2301.02967](#)].
- [137] TIANQIN collaboration, *TianQin: a space-borne gravitational wave detector*, *Class. Quant. Grav.* **33** (2016) 035010 [[1512.02076](#)].
- [138] TIANQIN collaboration, *The TianQin project: current progress on science and technology*, *PTEP* **2021** (2021) 05A107 [[2008.10332](#)].
- [139] K. Zhou, J. Cheng and L. Ren, *Detecting anisotropies of the stochastic gravitational wave background with TianQin*, [2306.14439](#).
- [140] T. Robson, N.J. Cornish and C. Liu, *The construction and use of LISA sensitivity curves*, *Class. Quant. Grav.* **36** (2019) 105011 [[1803.01944](#)].
- [141] G.M. Harry, P. Fritschel, D.A. Shaddock, W. Folkner and E.S. Phinney, *Laser interferometry for the big bang observer*, *Class. Quant. Grav.* **23** (2006) 4887.
- [142] S. Sato et al., *The status of DECIGO*, *J. Phys. Conf. Ser.* **840** (2017) 012010.
- [143] S. Hawking, *Gravitationally collapsed objects of very low mass*, *Mon. Not. Roy. Astron. Soc.* **152** (1971) 75.
- [144] R. Saito and J. Yokoyama, *Gravitational-Wave Constraints on the Abundance of Primordial Black Holes*, *Prog. Theor. Phys.* **123** (2010) 867 [[0912.5317](#)].
- [145] K. Inomata and T. Nakama, *Gravitational waves induced by scalar perturbations as probes of the small-scale primordial spectrum*, *Phys. Rev. D* **99** (2019) 043511 [[1812.00674](#)].
- [146] C.-M. Yoo, T. Harada, J. Garriga and K. Kohri, *Primordial black hole abundance from random Gaussian curvature perturbations and a local density threshold*, *PTEP* **2018** (2018) 123E01 [[1805.03946](#)].
- [147] R.K. Sachs and A.M. Wolfe, *Perturbations of a cosmological model and angular variations of the microwave background*, *Astrophys. J.* **147** (1967) 73.
- [148] U. Seljak and M. Zaldarriaga, *A Line of sight integration approach to cosmic microwave background anisotropies*, *Astrophys. J.* **469** (1996) 437 [[astro-ph/9603033](#)].
- [149] S. Dodelson, *Modern Cosmology*, Academic Press, Amsterdam (2003).
- [150] C.R. Contaldi, *Anisotropies of Gravitational Wave Backgrounds: A Line Of Sight Approach*, *Phys. Lett. B* **771** (2017) 9 [[1609.08168](#)].
- [151] N. Bartolo, D. Bertacca, S. Matarrese, M. Peloso, A. Ricciardone, A. Riotto et al., *Anisotropies and non-Gaussianity of the Cosmological Gravitational Wave Background*, *Phys. Rev. D* **100** (2019) 121501 [[1908.00527](#)].

- [152] N. Bartolo, D. Bertacca, S. Matarrese, M. Peloso, A. Ricciardone, A. Riotto et al., *Characterizing the cosmological gravitational wave background: Anisotropies and non-Gaussianity*, *Phys. Rev. D* **102** (2020) 023527 [[1912.09433](#)].
- [153] E. Dimastrogiovanni, M. Fasiello, A. Malhotra and G. Tasinato, *Enhancing gravitational wave anisotropies with peaked scalar sources*, *JCAP* **01** (2023) 018 [[2205.05644](#)].
- [154] G. Cusin, I. Dvorkin, C. Pitrou and J.-P. Uzan, *First predictions of the angular power spectrum of the astrophysical gravitational wave background*, *Phys. Rev. Lett.* **120** (2018) 231101 [[1803.03236](#)].
- [155] G. Cusin, C. Pitrou and J.-P. Uzan, *Anisotropy of the astrophysical gravitational wave background: Analytic expression of the angular power spectrum and correlation with cosmological observations*, *Phys. Rev. D* **96** (2017) 103019 [[1704.06184](#)].
- [156] G. Cusin, I. Dvorkin, C. Pitrou and J.-P. Uzan, *Stochastic gravitational wave background anisotropies in the mHz band: astrophysical dependencies*, *Mon. Not. Roy. Astron. Soc.* **493** (2020) L1 [[1904.07757](#)].
- [157] G. Cusin, I. Dvorkin, C. Pitrou and J.-P. Uzan, *Properties of the stochastic astrophysical gravitational wave background: astrophysical sources dependencies*, *Phys. Rev. D* **100** (2019) 063004 [[1904.07797](#)].
- [158] A.C. Jenkins, R. O'Shaughnessy, M. Sakellariadou and D. Wysocki, *Anisotropies in the astrophysical gravitational-wave background: The impact of black hole distributions*, *Phys. Rev. Lett.* **122** (2019) 111101 [[1810.13435](#)].
- [159] A.C. Jenkins, M. Sakellariadou, T. Regimbau and E. Slezak, *Anisotropies in the astrophysical gravitational-wave background: Predictions for the detection of compact binaries by LIGO and Virgo*, *Phys. Rev. D* **98** (2018) 063501 [[1806.01718](#)].
- [160] A.C. Jenkins, J.D. Romano and M. Sakellariadou, *Estimating the angular power spectrum of the gravitational-wave background in the presence of shot noise*, *Phys. Rev. D* **100** (2019) 083501 [[1907.06642](#)].
- [161] S. Wang, V. Vardanyan and K. Kohri, *Probing primordial black holes with anisotropies in stochastic gravitational-wave background*, *Phys. Rev. D* **106** (2022) 123511 [[2107.01935](#)].
- [162] S. Mukherjee and J. Silk, *Time-dependence of the astrophysical stochastic gravitational wave background*, *Mon. Not. Roy. Astron. Soc.* **491** (2020) 4690 [[1912.07657](#)].
- [163] S.S. Bavera, G. Franciolini, G. Cusin, A. Riotto, M. Zevin and T. Fragos, *Stochastic gravitational-wave background as a tool for investigating multi-channel astrophysical and primordial black-hole mergers*, *Astron. Astrophys.* **660** (2022) A26 [[2109.05836](#)].
- [164] N. Bellomo, D. Bertacca, A.C. Jenkins, S. Matarrese, A. Raccanelli, T. Regimbau et al., *CLASS\_GWB: robust modeling of the astrophysical gravitational wave background anisotropies*, *JCAP* **06** (2022) 030 [[2110.15059](#)].
- [165] A.C. Jenkins and M. Sakellariadou, *Anisotropies in the stochastic gravitational-wave background: Formalism and the cosmic string case*, *Phys. Rev. D* **98** (2018) 063509 [[1802.06046](#)].
- [166] S. Kuroyanagi, K. Takahashi, N. Yonemaru and H. Kumamoto, *Anisotropies in the gravitational wave background as a probe of the cosmic string network*, *Phys. Rev. D* **95** (2017) 043531 [[1604.00332](#)].
- [167] S. Olmez, V. Mandic and X. Siemens, *Anisotropies in the Gravitational-Wave Stochastic Background*, *JCAP* **07** (2012) 009 [[1106.5555](#)].
- [168] P. Adshead, N. Afshordi, E. Dimastrogiovanni, M. Fasiello, E.A. Lim and G. Tasinato, *Multimessenger cosmology: Correlating cosmic microwave background and stochastic gravitational wave background measurements*, *Phys. Rev. D* **103** (2021) 023532 [[2004.06619](#)].

- [169] E. Dimastrogiovanni, M. Fasiello and G. Tasinato, *Searching for Fossil Fields in the Gravity Sector*, *Phys. Rev. Lett.* **124** (2020) 061302 [[1906.07204](#)].
- [170] D. Jeong and M. Kamionkowski, *Clustering Fossils from the Early Universe*, *Phys. Rev. Lett.* **108** (2012) 251301 [[1203.0302](#)].
- [171] J. Liu, R.-G. Cai and Z.-K. Guo, *Large Anisotropies of the Stochastic Gravitational Wave Background from Cosmic Domain Walls*, *Phys. Rev. Lett.* **126** (2021) 141303 [[2010.03225](#)].
- [172] M. Li, Q.-S. Yan and M. Huang, *Anisotropic gravitational waves induced by hypermagnetic fields during the electroweak phase transition epoch*, *Phys. Rev. D* **107** (2023) 043527 [[2211.03368](#)].
- [173] Y. Li, F.P. Huang, X. Wang and X. Zhang, *Anisotropy of phase transition gravitational wave and its implication for primordial seeds of the Universe*, *Phys. Rev. D* **105** (2022) 083527 [[2112.01409](#)].
- [174] V. Domcke, R. Jinno and H. Rubira, *Deformation of the gravitational wave spectrum by density perturbations*, *JCAP* **06** (2020) 046 [[2002.11083](#)].
- [175] R. Jinno, T. Konstandin, H. Rubira and J. van de Vis, *Effect of density fluctuations on gravitational wave production in first-order phase transitions*, *JCAP* **12** (2021) 019 [[2108.11947](#)].
- [176] M. Geller, A. Hook, R. Sundrum and Y. Tsai, *Primordial Anisotropies in the Gravitational Wave Background from Cosmological Phase Transitions*, *Phys. Rev. Lett.* **121** (2018) 201303 [[1803.10780](#)].
- [177] S. Kumar, R. Sundrum and Y. Tsai, *Non-Gaussian stochastic gravitational waves from phase transitions*, *JHEP* **11** (2021) 107 [[2102.05665](#)].
- [178] D. Racco and D. Poletti, *Precision cosmology with primordial GW backgrounds in presence of astrophysical foregrounds*, *JCAP* **04** (2023) 054 [[2212.06602](#)].
- [179] L. Bethke, D.G. Figueroa and A. Rajantie, *Anisotropies in the Gravitational Wave Background from Preheating*, *Phys. Rev. Lett.* **111** (2013) 011301 [[1304.2657](#)].
- [180] L. Bethke, D.G. Figueroa and A. Rajantie, *On the Anisotropy of the Gravitational Wave Background from Massless Preheating*, *JCAP* **06** (2014) 047 [[1309.1148](#)].
- [181] A. Ricciardone, L.V. Dall’Armi, N. Bartolo, D. Bertacca, M. Liguori and S. Matarrese, *Cross-Correlating Astrophysical and Cosmological Gravitational Wave Backgrounds with the Cosmic Microwave Background*, *Phys. Rev. Lett.* **127** (2021) 271301 [[2106.02591](#)].
- [182] M. Braglia and S. Kuroyanagi, *Probing prerecombination physics by the cross-correlation of stochastic gravitational waves and CMB anisotropies*, *Phys. Rev. D* **104** (2021) 123547 [[2106.03786](#)].
- [183] G. Capurri, A. Lapi and C. Baccigalupi, *Detectability of the Cross-Correlation between CMB Lensing and Stochastic GW Background from Compact Object Mergers*, *Universe* **8** (2022) 160 [[2111.04757](#)].
- [184] G. Galloni, N. Bartolo, S. Matarrese, M. Migliaccio, A. Ricciardone and N. Vittorio, *Test of the statistical isotropy of the universe using gravitational waves*, *JCAP* **09** (2022) 046 [[2202.12858](#)].
- [185] R. Ding and C. Tian, *On the anisotropies of the cosmological gravitational-wave background from pulsar timing array observations*, [2309.01643](#).
- [186] B. Cyr, T. Kite, J. Chluba, J.C. Hill, D. Jeong, S.K. Acharya et al., *Disentangling the primordial nature of stochastic gravitational wave backgrounds with CMB spectral distortions*, [2309.02366](#).

- [187] G. Cañas Herrera, O. Contigiani and V. Vardanyan, *Cross-correlation of the astrophysical gravitational-wave background with galaxy clustering*, *Phys. Rev. D* **102** (2020) 043513 [[1910.08353](#)].
- [188] D. Alonso, G. Cusin, P.G. Ferreira and C. Pitrou, *Detecting the anisotropic astrophysical gravitational wave background in the presence of shot noise through cross-correlations*, *Phys. Rev. D* **102** (2020) 023002 [[2002.02888](#)].
- [189] K.Z. Yang, V. Mandic, C. Scarlata and S. Banagiri, *Searching for Cross-Correlation Between Stochastic Gravitational Wave Background and Galaxy Number Counts*, *Mon. Not. Roy. Astron. Soc.* **500** (2020) 1666 [[2007.10456](#)].
- [190] K.Z. Yang, J. Suresh, G. Cusin, S. Banagiri, N. Feist, V. Mandic et al., *Measurement of the cross-correlation angular power spectrum between the stochastic gravitational wave background and galaxy overdensity*, *Phys. Rev. D* **108** (2023) 043025 [[2304.07621](#)].
- [191] S. Libanore, M. Liguori and A. Raccanelli, *Signatures of primordial black holes in gravitational wave clustering*, *JCAP* **08** (2023) 055 [[2306.03087](#)].
- [192] M. Bosi, N. Bellomo and A. Raccanelli, *Constraining extended cosmologies with  $GW \times LSS$  cross-correlations*, [2306.03031](#).
- [193] A. Balaudo, A. Garoffolo, M. Martinelli, S. Mukherjee and A. Silvestri, *Prospects of testing late-time cosmology with weak lensing of gravitational waves and galaxy surveys*, *JCAP* **06** (2023) 050 [[2210.06398](#)].
- [194] G. Scelfo, M. Spinelli, A. Raccanelli, L. Boco, A. Lapi and M. Viel, *Gravitational waves  $\times$  HI intensity mapping: cosmological and astrophysical applications*, *JCAP* **01** (2022) 004 [[2106.09786](#)].
- [195] N. Seto and A. Cooray, *Cosmological constraints on the very low frequency gravitational-wave background*, *Phys. Rev. D* **73** (2006) 023005 [[astro-ph/0502054](#)].
- [196] L. Valbusa Dall’Armi, A. Nishizawa, A. Ricciardone and S. Matarrese, *Circular Polarization of the Astrophysical Gravitational Wave Background*, *Phys. Rev. Lett.* **131** (2023) 041401 [[2301.08205](#)].
- [197] G. Capurri, A. Lapi, L. Boco and C. Baccigalupi, *Searching for Anisotropic Stochastic Gravitational-wave Backgrounds with Constellations of Space-based Interferometers*, *Astrophys. J.* **943** (2023) 72 [[2212.06162](#)].
- [198] K. Schmitz, *New Sensitivity Curves for Gravitational-Wave Signals from Cosmological Phase Transitions*, *JHEP* **01** (2021) 097 [[2002.04615](#)].
- [199] G. Wang and W.-B. Han, *Alternative LISA-TAIJI networks: Detectability of the isotropic stochastic gravitational wave background*, *Phys. Rev. D* **104** (2021) 104015 [[2108.11151](#)].
- [200] G. Hobbs et al., *The international pulsar timing array project: using pulsars as a gravitational wave detector*, *Class. Quant. Grav.* **27** (2010) 084013 [[0911.5206](#)].
- [201] P.B. Demorest et al., *Limits on the Stochastic Gravitational Wave Background from the North American Nanohertz Observatory for Gravitational Waves*, *Astrophys. J.* **762** (2013) 94 [[1201.6641](#)].
- [202] EPTA collaboration, *The European Pulsar Timing Array and the Large European Array for Pulsars*, *Class. Quant. Grav.* **30** (2013) 224009.
- [203] R.N. Manchester et al., *The Parkes Pulsar Timing Array Project*, *Publ. Astron. Soc. Austral.* **30** (2013) 17 [[1210.6130](#)].
- [204] A. Sesana, A. Vecchio and C.N. Colacino, *The stochastic gravitational-wave background from massive black hole binary systems: implications for observations with Pulsar Timing Arrays*, *Mon. Not. Roy. Astron. Soc.* **390** (2008) 192 [[0804.4476](#)].

- [205] E. Thrane and J.D. Romano, *Sensitivity curves for searches for gravitational-wave backgrounds*, *Phys. Rev. D* **88** (2013) 124032 [[1310.5300](#)].
- [206] LIGO SCIENTIFIC, VIRGO collaboration, *GWTC-1: A Gravitational-Wave Transient Catalog of Compact Binary Mergers Observed by LIGO and Virgo during the First and Second Observing Runs*, *Phys. Rev. X* **9** (2019) 031040 [[1811.12907](#)].
- [207] LIGO SCIENTIFIC, VIRGO collaboration, *GWTC-2: Compact Binary Coalescences Observed by LIGO and Virgo During the First Half of the Third Observing Run*, *Phys. Rev. X* **11** (2021) 021053 [[2010.14527](#)].
- [208] LIGO SCIENTIFIC, VIRGO, KAGRA collaboration, *GWTC-3: Compact Binary Coalescences Observed by LIGO and Virgo During the Second Part of the Third Observing Run*, [2111.03606](#).
- [209] X. Wang, Y.-l. Zhang, R. Kimura and M. Yamaguchi, *Reconstruction of power spectrum of primordial curvature perturbations on small scales from primordial black hole binaries scenario of LIGO/VIRGO detection*, *Sci. China Phys. Mech. Astron.* **66** (2023) 260462 [[2209.12911](#)].
- [210] J. He, H. Deng, Y.-S. Piao and J. Zhang, *Implications of GWTC-3 on primordial black holes from vacuum bubbles*, *Phys. Rev. D* **109** (2024) 044035 [[2303.16810](#)].
- [211] J.-P. Li, S. Wang, Z.-C. Zhao and K. Kohri, *Angular bispectrum and trispectrum of scalar-induced gravitational-waves: all contributions from primordial non-Gaussianity  $f_{\text{NL}}$  and  $g_{\text{NL}}$* , [2403.00238](#).
- [212] M. Maggiore, *Gravitational Waves. Vol. 2: Astrophysics and Cosmology*, Oxford University Press (3, 2018).